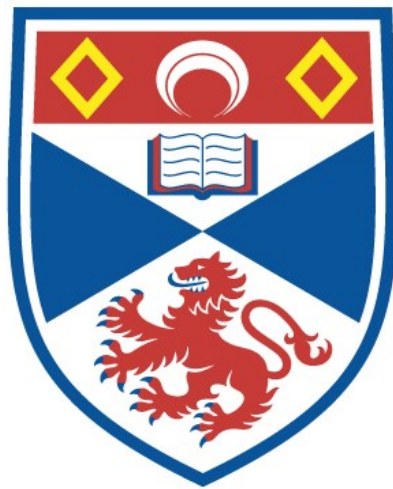


University of St Andrews



Full metadata for this thesis is available in
St Andrews Research Repository
at:

<http://research-repository.st-andrews.ac.uk/>

This thesis is protected by original copyright

THE FREQUENCY STABILIZATION OF GAS LASERS

A THESIS

PRESENTED BY

ANDREW J. WALLARD B.SC.

TO THE

UNIVERSITY OF ST. ANDREWS

IN APPLICATION FOR THE

DEGREE OF DOCTOR OF PHILOSOPHY



Th 7047

A.J. Wallard was born in Liverpool, England on 11th October 1945 and was educated at the Liverpool Institute High School for Boys. He entered the University of St. Andrews in October 1964 and graduated with a first class honours Bachelor of Science Degree in June 1968.

After graduation and until the present time he has been a member of the staff of the Division of Quantum Metrology of the National Physical Laboratory, Teddington, where his work has been concerned with the development of stabilized gas lasers as length standards.

I hereby certify that this thesis has been composed by me, and is a record of work done by me, and has not previously been submitted for a Higher Degree.

This research was carried out at the National Physical Laboratory, Teddington, Middlesex, under the supervision of Dr. W.R.C. Rowley. Mr A. Maitland has acted as my supervisor at the University of St. Andrews.

A.J. Wallard

I certify that A.J. Wallard B.Sc. has spent nine terms of research work at the National Physical Laboratory under my direction.

W.R.C. Rowley, Research Supervisor

I certify that A.J. Wallard B.Sc. has fulfilled the conditions of ordinance No. 16 (St. Andrews) and that he is qualified to submit the accompanying thesis in application for the degree of Doctor of Philosophy.

A. Maitland, Research Supervisor

ABSTRACT

This thesis contains a description of the design and development of a visible helium-neon laser stabilized to an absorption transition in an intracavity cell of iodine vapour. Two methods of frequency locking the laser have been studied, and a series of experiments has been performed in which the stability and reproducibility of the iodine stabilized laser have been investigated.

Chapter 1 discusses the frequency perturbations which might be expected to appear on an unstabilized laser and the steps which may be taken to minimise such perturbations. Three methods of mode selection have been studied in some detail: short lasers, saturated neon absorption and intracavity etalons. These will also be discussed in Chapter 1. The Chapter closes with a discussion of the definition and measurement of frequency stability.

The technological features of laser design are described in Chapter 2 together with some of the more important ancillary apparatus involved in these experiments. The Chapter concludes with a discussion of the servosystem techniques involved in frequency locking a laser.

Chapter 3 discusses theoretical aspects of the work including the nature of saturated absorption, and the width of the expected saturated absorption peaks to which the laser is stabilized; it concludes with an estimate of the laser powers required to achieve saturation.

The operation of the laser is outlined in Chapter 4 which points out the advantages of the third derivative locking technique. A short discussion of laser noise problems is incorporated in this Chapter.

Finally, Chapter 5 presents results obtained in experiments with two stabilized lasers and investigates the effects of saturated absorption linewidth broadening and shifts introduced by the detection system, the iodine pressure, and the laser power. Measurements of the long term stability have been made, and indicate that the laser frequency has a reproducibility better than 1 part in 10^{10} .

The experiments discussed here indicate that a laser stabilized in this way possesses a stability and reproducibility superior to that of the existing length standard. These properties, together with the optical advantages of a laser source, could make this laser an eminently suitable successor to the existing Krypton lamp standard.

ACKNOWLEDGEMENTS

I acknowledge with gratitude the support and encouragement given to me during the past four years by my colleagues at the National Physical Laboratory, and wish to thank Dr. P. Dean, the Superintendent of the Quantum Metrology Division, and the Directorate of the Laboratory for permission to publish this work.

I am particularly grateful to my friends and team-mates, Dr. W.R.C. Rowley, Dr. K.C. Shotton, and Mr P.T. Woods, who have contributed so much to my understanding of laser physics, and Mr. D.C. Wilson who has patiently afforded generous and valuable practical and electronic enlightenment.

Mr. A. Maitland, of the University of St. Andrews, originally aroused my interest in lasers, and his continued enthusiasm and timely encouragement have been a source of great stimulation to me.

Elizabeth Oates has typed this thesis with exceptional patience and great skill. I am extremely grateful for the many hours which she has spent on this task.

Lastly, I thank my wife, Barbara, for her invaluable help. In addition to her general encouragement, she has spent many hours reading through my manuscript and helping me to an awareness of the finer points of English grammar, in return for which I hope that she may have absorbed just a few of the principles of laser physics!

May, 1972.

Chapter 1	INTRODUCTION, DESIGN CONSIDERATIONS, AND FREQUENCY STABILITY	page 1
1.1	Introduction	
1.2	Choice of laser to be studied	
1.3	Factors affecting laser stability	
1.4	Single mode lasers	
1.5	Definitions of Frequency Stability	
1.6	Measurement of Frequency Stability	
Chapter 2	LASER DESIGN AND ANCILLARY APPARATUS	page 24
2.1	Cavity design	
2.2	Laser tube construction	
2.3	Absorption tube construction	
2.4	Cavity length modulators	
2.5	Antivibration Mountings and Temperature Control	
2.6	Optical Spectrum Analysis	
2.7	Beat Frequency Measurement	
2.8	Servosystem design	
Chapter 3	SATURATED ABSORPTION THEORY	page 41
3.1	Introduction	
3.2	The Lamb Dip	
3.3	Saturated Absorption	
3.4	Linewidth of the Saturated absorption features	
3.5	Power required to saturate the iodine absorption	
3.6	Spectroscopy of the iodine molecule	
Chapter 4	INITIAL EXPERIMENTS WITH IODINE AND THE DEVELOPMENT OF THE IODINE STABILIZED LASER	page 53
4.1	Choice of absorbing vapour and laser design	
4.2	Iodine absorption coefficient	
4.3	Iodine absorption coefficient frequency variation measurements	
4.4	Laser parameters in these experiments	
4.5	Laser noise problems	
4.6	Experiments investigating moving striations	
4.7	Observation of saturated iodine peaks	
4.8	Effect of the gain curve on the shape of the component	

- 4.9 Third Derivative locking
- 4.10 Shape of the Saturated absorption features
- 4.11 Third Derivative observation of saturated absorption features

Chapter 5 EXPERIMENTAL RESULTS

page 66

- 5.1 Summary of known data on iodine absorption lines
- 5.2 Effects of the scan width
- 5.3 Power Broadening
- 5.4 Pressure Broadening
- 5.5 Beat frequency measurements for different integration times
- 5.6 Long term stability and Allan Variance Plots
- 5.7 Frequency offsets - beat frequency experiments with lasers locked to the same line
- 5.8 Separation of Hyperfine component centres
- 5.9 Summary and conclusions

APPENDIX I Summary of known absorption coincidences

page 83

REFERENCES

page 84

CHAPTER 1

INTRODUCTION, DESIGN CONSIDERATIONS AND FREQUENCY STABILITY

1.1. Introduction

Since the first gas laser was developed in 1961, there has been a great deal of interest in the problem of developing stable frequency lasers. These devices have many important applications in the fields of communications, metrology and spectroscopy, and the techniques of frequency stabilization have now been advanced to the point when a frequency stabilized laser is a suitable contender for establishment as the primary standard of length.

Since 1960, the standard of length, and the spectroscopic wavelength standard have been defined in terms of the 605.8 nm. radiation from a Krypton 86 discharge lamp operated under specified conditions (1). This standard is reproducible to an accuracy of one part in 10^8 , and has a coherence length of about 80 cms. which limits its use in interferometry. The Krypton lamp also suffers from practical disadvantages: the light emitted is not properly collimated, and is moreover of fairly low power - of the order of 10 microwatts. This necessitates carefully designed interferometers and sensitive detector systems.

The laser presents a solution to many of these problems. The spatial and temporal coherence properties allow the formation of well defined interference fringes over distances of more than 200 metres; the high power directional beam makes the design of interferometers more simple and permits the use of photoelectric detectors. However, although the laser possesses a very high spectral purity, its optical frequency may drift over a range of a few parts in 10^6 for visible lasers, and its potential may only be realised if its frequency is stabilized. Without any form of stabilization, the frequency of these lasers may drift with time over the entire frequency range for which laser gain is possible, giving an uncertainty of ± 1 part in 10^6 . This variation is caused by changes in the optical length of the laser due to vibration, thermal expansion and refractive index changes. However, frequency control of the laser using an electronic servocontrol mechanism is a well established technique which enables high stabilities to be obtained. The technique involves modulating the laser frequency and then performing phase sensitive detection on the resulting amplitude modulation of the light output. An error signal proportional to the deviation of the laser frequency from some reference frequency is fed back to retune the laser frequency to this reference.

Early stabilization schemes referred the laser frequency to features of the atomic linewidth, such as the peak of the gain profile (2) or to external interferometers (3). Perhaps the most widely applied method has entailed the use of the centre of the Lamb Dip (4) as a reference frequency. This dip occurs in the centre of the power output curve as the laser frequency is tuned over the range of frequencies available. Usually this dip is some 5-10% of the total laser output power and may be up to 200 MHz wide. A limitation of this method lies in the breadth of the Lamb Dip and its flatness near the centre. An ideal frequency reference should be narrow and well defined to provide a sharp discriminant shape from which error signals may be derived to control the laser.

Using this stabilization method, Lamb Dip stabilized lasers achieve frequency stabilities of a few parts in 10^8 over several minutes. However, lasers stabilized in this way are subject to a slow frequency shift of the centre of the Lamb Dip since, due to diffusion of the gases out of the tube, the pressure inside the tube varies. The resultant changing pressure shift limits the long term stability to 1 part in 10^7 (5). This pressure shift is a feature common to all stabilization schemes where the reference frequency is derived from features of the spectral line involved in the lasing transition. The effect is less severe in tubes containing neon alone as this diffuses much less rapidly than helium (6). This has led to the use for stabilization of intra cavity low pressure neon discharge tubes, and reference frequencies stable to 1 part in 10^9 (7, 8) have been achieved by this means.

Recently considerable improvements in stability have been obtained by using absorption lines in the spectrum of a molecular gas to provide the reference frequencies. A significant advantage is that this absorption takes place from the ground state of the molecule so that perturbing discharge effects are entirely eliminated. This technique, known as stabilization by saturated absorption, involves placing inside the laser cavity a tube containing a low pressure gas which has an absorption line falling within the gain bandwidth of the laser. The strong, standing-wave electric field inside the laser cavity gives rise to a saturation of the absorption, and a Lorentzian shaped dip forms at the centre of the absorption line. This dip produces a corresponding increase in laser power output as the laser frequency is tuned through it. As with the Lamb Dip in emission, this dip has a width which is determined not by the large Doppler broadening effect but by the small natural width of the levels involved in the transition.

However, the molecular lifetimes involved are much longer than those of the neon laser level lifetimes, and this leads to a much smaller natural width. Moreover, pressure broadening of the saturated absorption dip may be made small, since low pressure absorbing gases are used. This is made possible since lasers are very sensitive to the small changes in the cavity gain and loss parameters which occur in the region of the saturated absorption features. When the laser is stabilized to the centre of the dip in absorption, stabilities better than 1 part in 10^{10} may be expected with the use of suitable molecular lines. The most suitable molecules are those with symmetry giving small dipole moments and thereby ensuring insensitivity to Stark shifts and also Zeeman shifts.

The experiments to be described in this thesis involve the stabilization of a helium-neon laser to saturated absorption transitions in iodine vapour. Reference will be made, from time to time, to methane stabilized helium-neon lasers operating at $3.39\mu\text{m}$. This latter laser system is also a contender for establishment as a future length standard, largely due to American work. It is part of the function of the Gas Laser Section at N.P.L. to evaluate the performance of this device, and lasers of this type have been constructed and investigated during the period covered by this thesis.

The work forms part of the research programme of the Quantum Metrology division of the National Physical Laboratory, and is concerned with progress towards a new definition of the Metre, using a laser wavelength standard.

1.2. Choice of a laser to be studied

The obvious choice for study was the visible 633 nm. He - Ne laser line. The other possible choices were the infra red $3.39\mu\text{m}$. He - Ne line, the ionised argon laser and the carbon dioxide laser. Typical properties of these lasers are summarised in table 1.1. A laser suitable for a length or wavelength standard should possess certain characteristics. The discharge should be smooth, easy to maintain and not require high voltages or currents which would necessitate complicated smoothing techniques. These features lead to a stable output power and minimise possible Stark shifts and refractive index variations due to large varying electric fields in the plasma. Furthermore, the laser should be easily constructed and not dissipate power to any extent which would require cooling. This leads to easy design and the construction of reasonably stable cavities. The laser frequency is particularly susceptible to thermal length changes and so the absence of any heat source is a considerable practical advantage. Sealed off lasers are not subject to pumping pressure changes and the associated vibrations from pumping apparatus. The gain and output power may be kept fairly low as output powers in the 50 microwatt region are quite adequate for interferometry and standards work.

TYPICAL PARAMETERS OF POSSIBLE LASERS

	He-Ne	He-Ne	CO ₂	Ar ⁺
Wavelength	633 nm	3.39 μm	10.6 μm	488 nm/514 nm
Frequency (Hz)	5×10^{14}	1×10^{14}	3×10^{13}	7×10^{14}
Gain bandwidth (MHz)	1200	240	36	2000
Gain (%/metre)	small (2%)	medium	high (30%)	high (20%)
Typical Power	50 μW-10 mW	several mW	several watts	several watts
Discharge Parameters				
current	4-15 mA	4-15 mA	30 mA	few amps
pressure	1-2 torr	1-2 torr	20 torr	1 torr
Discharge characteristics	Smooth	Smooth	High voltages. Needs careful current stability	Very noisy
Convenience	Small	Small. Materials problems.	Water cooling. Materials problems.	Water cooling. High power input. Bulky.

Although there can be no logical objection to an infra-red length standard, there are considerable and obvious advantages in maintaining a visible standard of length. Conventional interferometry is easily modified to accommodate laser sources and high sensitivity, fast detectors are available. Infra red work, however, is beset with problems: good quality optical materials are scarce and detectors are, in general, slow and insensitive. These difficulties are slowly being overcome, and the liquid nitrogen cooled CdHgTe and PbSnTe detectors have response times and output impedances of 1μ sec. and 50Ω and 10μ sec. and a few ohms respectively for 10μ m. radiations.

A synthesis of the above facts led to the choice of the 633 nm. He - Ne system as the primary object of study. As a result of some American work on the methane absorption bands around 3.4μ m the 3.39μ m line was also considered and lasers of this type have been constructed. At the time that these problems were being considered (1967) results were published by Lee and Skolnick (9) on saturated absorption experiments with neon for the visible transition. This phenomenon has been exploited in schemes for single mode lasers which are discussed in section 4 of this Chapter.

1.3. Factors affecting laser stability

A free running or unstabilized laser is subject to many perturbations of its optical length. The following discussion considers their nature and magnitude.

If we consider a laser operating in TEM_{00q} mode, (off axis modes have been eliminated by a careful choice of mirror radii and tube bore diameter) the cavity resonant frequencies ν_q are given by

$$\nu_q = q \frac{c}{2nL} \quad (1.1)$$

here q is the order of the mode and is an integer, about 10^6 , c is the velocity of light, n is the refractive index of the medium between the laser mirrors, and L is the cavity length.

The number of modes which contribute to the multimode power output of the laser depends on the gain of the medium and the axial mode separation, $c/2nL$. We see from equation 1.1. that changes in cavity length affect the frequency of an oscillating mode:

$$\frac{d\nu}{dL} = - \frac{mc}{2L^2 n} \quad \text{or} \quad \frac{d\nu}{\nu} = - \frac{dL}{L} \quad (1.2)$$

Any changes in cavity length must be minimised if the laser frequency is to remain stable, and this maintenance of constant cavity length is the prime

objective in frequency stabilization schemes. There are various possible perturbations on the cavity length and these will be listed and discussed under two groups; those perturbations which arise from external phenomena, and those which arise from effects internal to the plasma tube.

1.3.1. External effects

i) Thermal

Variations occur in the temperature of the spacer material between the end plates of the cavity which carry the mirrors. This leads to a fractional change $\Delta L/L$ in the mirror separation which is given by $\alpha \Delta T$ where α is the coefficient of expansion of the spacer bars, and ΔT the temperature rise. Materials with a low value of α , such as invar and fused quartz, are therefore used. Typical α values for these materials may be found in Table 1. Various ceramic glasses have been developed, such as Cer-Vit (Owens-Illinois Ltd) and Zero-dur (Zeiss-Jena) which have even smaller coefficients of expansion. Some ceramic samples have been produced which have negative α values over certain temperature ranges near room temperature. These are not yet totally reliable from sample to sample, as their mechanical properties depend critically on the composition of the ceramic and its treatment during manufacture. Even with low expansion materials thermal tunings of the cavity of 500 MHz per degree Centigrade are typical. These effects are generally slow and occur over several minutes. For a frequency stability of 5 MHz, the cavity temperature must be constant to 0.01°C . These temperature instabilities increase with longer lasers since it is difficult to maintain a constant temperature over the whole laser. Obviously lasers with high power inputs and a large heat dissipation would be severely affected by this problem.

ii) Atmospheric variations

Lasers of the external mirror type have a fraction x of the cavity length open to the air. Changes in atmospheric conditions will alter the refractive index of the air and therefore shift the cavity resonant frequency under the laser gain curve. The factors affecting the refractive index are temperature rise (ΔT), pressure changes (Δp) and humidity changes (Δh) and we may represent the effects on the average laser frequency, ν , by:

$$\left(\frac{\Delta\nu}{\nu}\right)_T = x \beta_T \Delta T \quad \text{where } \beta_T = +9.3 \times 10^{-7}/^\circ\text{C} \quad (1.3.a)$$

$$\left(\frac{\Delta\nu}{\nu}\right)_p = x \beta_p \Delta p \quad \text{where } \beta_p = -3.6 \times 10^{-7}/\text{torr} \quad (1.3.b)$$

$$\left(\frac{\Delta\nu}{\nu}\right)_h = x \beta_h \Delta h \quad \text{where } \beta_h = +5.7 \times 10^{-8}/\text{torr} \quad (1.3.c)$$

These coefficients have been calculated for a mean temperature, pressure and humidity of 20°C , 760 torr and 8.5 torr of water vapour (1 torr = 133.3 N/m^2).

	α (per°C)	γ (N/m ²)	ρ (g/cc)	$\frac{\gamma}{\rho}$ (arby.)
INVAR	1.26×10^{-6}	1.44×10^{11}	8.0	18
FUSED QUARTZ	5.5×10^{-6}	3.03×10^{10}	2.0	1.52
CERVIT	$0 \pm 15 \times 10^{-7}$	9.23×10^{10}	2.3	4.0
ZERODUR.	5×10^{-8}	8×10^{10}	2.52	3.17

TABLE 1.2
CAVITY SPACER BAR MATERIALS

To provide an estimate of the magnitude of these shifts, let us assume a cavity for which $x = 0.1$ (10% is open). We find that $(\frac{\Delta\nu}{\nu})_T = 1 \times 10^{-7}$ for a 1°C rise, $(\frac{\Delta\nu}{\nu})_p = -4 \times 10^{-7}$ for a 10 torr change and $(\frac{\Delta\nu}{\nu})_h = 6 \times 10^{-9}$ for a 1 torr change. These atmospheric changes are larger than one would expect in a well controlled laboratory environment (except for pressure changes) and, in general, lasers are designed to minimise the amount of free space in a cavity. Internal mirror lasers do not, of course, suffer from this type of effect, although pressure changes can constrict a non-rigid structure and temperature changes have the effects discussed in the previous section. Air turbulence, caused by draughts in an external mirror laser, can cause fast frequency fluctuations over several MHz in a few seconds, and such lasers must be well shielded from draughts.

iii) Mechanical Vibrations

To maintain a frequency stability of $\frac{\Delta\nu}{\nu} = 1 \times 10^{-8}$ the length of a 100 cm. long cavity must be maintained constant to 10^{-6} cm. or 100 Å. This magnitude of disturbance is easily produced by mechanical movements transmitted through the working surfaces, or airborne disturbances from temperature control or air conditioning systems.

At the N.P.L. we have counteracted ground-borne vibrations by the use of heavy steel tables supported with damped and sprung vibration isolation systems constructed on to deep concrete foundations. Alternative methods use inflated car inner tubes sandwiched between rigid bench tops and a steel working surface. This simple method of isolation is extremely effective: high frequency vibrations are virtually eliminated, although those of a lower frequency may be present due to resonances of the support system. In the steel table method, resonant frequencies of a few Hertz are readily achieved. At these low frequencies, one expects the laser to be sufficiently rigid so that the complete system moves slowly up and down over a small amplitude at low frequencies. Acoustically borne vibrations are reduced by shielding the laser with some form of enclosure. These vibrations, emanating from nearby equipment or environmental control systems are often sufficient to cause substantial amplitude and frequency variations of up to several per cent and several parts in 10^7 respectively. Some workers have gone to extreme care to isolate their lasers from vibrations. Jaseja et al. (10), in measuring the spectral purity of a $1.15 \mu\text{m}$ He - Ne laser, required the degree of isolation provided by huge shock proof tables in the cellar of an isolated building. Equipment was operated in a separate room from the lasers, and a frequency drift of 10 Hz per second (a stability of about 1 in 10^{13}) was obtained under the optimum conditions which included the quiet wind conditions outside!

There are two differing approaches to the problem of vibrational stability. One uses very heavy equipment, for example steel endplates to a laser with large diameter invar bars, to give good rigidity and low thermal expansion. The other approach attempts to make the whole structure as light as possible, in the belief that all disturbances in the frequency range of interest impinging upon one end of a laser would immediately be transmitted to the other. The entire laser cavity then moves in unison, thereby keeping the mirror separation constant. Such cavities are frequently fabricated entirely with light quartz spacer rods and aluminium end plates or a solid quartz block with a capillary drilled down the centre. (11, 12, 13). The approach can be useful for short internal mirror lasers where the mirrors are sealed on to the ends of the quartz block. The disadvantages are that there is no means of mirror alignment, the long cavities are mechanically weak, and frequency tuning must be by thermal means.

The lowest limit on mechanical vibrational stability is that of variations in the resonator length from excitation of the fundamental stretching frequency of the spacer bars. We represent this by

$$-\frac{\Delta\nu}{\nu} = \frac{\Delta L}{L} = \left(\frac{2kT}{YV} \right)^{\frac{1}{2}} \quad (1.4)$$

where k is Boltzman's constant, T is the temperature, V is the spacer volume, and Y is Young's Modulus for the spacer bars. From this, we see that spacer bars of large volume and with a large value of Young's Modulus minimise $\Delta\nu/\nu$. For a given length of laser, the volume requirement is reduced to that of large diameter bars. Typical values for Young's Modulus may be found in table 1.2., together with density values (ρ). The ratio $\frac{Y}{\rho}$ should be made as high as possible since the resonant frequency is proportional to $\left(\frac{Y}{\rho} \right)^{\frac{1}{2}}$ and this must be far away from easily coupled low frequencies. Hence, for a mechanically rigid design, a high Young's Modulus and a low density are required, and for typical values we find $\frac{\Delta\nu}{\nu}$ to be of the order of 10^{-14} . This is claimed to be a realistic practical limit to the attainable frequency stability.

iv) Variations in the position of optical components

External mirror lasers suffer from the variations in optical path length arising from movement of the plasma tube or other intra-cavity components. In passing through a Brewster Angle window of thickness t and refractive index n , the light travels a path $p = \frac{tn}{\cos r}$ where r is the angle of refraction. At the Brewster Angle, i_B we have that $i_B = \pi/2 - r$, and also $\tan i_B = n$. So we may write, for a variation Δp in the window position:

$$\frac{\Delta p}{\Delta i_B} = \frac{-t}{\sin i_B} \quad (5)$$

The frequency variation caused by this is:

$$\frac{\Delta\nu}{\nu} = \frac{\Delta p}{\rho L} = \frac{-t}{L \sin i_B} \quad (6)$$

where μ is the mean refractive index of the medium between the laser mirrors, and is nominally unity. L is the laser length. We may calculate $\Delta\nu$ for a 2 mm thick window, a length L of 100 cm. and a 1 microradian change in i_B which is 57° for red light in fused quartz. This results in a frequency instability of 3 parts in 10^8 , and indicates the necessity to support any intracavity element rigidly.

v) Magnetic fields

If invar bars are used as spacer bars, then there is the possibility of cavity length changes due to the magnetostrictive properties of invar. Jaseja et al. (10) have found that shifts of 140 KHz may be found in $1.15 \mu m$ lasers due to effects of the earth's field alone. Stray magnetic fields from local electronic apparatus may have an effect which must be considered in highly stable lasers or those stabilised by magnetic effects. Magnetic fields also have an effect on the spectral linewidth. This results in the splitting of the gain curve by the field into two Zeeman shifted curves of opposite circular polarisation. This splitting is symmetric about the unshifted line centre and, for the 633 nm. line, is of the order of 2 MHz. for a field of one gauss. (14, 15).

1.3.2. Internal effects

i) Discharge noise

In general, gas discharges are not well understood, and comparatively little is known about discharge mechanisms and the effect of different discharge parameters. Bunching or local variations in the electron density N_e , have an effect on the refractive index as given by

$$n = 1 - \frac{N_e e^2}{2 \pi m \nu^2} \quad (1.6)$$

where e and m are the electronic charge and mass. Typically N_e is of the order of 10^{12} electrons/cm³ and changes of 1% lead to a frequency instability of about 2×10^{-12} , Hence electron density variations are not usually significant unless the discharge is particularly noisy.

Fluctuations in the upper laser level population may be caused by variations in discharge current from instabilities or plasma oscillations. This leads to a white noise spectrum on the laser power output although oscillations of the power supply-ballast resistor plasma circuit of a D.C. excited laser frequently lead to intensity variations in the kilohertz region. In the low frequency (10 Hz. - 1 MHz.) region, individual tubes vary depending

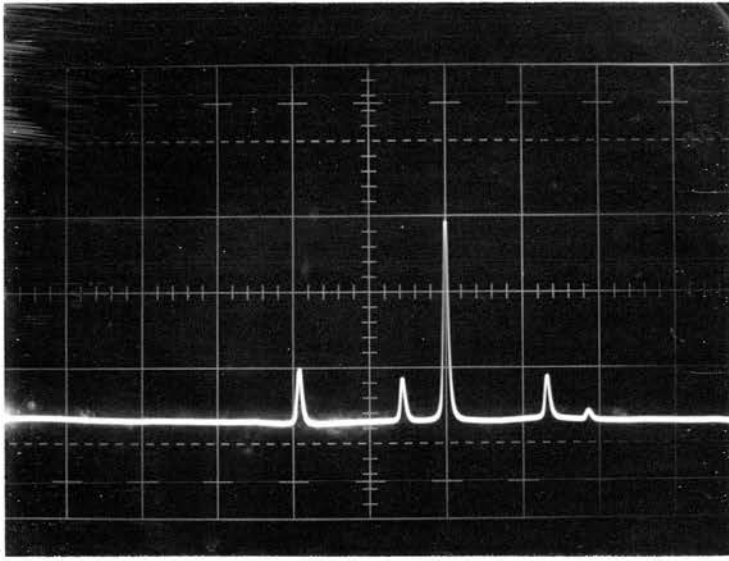
on their processing procedure and geometry, but the appearance of strong peaks in the audio frequency discharge spectrum is a common phenomenon. These peaks are associated with moving striations in the discharge, and the nature of the spectrum depends critically on the discharge current (16). Small variations in tube filling pressure can cause considerable differences in the smoothness of the discharge. The use of either R.F. or a mixture of R.F. and D.C. excitation often leads to a quieter discharge than D.C. excitation alone. (17).

In multimode lasers, competition for the available gain may exist between the various modes, and this leads to modulation on the laser output. Figure 1.3. shows the noise levels observed on the output power of a 633 nm. He - Ne laser for a multimode output and a TEM_{00q} mode output. The optical spectrum analysis showed violent variations of the power contained in a particular mode in the multimode case, and the effect is clearly visible in the noise photographs. The noise was observed on an oscilloscope monitoring a silicon photodiode signal of the laser output.

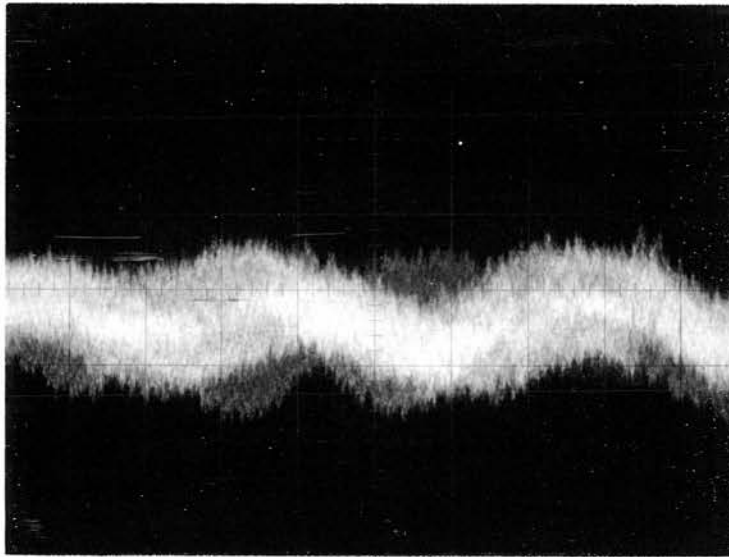
ii) Shifts with gas pressure

Many stabilized lasers have used the centre frequency of the neon spectral line as a frequency reference, for example, Lamb Dip stabilized lasers. However, this frequency is itself subject to a variation with gas pressure and is the cause of the long term drift in the wavelength of a laser during its lifetime as the helium, in particular, diffuses out of the plasma tube (6, 18)

The subject of pressure broadening, shift, and asymmetry is both complex and extensive and involves the interactions of colliding atoms and the effects of the various interatomic fields during the close atomic proximity during an interaction. Basically, an atom emitting a photon 'collides' with another, the 'collisions' being of two distinct types: a hard collision is thought of as an interaction which produces a termination of photon emission from the first emitting atom. This may be represented by an increase δ_{coll} in the total decay rate from the natural rate δ . This leads to a broadening of the Lorentzian shaped linewidth the full width of which at half maximum intensity is $\Gamma = \delta + \delta_{coll}$. This broadening is not, in general, sufficient to explain the shifts and broadening experienced in practice, and the effects of 'soft' collisions are now considered. It is usual to illustrate this additional contribution by considering the Frank-Condon potential curves in Figure 1.4. If, during the period while an atom is emitting a photon, a second atom approaches closely, then the emitting atom comes under the influence of the electric field of the perturbing second atom.

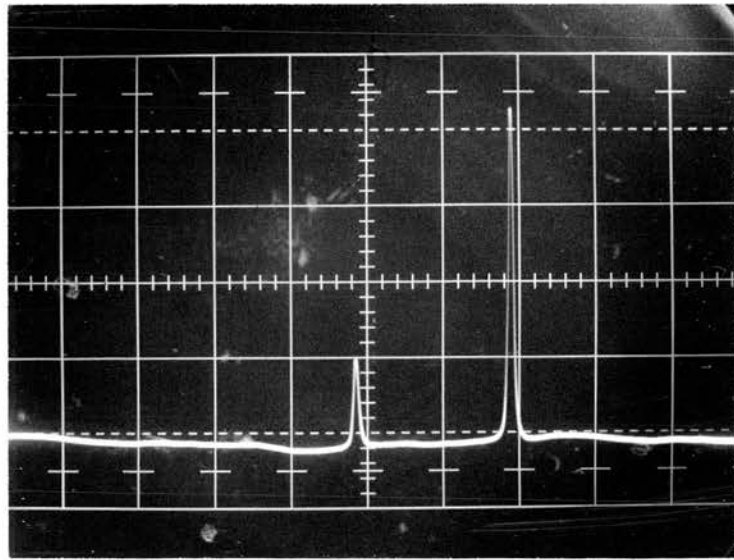


MULTIMODE OPTICAL SPECTRUM.

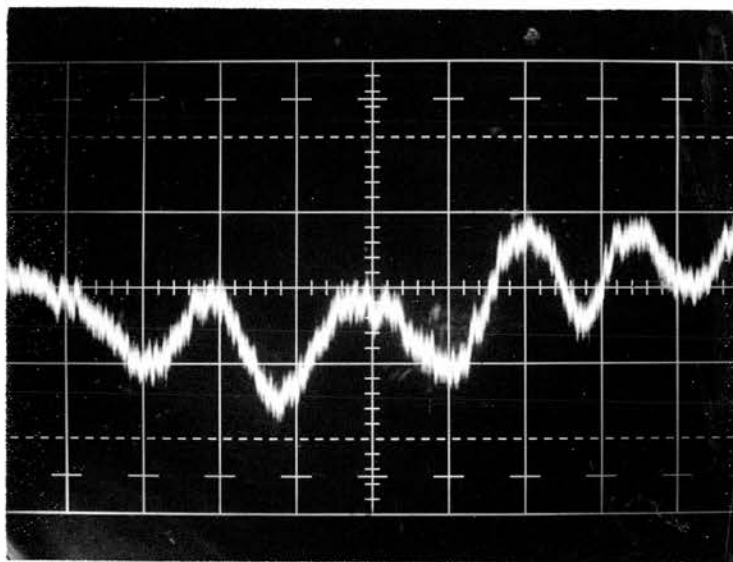


POWER OUTPUT NOISE.
(0.4 mV/cm : 80 mV total power)

FIGURE 1.3
MODE NOISE ON THE LASER OUTPUT.



TEM_{00q} MODE OPTICAL SPECTRUM.



POWER OUTPUT NOISE.
(0.2 mV/cm: 80 mV total power.)

FIGURE 1.3 continued.

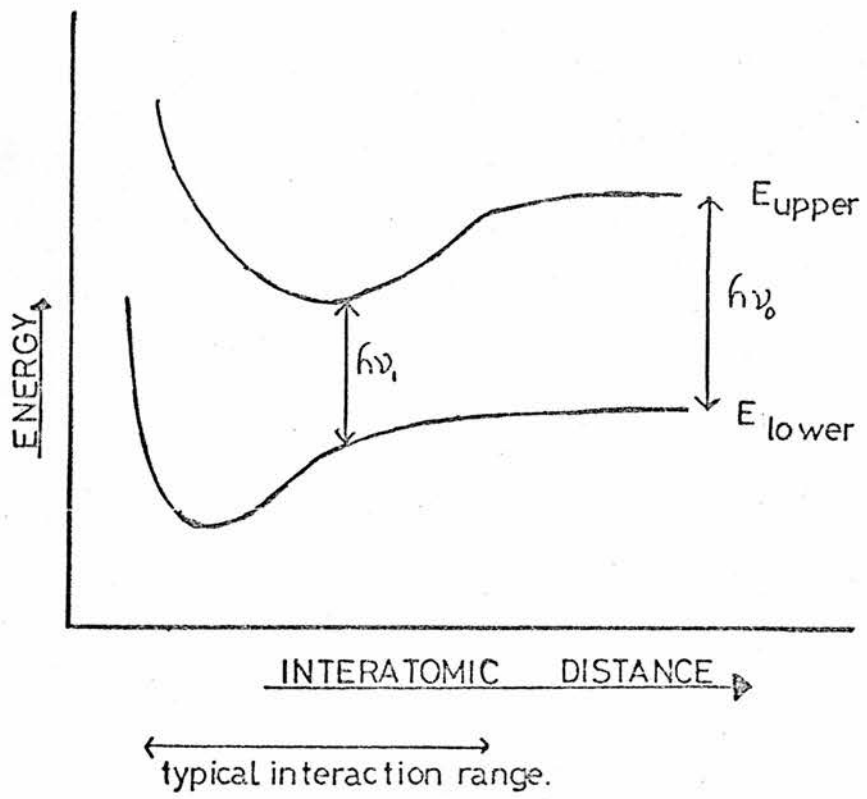


FIGURE 14

POTENTIAL ENERGY CURVES FOR LASER LEVELS.

This leads to an energy shift in the energy levels of the emitting atom during the emission of the photon. Because of the shape of the typical atomic energy level curves shown in the figure, their separation is not constant throughout the interaction and varies with interatomic distance. The instantaneous photon frequency therefore also varies during the emission time and Figure 1.4. indicates the unperturbed energy levels with a spacing h_0 when the perturber is far away, and a typical smaller energy gap h during the interaction. The resulting spectral distribution is both broadened, and shifted, and possesses asymmetry.

These naive pictures of the effects of atomic collisions indicate that the observed spectral widths will be dependent on the number of interactions and thereby on perturber density or pressure. As mentioned previously, the laser gases diffuse out of a laser tube during its life. The diffusion rate of helium is larger than that of neon through both quartz and pyrex tubes and it is this partial pressure variation which is particularly serious. It has been found by various workers (19, 20) that the main source of the observed shift of the centre of the neon line in the 633 nm laser is due to collisions between excited neon atoms and ground state helium atoms. The shift is to higher frequency and increases at the rate of 20 MHz per torr.

iii) Stark effect

The D.C. discharge inside the plasma tube induces an ambipolar flow of charged particles which, because of the differing electron and ion mobilities sets up a radial ambipolar electric field. It is this field which results in a second order Stark Effect broadening and shift of the neon energy levels involved in the laser transition. Meyer (22) calculates that the frequency shift of the upper $3s_2$ neon laser level (shifts in the lower $2p_4$ level are neglected) to be:

$$\Delta \nu \approx -2.8 \times 10^6 \left(\frac{T_e}{R} \right)^2 \eta \text{ Hz.} \quad (1.7)$$

T_e is the electron temperature in tens of eV., R the discharge tube radius (mm.),

$$\text{and } \eta = \left\{ \frac{J_1 \left(\frac{2.4r}{R} \right)}{J_0 \left(\frac{2.4r}{R} \right)} \right\}^2 \quad (1.8)$$

the J 's are Bessel functions and r and R are the radial distance from the centre and the tube radius. Meyer goes on to assume that the electron temperature T_e is proportional to the gas pressure p , $T_e = \left(\frac{P_0}{p} \right)^{\frac{1}{2}}$ where $P_0 = 2.88$ torr, and calculates the frequency shift with pressure due to this electron temperature change. He finds $\Delta\nu \sim -2.8 \times 10^6 \left(\frac{2.88}{p} \right) \eta$ where $\Delta\nu$ is the frequency shift of the line centre from a field free situation. The function η varies from very small values (0.1) at the centre to values nearing 100 at the walls. However, in view of the assumptions made, the shifts expected in an intermediate region are of the order of several MHz, for tube bores of a few mm. Meyer shows that in comparing the measured pressure shifts of the 633 nm and the 1.15 μ m lines that their ratio agrees closely with that predicted by this theory. However, the line shift is measured to be directly proportional to pressure, whereas the theory indicates an inverse proportionality. This may be resolved, however, by better measurements of electron temperatures.

It is not completely clear yet as to the real mechanism of the observed shifts. White (23) suggests that certain aspects of pressure broadening and second order Stark Effect may be treated in the same way. More experiments need to be performed to give accurate measurements of the various relationships involved in this complex subject.

iv) Effect of neighbouring spectral lines

The frequency ν_0 of a laser mode is influenced by the value of the refractive index of the lasing medium. This varies over the spectral line with the well known dispersion shape. However there are also contributions at ν_0 from the tail of the dispersion curve of neighbouring spectral lines. It is to variations in this contribution, arising from discharge current variations, that Arrathoon and Siegman (24) attributed an observed frequency shift. They observed a shift to higher frequencies of 2.5 to 0.5 MHz/mA. with current over a range from 3 mA. to 8 mA. in a Spectra Physics 119 laser and also predicted the observed decreasing shift with increasing mean current. They argued that the varying contribution to the refractive index arose from the nearby 633.4 nm. and 640.2 nm. absorptive transitions from the neon $1s_5$ metastable level to levels in the 2p group. A current shift was also observed by White (19) in a Ne^{20} cell, however this was to lower frequencies and varied with pressure.

1.4. Single Mode Lasers

If a laser is to be a suitable length standard, it is essential that only one frequency be emitted, in other words that the laser operates in a single mode. Off axis modes of the laser cavity may be eliminated by a careful choice of mirror curvatures, and gain tube bore diameter. Longitudinal modes, however, pose a more difficult problem.

In the visible helium-neon laser, the gain bandwidth is inhomogeneously broadened and has a Doppler full width, at half maximum, of about 1200 MHz. The infra red $3.39 \mu\text{m}$. line is also inhomogeneously broadened but has a Doppler width of about 300 MHz. full width at half maximum (F.W.H.M.) The collisionally broadened natural width is about 100 MHz. F.W.H.M. at the pressures used of 1-2 torr.

Since the longitudinal mode spacing of the cavity is given by $C/2L$ (where C is the velocity of light and L the cavity length) single mode visible lasers must have lengths of less than 15 cms., while infra red lasers may be up to 50 cms. long. In practice, the $3.39 \mu\text{m}$. lasers were constructed about 50 cms. long to enable commercially available 30 cm. tubes to be used with 10 cm. long absorption cells thereby ensuring little empty space in the cavity.

As the gain of the 633 nm. laser is small (5% per metre) only small losses are needed to stop the laser oscillating. The laser must be made as long as possible to give sufficient intracavity power to saturate the iodine absorption (about 30% per metre) and yet remain in a single mode - at least when oscillating at frequencies corresponding to the saturated absorption peaks on the power output curve.

If the visible laser were made longer than 15 cm., there would be a welcome increase in power, but an unwelcome increase in the number of longitudinal modes oscillating. However the presence of an intracavity iodine vapour cell with a measured absorption coefficient of a few per cent at room temperature would reduce the gain/loss ratio. This would permit the use of longer cavities and still enable the laser to oscillate in a single mode.

It was decided to construct the visible laser with a mirror spacing of approximately 30 cm. which was filled with a 10 cm. absorption tube and a 17 cm. long gain tube. The dead space was occupied by the inside of the piezo-electric tube used to control the laser length (Section 2.4). This scheme seemed to be the simplest to construct, but, because there seemed to be so many unknowns at first (e.g. absorption coefficient of iodine and the optimum relative lengths and dimensions of the gain and absorption cells), some attention was given to alternative methods employing mode selection for the visible laser.

The experiments, or reasons for their rejection, are outlined in the following paragraphs.

1.4.1. Fox Smith or Three mirror cavity (25,26)

This well known mode selecting technique would have the attractive property of a high power single mode which could be tuned over the entire laser gain profile. It would, however, necessitate the use of a servo-loop to maintain the long cavity laser mode at the centre of the more stable short cavity resonance.

As the final iodine stabilized laser would itself have a servo-loop to stabilize the laser frequency, this second Fox-Smith servo-loop was considered undesirable and the scheme was rejected for this reason and on the grounds of simplicity and compactness.

1.4.2. Modulator Technique

The internal-external modulator technique of Harris and McDuff (27) was another possibility which gave a high power single frequency, since it could also be applied to long lasers. This was rejected again on the grounds of simplicity but also because of the difficulty of driving the two modulators in the required phase relationship.

1.4.3. Mode Selection by Saturated Absorption in Neon

This technique has been used by several workers (7, 8, 9) to provide high power single frequency lasers. A tube containing neon, in which a discharge is run, is also placed inside the laser cavity. The neon is at a lower pressure than the helium and neon inside the gain tube. The neon atoms in the second tube are excited to the lower laser level and so may absorb the 633 nm. laser radiation from the gain tube. If a similar gas temperature is assumed for neon atoms in both discharge tubes then the inhomogeneously broadened neon linewidths are also similar. The absorbing neon atoms therefore exhibit absorption over the entire neon gain curve. However, since the neon absorbing cell is operated at a lower pressure than the gain cell, the homogeneous pressure-broadened component of the absorbing neon linewidth is much smaller than for neon in the gain cell. The intracavity electric field strength is high, and so a deep narrow Lamb Dip forms at the centre of the absorption linewidth as a laser mode is tuned to its centre. The width of this Lamb Dip in absorption is of the order of the homogeneous width which, we have already remarked, is narrow in the absorption tube. This situation may be represented by the gain and absorption curves of Figure 1.5. If the saturated absorption of the neon cell is greater than the laser gain for all frequencies except those near the centre of the absorption curve, then the laser may only begin to oscillate when a cavity mode is tuned to ν' .

The neon homogeneous linewidth is about 40 MHz. F.W.H.M. for typical

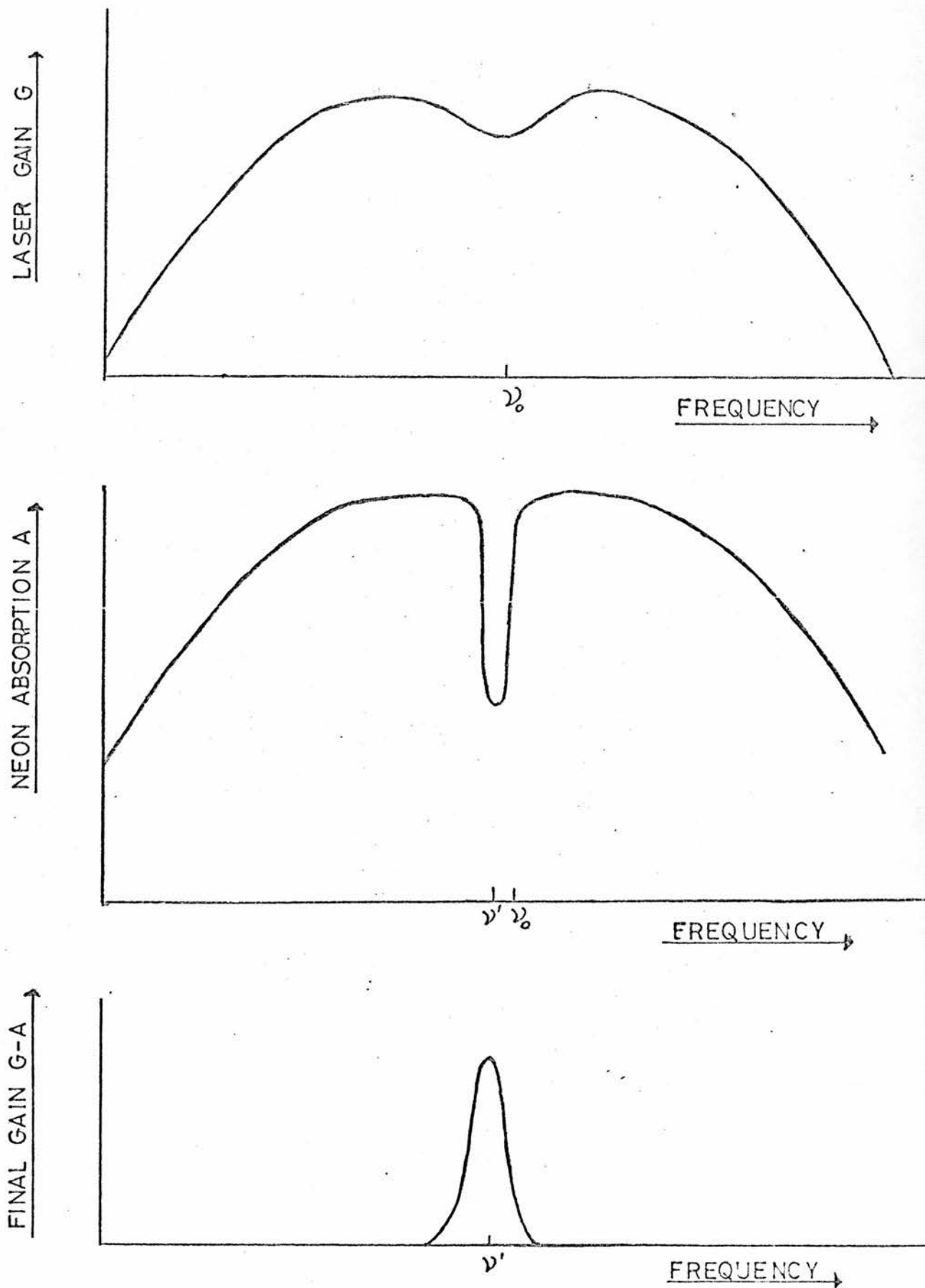


FIGURE 1.5
SATURATED ABSORPTION IN NEON

neon pressures of 0.3 torr. A laser 380 cm. long having a mode spacing of 40 MHz. will therefore oscillate in only a single mode at ν' . The gain for all other modes is exceeded by the losses; only for ± 20 MHz around will the gain exceed the losses, as shown in the Figure where $(G - A)$ is plotted against frequency. In this condition, however, where all modes except one have been suppressed, some of the atoms potentially supplying gain for these suppressed modes become available to the single oscillating mode. As with the Lamb Dip in emission, only zero longitudinal velocity atoms provide gain at the Dip. The frequent velocity changing collisions in the higher pressure gain tube transfer excited neon atoms from one velocity group to this zero velocity group. Therefore, atoms with velocities far away from the zero velocity group contributing to gain at ν' may change their velocity and fall near zero longitudinal velocity. Because of the large homogeneous width in the gain cell, some 70% - 80% of multimode power becomes available to the single oscillating mode. When this condition has been established, the oscillating mode may be tuned in frequency. Once the dynamic situation of a single frequency is achieved, the hole burned in the absorption curve at its centre may be tuned over the absorption linewidth. Single frequency operation is still maintained, even though other modes may possess potentially more unsaturated gain than the oscillating mode. The shape of the resultant power output curve depends on the shape of the neon absorption curve and the gain curve shape. Different neon isotopes or isotope mixtures have considerable effects on this shape.

Originally, this curve shape changing property was to be employed in a laser stabilized by passive absorption in iodine. As will be discussed in Chapter 4, a sloping gain curve shape produces an error in the iodine reference frequency. A suitable intracavity neon cell would have been useful for flattening the gain curve background in the vicinity of the iodine reference frequency. However, a more suitable, simple method of eliminating the background slope has been developed (Third Derivative Locking - Chapter 4) which obviates the need for such a development.

As this new technique was discovered some time after the experiments described in this thesis were initiated, some considerable work was devoted to the development of intracavity neon cells. Many practical difficulties were discovered in this work which made neon cells progressively less attractive propositions and the reasons contributing to its abandonment will be briefly outlined.

1) The technique involved insertion of an active discharge cell inside the laser cavity. In the experiments conducted, the laser cavity was some

80 cm. long, the gain tube was 30 cm. long and a similar length neon absorption tube was used. Cold cathode neon tubes were constructed and filled as described in Chapter 2. The requirements of cleanliness and careful construction of laser tubes were not always achieved in these early stages of technological development. The resulting tubes frequently reduced the laser power by 50% for an insertion loss alone and by some 75% when low current discharges were run. This resulted in lasers with output powers of only a few hundred microwatts. These excessive power losses were due to poor construction and Brewster window contamination by the neon discharge.

ii) Neon discharges tended to be extremely noisy and attempts with R.F. and microwave power smoothing were unsuccessful. The noise could approach 5% peak to peak of the total laser power and would have been extremely detrimental in the eventual saturated iodine absorption application.

iii) At the stage when the work was abandoned in favour of third derivative locking in short lasers, a successful single mode laser with 0.5 milliwatts output power was operated with a tunable frequency range of about 300 MHz. 70% conversion from multimode to single mode power was obtained with a neon cell filled to 0.3 torr. The laser noise was 2% peak to peak white noise over the 1 KHz. to 10 MHz. range.

1.4.4. Intracavity Tilted Etalons

The intracavity etalons technique had been developed particularly by Hercher (28) and its seeming simplicity, and likelihood of high power single frequency made it an attractive proposal. Some experiments were carried out with fused quartz etalons. This technique has been known for some years and has been particularly successful in high gain lasers such as the argon system. A summary of the technique will be given, and some experimental results discussed below.

The Fabry Perot etalon is here used as a frequency selective device. In this case it consists of a solid block of fused quartz, the ends of which are ground optically flat and parallel, to within $\frac{\lambda}{10}$.

If light of wavelength λ is incident on the etalon surface at an angle θ to the normal (Figure 1.6), then the transmitted light will be a maximum when

$$2nt \cos \theta = m\lambda \quad (1.9)$$

where n is the refractive index of the etalon material and m is an integer. This means that the optical length of the etalon is a whole number of half wavelengths of the incident light. As the tilt of the etalon is varied, the resonant wavelength varies in accordance with the expression given above (1.9).

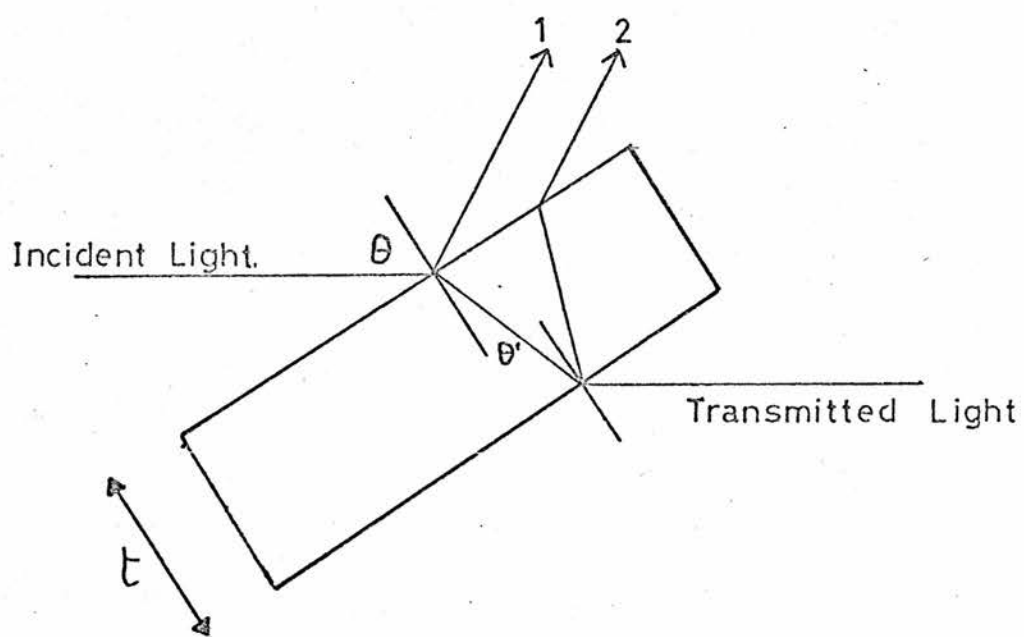


FIGURE 1.6
INTRACAVITY TILTED ETALON

It is easy to show that the shift in frequency $\Delta\nu$ of the resonance maximum with tilt Θ , is given by

$$\Delta\nu = \Theta^2 / 2 t^2 \quad (1.10)$$

A graph illustrating this is shown in Figure 1.7. for light of frequency 4.74×10^{14} Hz. (633 nm.) and an etalon length of 1 cm. By altering the orientation of such an etalon placed inside a laser cavity, it is possible to tune a transmission maximum of an etalon into coincidence with a laser mode frequency. All other laser modes would have a reduced transmission, and by choosing the transmission to be a steeply varying function of frequency the gain available to these modes may be reduced below the loss level of the cavity. The steepness of this transmission band increases if the reflectivity of the etalon surfaces is increased, and also if the etalon length is increased. The Free Spectral Range, that is the separation of the transmission maxima, is $c/2nt$, and so decreases for longer etalons. The etalon length should be chosen such that the Free Spectral Range is greater than the gain bandwidth of the laser. Only one mode now remains with sufficient gain to oscillate.

As with the saturated neon absorption technique, suppression of all but one laser mode allows the gain available from the suppressed mode to become available to the oscillating mode. One might again expect a mode selection efficiency of around 80% of the multimode power, but losses introduced by the etalon reduce this. Absorption and scattering losses occur in the material, and these are reduced by selecting a strain free quartz block and by good polishing of the surfaces. The absorption losses in good fused silica are less than 0.1% per cm. in the visible portion of the spectrum.

The etalon is not normally used perpendicular to the laser axis as this forms several closely coupled resonant cavities of different lengths. Small movements of the etalon change their relative lengths resulting in a very unstable arrangement. In normal use, the etalon is operated at an orientation of a few milliradians. In this position, however, the light beams due to a reflection at the first surface and that from a reflection inside the etalon (beams 1 and 2 in Figure 1.6.) do not overlap each other entirely. The resultant interference effect between the two beams is therefore not complete, and a reflection loss, ℓ is introduced. This is given by

$$\ell = 4 t R / nD \quad (1.11)$$

where D is the beam diameter, R the reflectivity of the etalon surfaces and other symbols are as before. This loss increases as the etalon length increases and also as the reflectivity increases. Typically for an etalon 3 cm. thick, an orientation of 1 milliradian and a beam diameter of 1 mm. we find that $\ell = 0.3\%$. This may represent quite an appreciable loss in low gain systems such as the visible Helium - Neon laser.

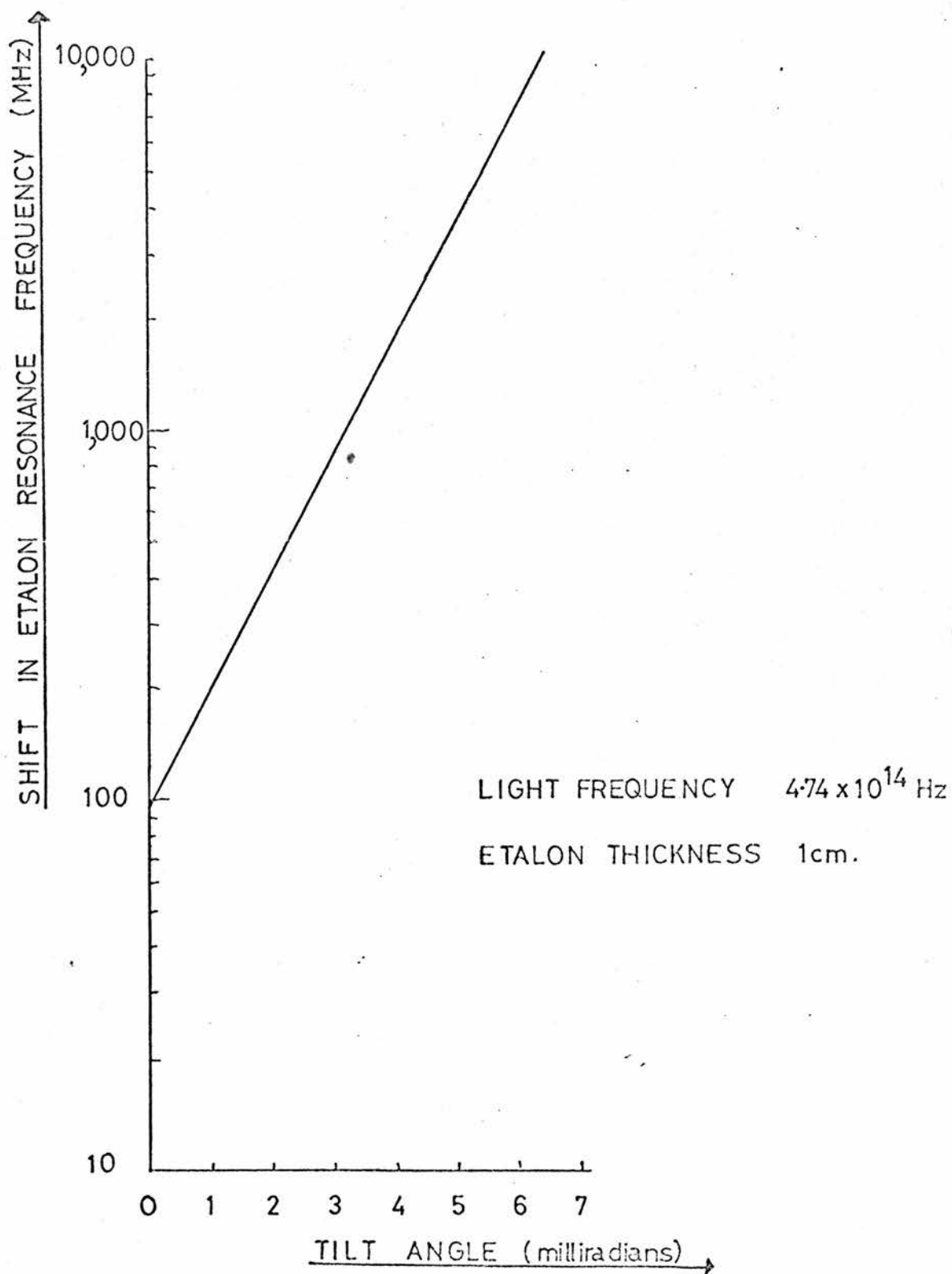


FIGURE 17
INTRACAVIDY ETALON TUNING CURVE.

The reflection loss becomes more serious still if long etalons or high reflectivities are needed to obtain a sufficiently steep transmission curve. The width of the transmission band halves if the length is doubled, and is reduced by $1/\sqrt{2}$ if the etalon reflectivity is doubled. The losses due to incomplete superimposition double in each case; but absorption losses in the etalon double if the length is doubled. It generally appears more satisfactory to increase reflectivity rather than length, and low absorption and low scattering coatings of Zinc Sulphide have been used with some success.

The orientation stability of the etalon requires careful attention, since vibrations may alter the orientation by amounts which detune etalon and laser. In particular airborne vibrations may be serious, and it is necessary to mount the etalon in a rigid manner which also allows precise angular adjustments.

Barber (29) reports a thermal detuning of the system over a few minutes, and it has been suggested that servo systems may be used to counteract angular and length detunings, but, as yet, no successful system has been reported. Manger and Rothe (30) have suggested the use of KDP as an etalon material. The electro-optic effect could be used as a means of changing the etalon length, but its hygroscopic properties and softness for optical working are considerable disadvantages.

Experiments were carried out with 1, 2 and 3 cm. long quartz etalons mounted in an Oriel Optics laser mirror mount and rigidly placed inside an 80 cm. long 633 nm. laser cavity. The gain tube was 30 cm. long with a bore diameter of 0.2 cm. and gave a laser power (1% output mirror) of about $1\frac{1}{2}$ mW.

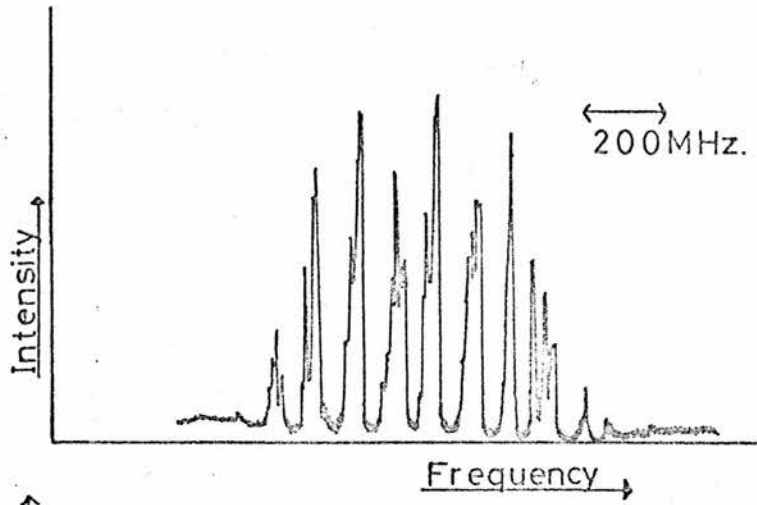
The etalons used were polished flat and parallel to $\lambda/10$, and single layer low absorption reflective films of Zinc Sulphide were deposited on both surfaces to give reflectivities of approximately 10%, 15%, 20%, and 25%. Table 1.8. gives the calculated values for various parameters of these etalons. The bandwidth figures give an indication of the narrowing of the pass band (at half power levels) with increasing reflectivity. In this experiment, however, we are really only concerned with changes of transmission of a few percent at the maximum of the Lorentzian shaped transmission band. The Scanning Spectrum Analyser photographs taken of the laser spectral output, which are shown in Figure 1.9. indicate the mode selecting effects of various etalon length reflectivity combinations.

The frequency range transmitted by the etalons may be estimated from the spectra shown in Figure 1.10. which were taken with an etalon in place while the laser cavity length was varied. The envelope of the transmission band is traced out by the scanned laser modes and its width is determined by calibration of dispersion of the oscilloscope trace.

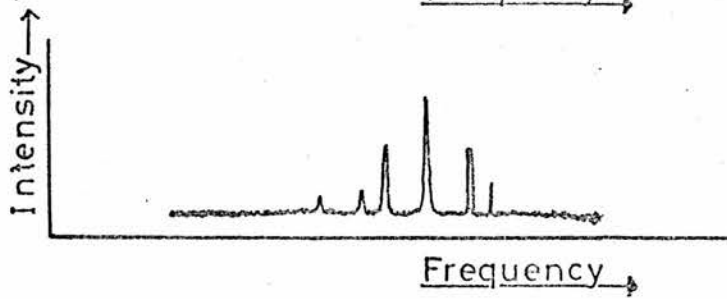
Length	Reflectivity	F.S.R. $\Delta\nu = \frac{c}{2Ln}$	Bandwidth $\delta\nu = \frac{c(1-R)}{2L\pi R^{1/2}}$ GHz	Reflec ⁿ loss/ transit $\frac{4d\theta R}{Dn}$ % $\theta = 2 \times 10^{-3} \text{c}$ $D = 0.2 \text{cm.}$	Abs ⁿ loss/ transit %
1cm	0.10	10 GHz	90	0.3	0.1
	0.15		6.7	0.45	
	0.20		6.2	0.59	
	0.25		4.7	0.75	
2cm	0.10	5 GHz	4.5	0.6	0.2
	0.15		3.35	0.9	
	0.20		3.10	1.18	
	0.25		2.35	1.5	
3cm.	0.10	2 GHz	1.82	0.9	0.3
	0.15		1.34	1.35	
	0.20		1.24	1.77	
	0.25		0.95	2.25	

TABLE 1.8

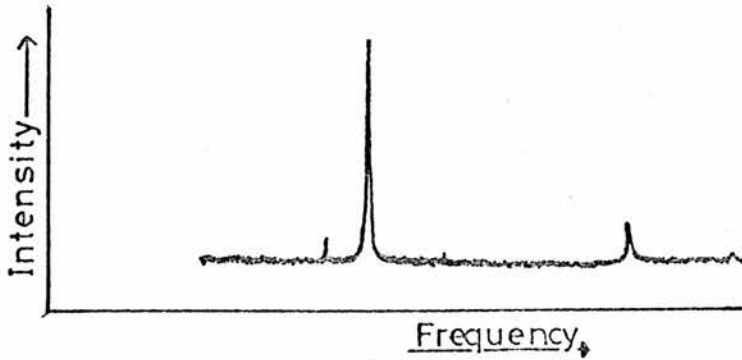
INTRACAVITY ETALONS



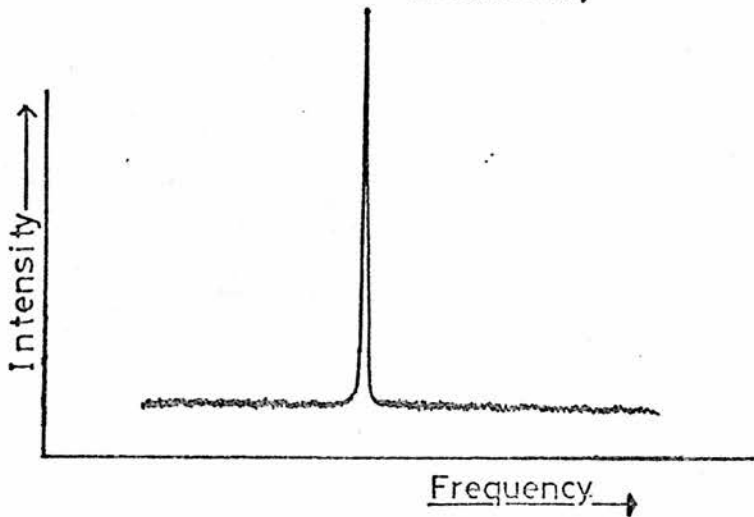
No etalon present.



1cm. long : 7% reflectivity.



3cm. long : 10% reflectivity.



3cm long: 17% reflectivity.

FIGURE 1.9
 MODE SPECTRA OF A LASER OPERATING
 WITH DIFFERENT INTRACAVITY ETALONS.

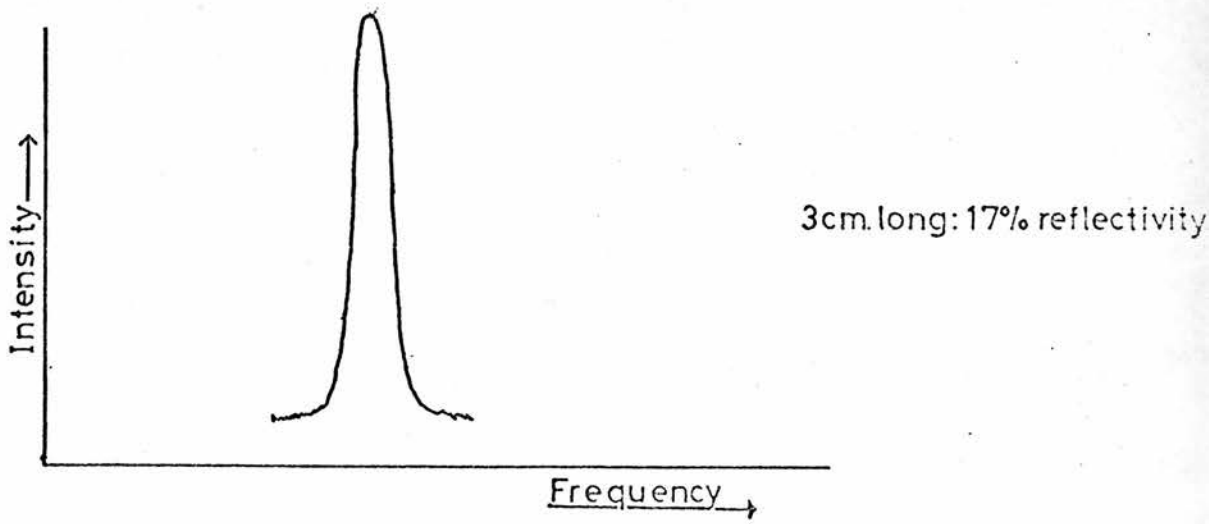
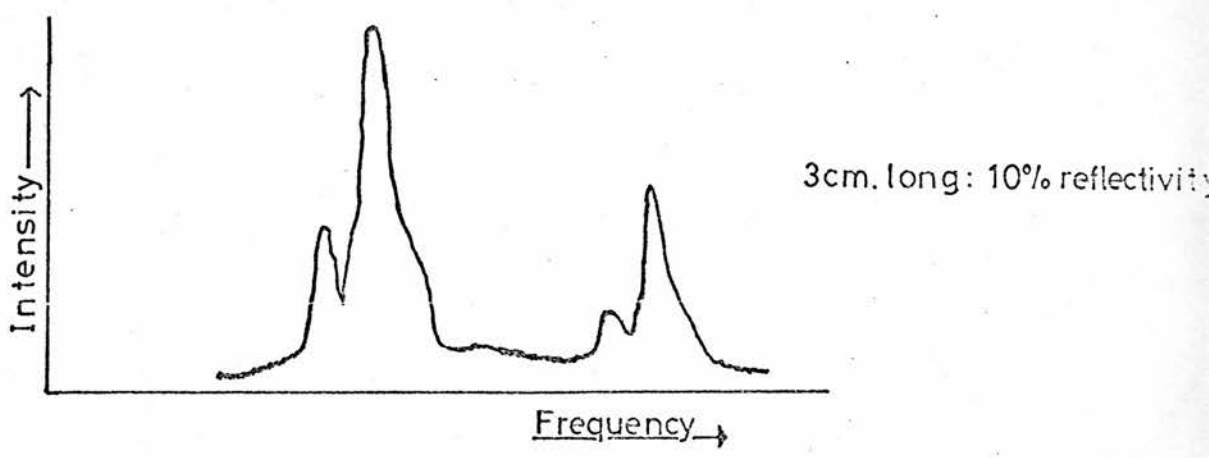
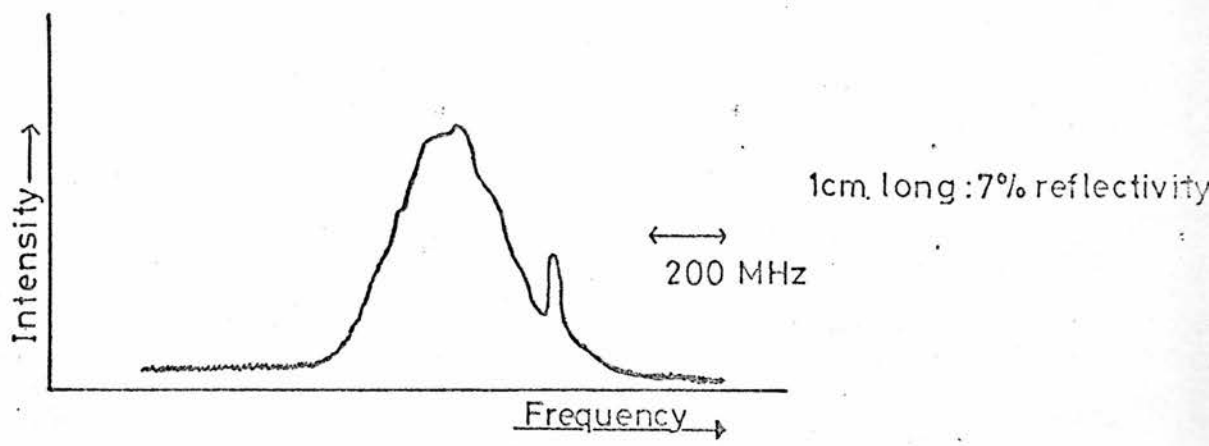


FIGURE 1.10

OPTICAL SPECTRA ILLUSTRATING THE PASS BANDS FOR DIFFERENT INTRACAVITY ETALONS.

It was found, from a series of experiments, that the following features of intracavity mode selectors made this technique unsuitable as a means of achieving single mode lasers with the required degrees of frequency stability, power and output noise.

1. In most cases, etalon reflectivities of 20% or more were needed to produce a single frequency which then was only tunable (by altering the cavity length) over a few hundred MHz. The iodine hyperfine structure spectrum extends over almost 500 MHz.
2. This high reflectivity means that the reflection losses were typically 2% per pass and this reduced the gain/loss margin, resulting in low laser power. The insertion losses from poor surface polish, absorption and scatter were such that the laser power was reduced by 40% in the best case and frequently by more. This 'best case' was when the etalon was aligned "exactly" perpendicular to the laser beam and not in a single mode position. In the latter case, the power was reduced by about 80% or more.

The high reflectivity led also to the formation of coupled cavities with sufficient finesse to pull the laser frequency.

3. This power loss is compensated for in some cases by the increased power available to the one lasing mode from the suppressed mode atoms which are made available via velocity changing collisions amongst excited neon atoms occurring within the upper laser level lifetime. A measure of the extent of this transfer lies in the collisionally broadened linewidth and the mode spacing. In this experiment the laser was filled to approximately 1.2 torr total pressure giving a Lorentz pressure broadened linewidth of 100 MHz. FWHM. The laser axial mode spacing was 180 MHz. Better transfer of power occurs, therefore, in longer lasers or in those operated at higher pressures.

4. Probably the most severe restriction leading to the rejection of this scheme lies in the vibrational stability requirements of the etalon. Simple calculations indicate that the pass band centre frequency shifts 200 MHz. for a change in tilt from 1 milliradian to 2 milliradians. (1 cm. etalon). If we stipulate a laser stability of a few MHz. drift per second in the free running laser, this demands a vibrational stability of a few hundredths of a milliradian per second. Slow thermal changes will also alter the resonance frequency and, because of these effects, it seems likely that some servo-system would be necessary to maintain the alignment of the etalon. Experimentally, shifts of about 10 MHz. in a few seconds were seen from a shielded laser on a vibration isolated table. This was double that from the free running laser. Improvements in acoustic shielding could probably increase the stability. These additional complications were a severe discouragement

in the use of etalon mode selectors. Vibration could also sufficiently detune the laser cavity mode and the etalon transmission peak, thus causing an instability in the frequency which could lead to mode competition, which, in turn, would lead to noise levels of a few per cent on the laser output power.

1.5. Definitions of frequency stability

This is a subject about which no really satisfactory agreement has been reached. There are several items of information needed to specify the stability of a laser completely, and these will be discussed individually. The particular application of a stabilized laser often demands knowledge of one aspect more than another.

i) The frequency variations of a laser within a certain observation bandwidth should be measured over short periods - say up to one second. These variations may or may not be controlled by the servo-system depending on the gain of the system and the time constants involved in the electronics. (Section 2. Usually such short term variations are averaged out in many applications.

ii) More importantly, the frequency fluctuations need to be ascertained over long periods, which may extend to several hours. This involves long term frequency drift, and changes of a regular nature which may have periods of several seconds or longer, also any drift in the control electronics such as psd zero drift (section 5).

iii) It is necessary to specify the nature of any frequency limiting or averaging process used to reduce and observe laser frequency variations. Practically the former refers to the time constants in the laser servo-loop which limit the bandwidth of controlled frequency variations. In the case of the latter, if a beat frequency experiment is used to observe the frequency stability between two lasers, then the mutual frequency variations within a certain electronic bandwidth may be time averaged and counted by some frequency counter system. One would expect the average frequency variation to decrease, until some limit is reached, as the averaging period is increased and so this time should be stated for a complete specification of the laser frequency stability.

iv) The reproducibility of the laser reference frequency is of great importance. If two similar lasers are locked to their individual references, the departure from zero mean beat frequency indicates how closely the lasers emit the same frequency when nominally under the same conditions. One should also determine how well the lasers reproduce the same beat frequency when both lock loops are opened and relocked. This carries information about how accurately the servo system may be adjusted to sense the reference frequency and control the laser to the reference frequency.

v) Frequency shifts due, for example, to possible variations, in the reference frequency environment e.g. temperature or laser power, will determine the reproducibility of the reference frequency. Ideally, the reference should not shift under different environmental changes and the sensitivity to shifts must be specified for an international standard.

vi) To gain information about the efficiency of the servo system in controlling the laser frequency, the nature of the limiting noise source influencing the laser frequency should be determined. If, for example, (1/f) type noise limits the performance, then no further improvements in frequency control are possible. If, however, the laser fluctuations appear to be typical of white noise, then further averaging and better control will reduce the extent of the frequency fluctuations and improve the stability of the system.

Frequency stability is a function not only of the bandwidth of the frequency measuring system used to observe any fluctuations, but also of the total observation time τ . A useful measure of frequency stability S may be written as:-

$$S = \frac{[\Delta \nu_{\text{rms}}]_t^{t+\tau}}{\int_t^{t+\tau} \nu(t) dt} = \frac{\Delta \nu_{\text{rms}}(\tau)}{\bar{\nu}} \quad (1.12)$$

where $\nu(t)$ is the frequency at any time t within the observation period t to $t + \tau$; $\bar{\nu}$ is the mean laser frequency during this period, and $\Delta \nu_{\text{rms}}(\tau)$ is the root mean square value of the frequency deviations observed within some bandwidth B during the observation period. Clearly, during the period τ , some extremely large frequency variations might occur and, indeed, could appear at any time if the noise spectrum were white and the bandwidth infinite. This would bias the estimation of frequency variations if a simple mean value of the maximum frequency excursions was to be taken as an estimate of the frequency variations. One intuitively feels that these large variations should have less weight than a 'typical' variation and that a statistical frequency fluctuation has most relevance in this definition. For this reason the RMS deviation is specified.

Practically, the observation time limits the slowest observable fluctuation: the electronic system detecting the laser frequency may, for example, have the capability of measuring frequency variations from d.c. to 100 MHz. However, if one only observes the laser frequency for 10 seconds, no sensible information may be extracted involving fluctuations with periods longer than 10 seconds. Similarly, any time constant averaging of the laser frequency (either electronically or by eye if observed in a beat frequency experiment) would prohibit the observation of fast fluctuations.

This complicated definition is conventionally interpreted in two specific cases. The short term stability of a laser locked to a reference

frequency usually refers to the observed frequency variations over periods of up to about a second. For observation times and corresponding integration times longer than 1 second the stability is referred to as long term stability.

A parameter which is slowly becoming recognised as a very useful way of specifying frequency stability and learning of the type of noise limiting the performance of the laser is the Allan Variance (32, 33). This measure of stability has been used in the microwave frequency standards field for some years where similar problems of measurement and specification exist. The classical variance σ of the laser frequency ν_i is :

$$\sigma^2(M, \tau) = \frac{1}{M-1} \left[\sum_{i=1}^M \nu_i^2 - \frac{1}{M} \left\{ \sum_{i=1}^M \nu_i \right\}^2 \right] \quad (1.14)$$

where M is the number of samples of the laser frequency ν_i and τ is the sample integration time.

One would require this variance to decrease as the noise fluctuations are averaged out using longer sample integration times and the value to converge as more averages are taken. However, for noise sources which contain a great deal of their noise power in the Fourier frequency range corresponding to long times, then the value of σ^2 begins to diverge as the number of samples of frequency is increased. These noise sources, such as $1/f$ type or flicker noise are frequently found in atomic standards of frequency such as we are discussing and this unsatisfactory state of affairs may be remedied by the following procedure. Let us first take a value of M equal to 2, in other words two adjacent samples of the laser frequency are taken, both averaged over a time then formula (1.14) gives:

$$\sigma^2(2, \tau) = \frac{(\nu_1 - \nu_2)^2}{2} \quad (1.15)$$

The Allan Variance is the averaged value of N pairs of readings of the laser frequency

$$\langle \sigma^2(2, \tau) \rangle = \frac{1}{N} \sum_{i=1}^N \left[\frac{\nu_{2i} - \nu_{2i-1}}{2} \right]^2 \quad (1.16)$$

This value does decrease with increasing N for just the same noise sources which make (1.14) diverge.

Strictly speaking, this average should be over an infinite time, however a large N value approximates to this statistical requirement and good confidence levels are achieved with N typically 100. However, for integration periods above about 1 second, the time required to compute $\langle \sigma^2(2, \tau) \rangle$ becomes very large, reaching 200 seconds for a 1 second period and over 30 minutes for a 10 second period. The values of the Allan Variance for smaller numbers of N are more conveniently taken, but with a corresponding loss in the confidence level of the result, so the value of N should also be specified in a measure of the Allan Variance.

The evaluation of the Variance gives information, in a beat frequency experiment about the average difference between two adjacent samples of the beat frequency as a function of the sampling time. Usually, one finds logarithmic plots of $\langle \sigma^2(2, \tau) \rangle$ as a function of time τ and the slope of these plots carries information about the nature of the dominant noise perturbing the laser over a particular time averaging period. We shall evaluate the slope for two commonly encountered noise sources which we may think of as determining the frequency spectrum $P(f)$ of the fluctuations in ν .

For $1/f$, or flicker noise, $P(f) = \alpha/f$ which indicates the increase of importance of this noise at low frequencies. The Allan Variance is:

$$\langle \sigma^2(2, \tau) \rangle = 2\alpha \log_e 2 \quad (1.17)$$

and the slope of the logarithmic plot of the variance is zero.

For white frequency noise $P(f) = \beta$ and the noise has the same magnitude independent of bandwidth. In this case

$$\langle \sigma^2(2, \tau) \rangle = \frac{\beta}{2} \tau \quad (1.18)$$

and so the plot has a slope of -1

The significance of these calculations is that if one finds, by performing an experiment to plot the Allan Variance as a function of τ that white noise dominates the fluctuations between the lasers at a particular value of τ then improvements in the laser stability are possible which would reduce the extent of the fluctuations by better or longer averaging. If, however, the Allan Variance is flat, then no further averaging will result in an improved stability for that value of the sample time.

Frequently one finds published plots (34, 35, 91) of the square root $\langle \sigma(2\tau) \rangle$ of the Allan Variance. In the plots discussed above, for this expression of stability we find that the slope is again zero for flicker noise, but is ($-\frac{1}{2}$) for white frequency noise.

The reproducibility of the laser is an item of considerable interest. This feature expresses how well the laser reproduces the same frequency when the servo loop is opened, and closed, and also the day to day reliability of the laser frequency.

We are also interested in how closely the same frequency is emitted from different lasers nominally stabilized to the same reference frequency. These characteristics may be measured by the reproducibility R which may be expressed as

$$R = \frac{\Delta \nu}{\bar{\nu}} \quad (1.19)$$

where $\bar{\nu}$ is the main frequency in a series of measurements, say, between two nominally similar lasers when their servo loops are continually opened and closed, locking the lasers to their individual reference frequencies. The measure of the variations, $\Delta \nu$, from this mean, invoking a similar argument to that of the stability definition, following equation (1.12), should be expressed in some statistical form. One convenient measure is the 3σ uncertainty where here σ expresses the standard deviation of a number of individual settings. This measure

then gives more information about the likelihood of a particular pair of lasers emitting the same frequency than does a statement of the poorest agreement achieved, which, statistically is unlikely.

The reproducibility is related to the long term stability since perturbations occurring over long periods influence both figures. An example of such a perturbation is the slow drift in the centre of the Lamb Dip which is used as a reference frequency. For one particular frequency lock, the long term stability may be superior to the laser reproducibility. In other words, the laser has a slightly different mean frequency each time it is locked and the variations about this frequency are smaller than the variation in mean frequency.

This concern with definition, both mathematical and semantic has recently been the subject of some considerable study particularly since lasers are now available with extremely high values of long term stability and reproducibility. The specification and careful comparison of the performance of the lasers has been hampered, to some extent, by a lack of uniformity in expression and it is encouraging to see that many recent publications specify more carefully statements of laser performance.

1.6. Measurement of Frequency Stability

The most usual form of measurement is the beat frequency technique already referred to and further discussed in section 2.7. A typical display of beat frequency over 0-100 MHz is shown in Figure 2.16. Two iodine stabilized lasers are locked to the d and e lines, and the Figure shows the beat centred at 13 MHz. The width of the beat is dominated by the 1 KHz applied modulation. The short term stability may be estimated by observing the fast fluctuations of the beat, and the long term stability by observing the slow drift of the centre of the beat.

In these experiments an analogue signal linearly proportional to the beat frequency was generated (Chapter 2.7) and this could be displayed as a function of time on a chart recorder, to plot long term stability over several hours. A suitable filter placed across the input of the chart recorder created a smoothing time constant, and an averaged stability scan versus time could be plotted. Alternatively, averaged values of the beat frequency could be measured in digital form by counting the beat frequency on a frequency counter with suitable integration times.

The reproducibility was also measured by a beat frequency experiment; one or both of the lasers were unlocked, relocked to the same components and the beat frequency counted. The resetability of the lasers manifested itself as different averaged beat frequencies. This experiment could also be performed with both lasers locked to the same line: the shift of the beat frequency from zero frequency indicated any offset, the constancy of which could again be measured by relocking and remeasuring. Wavelength comparisons between lasers are possible to an accuracy approaching 1 in 10^9 using a pressure scanned Fabry Perot interferometer (5). However comparisons against the primary standard are only possible to its own accepted accuracy of 1 part in 10^8 . (1)

Measurement of the Allan Variance are discussed in detail in Section 5.6.

CHAPTER 2

LASER DESIGN AND ANCILLARY APPARATUS

We shall describe here the general features of the type of laser used in these experiments. For these purposes the discussion will be divided into four sections.

2.1. Cavity Design

As discussed earlier, the prime requirement of the cavity support structure is to keep the mirror separation as constant as possible. The basic cavity design is shown in Figure 2.1. and is a modification of cavities which have successfully been used in this laboratory for some time.

The end plates (A) supporting the mirrors, are constructed of steel and are kinematically mounted against large, heavy, steel plates (B). These plates are linked by three $1\frac{1}{4}$ " diameter invar bars. The orientation of plate A is altered, with respect to the cavity axis, by spring loaded screws which give orthogonal movements with an angular sensitivity of $\frac{1}{3}^{\circ}$ per turn.

Various laser tube mounting arrangements were used. In the majority of cases the tubes were held in two Terry Clips which were supported from the upper invar bar. Alternatively, platforms resting on the bottom two spacer bars were used, in conjunction with micrometer movement plates which were bolted together to give horizontal translation of the tube. A spring loaded clamp provided vertical movement.

The absorption tubes were mounted (Figure 2.2.) in vee blocks on small tilting platforms and held in position with red wax. The platform was fixed to a micrometer cross slide bolted on to a magnetic base which was clamped to the steel vibration isolated table. This arrangement allowed tilt of the tube in two orthogonal directions and also translation of the tube perpendicular to the laser axis. Using these adjustments, it was possible to align empty absorption tubes in the laser cavity with a power loss of less than 5%.

Photographs of the laser system taken in plan and elevation are shown in Figures 2.3., and 2.4. The photographs show a laser with a hot cathode gain tube and an absorption tube. Normally, plastic dust screens surround the air gaps between tubes and mirrors. A plastic acoustic shield also surrounds the complete laser.

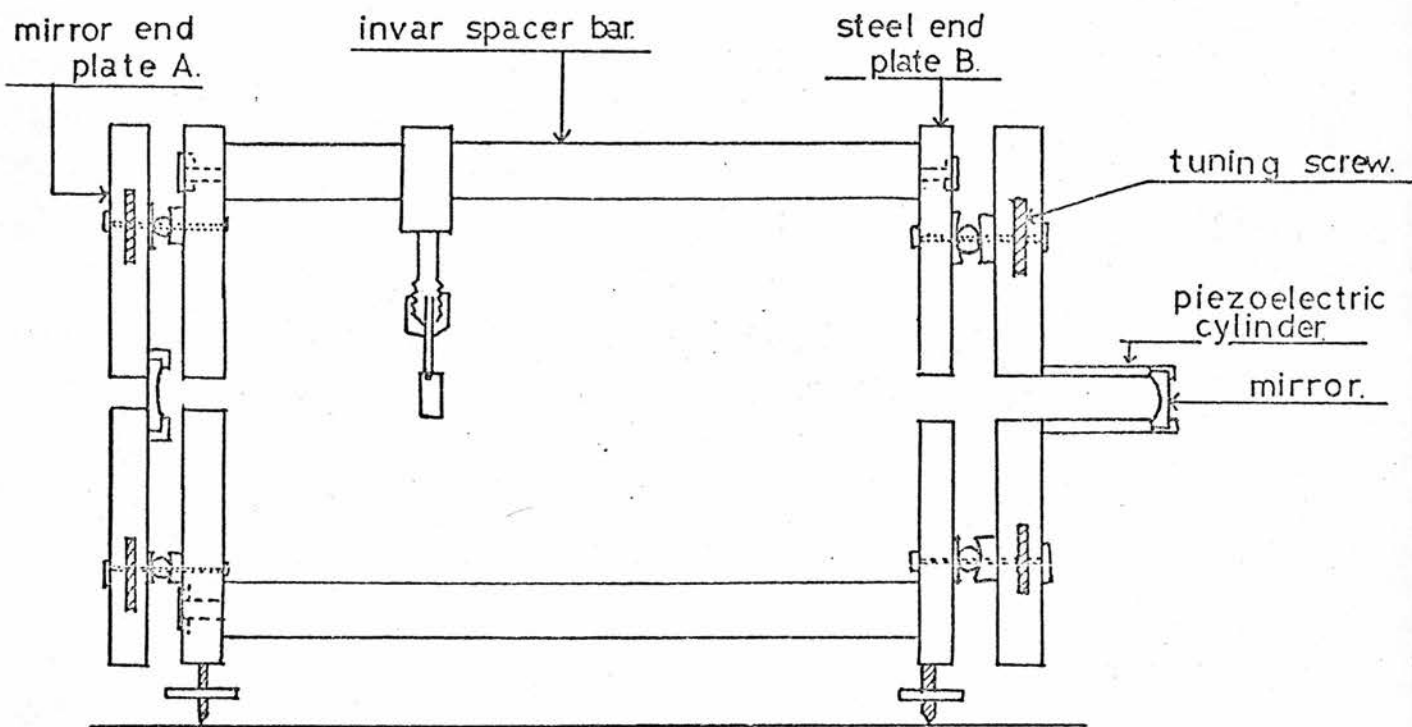


FIGURE 2.1
LASER CAVITY DESIGN

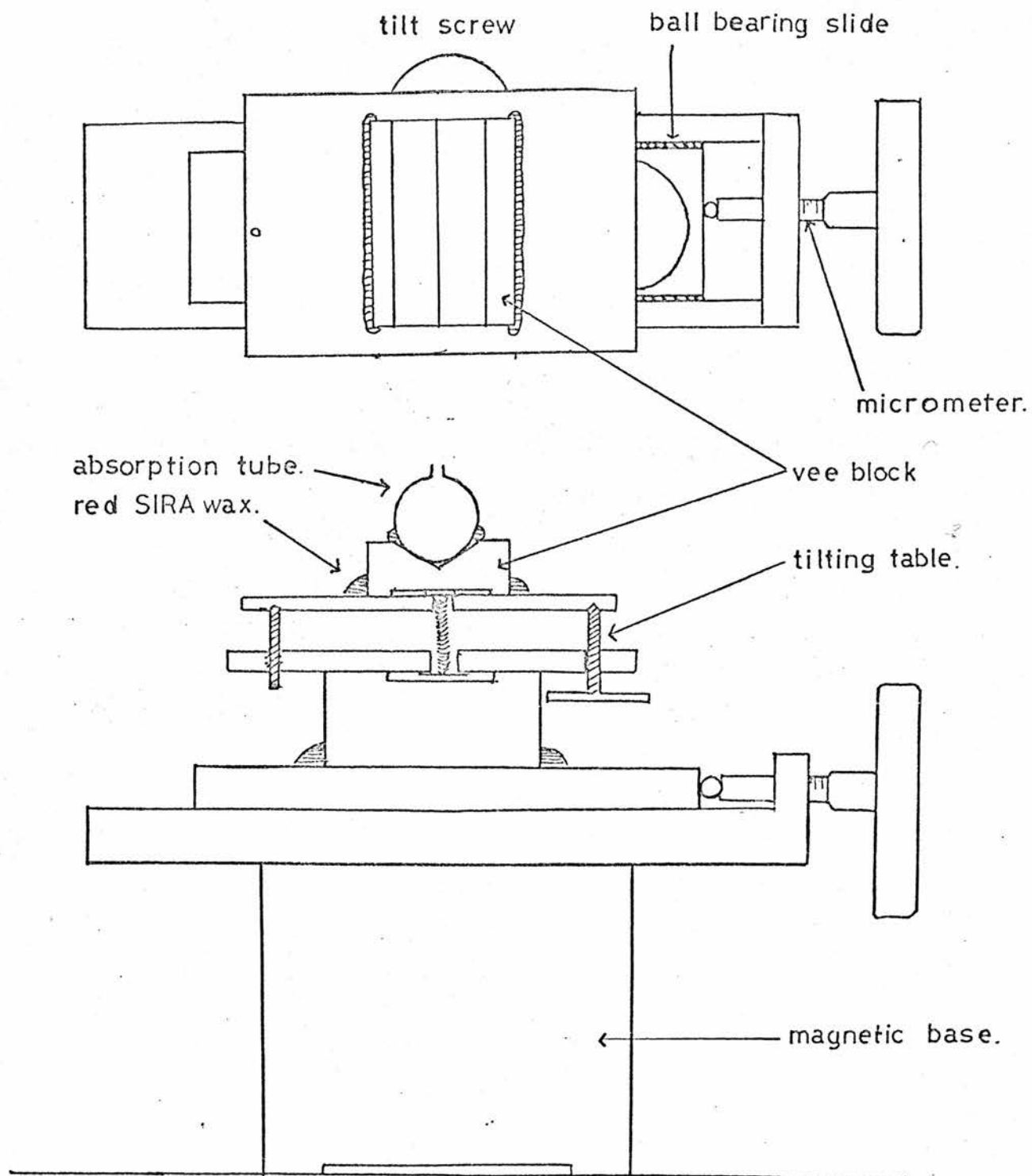


FIGURE 2.2

PLAN AND ELEVATION VIEWS OF THE ABSORPTION TUBE MOUNTING

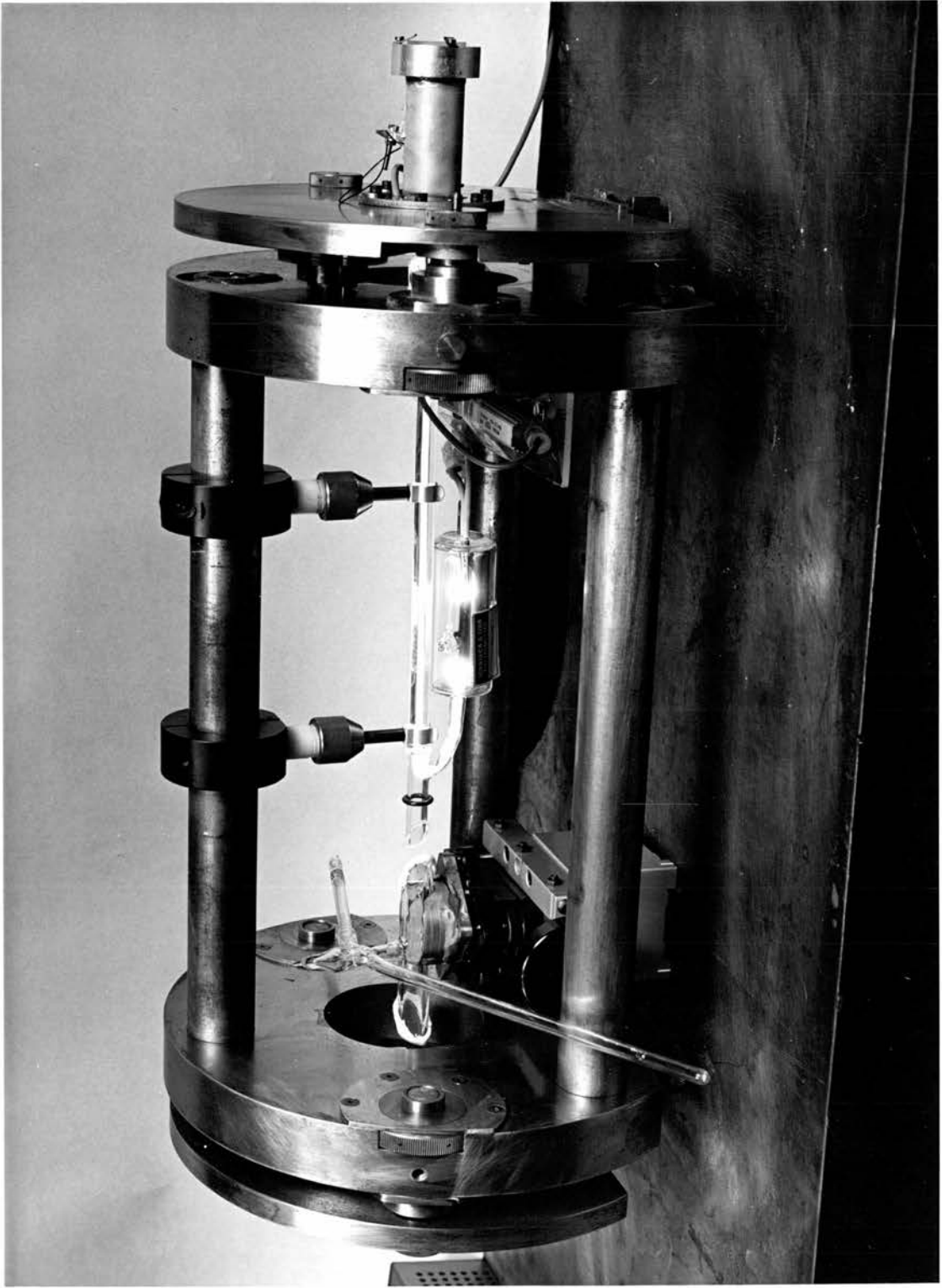


FIGURE 23
SIDE VIEW OF THE LASER.

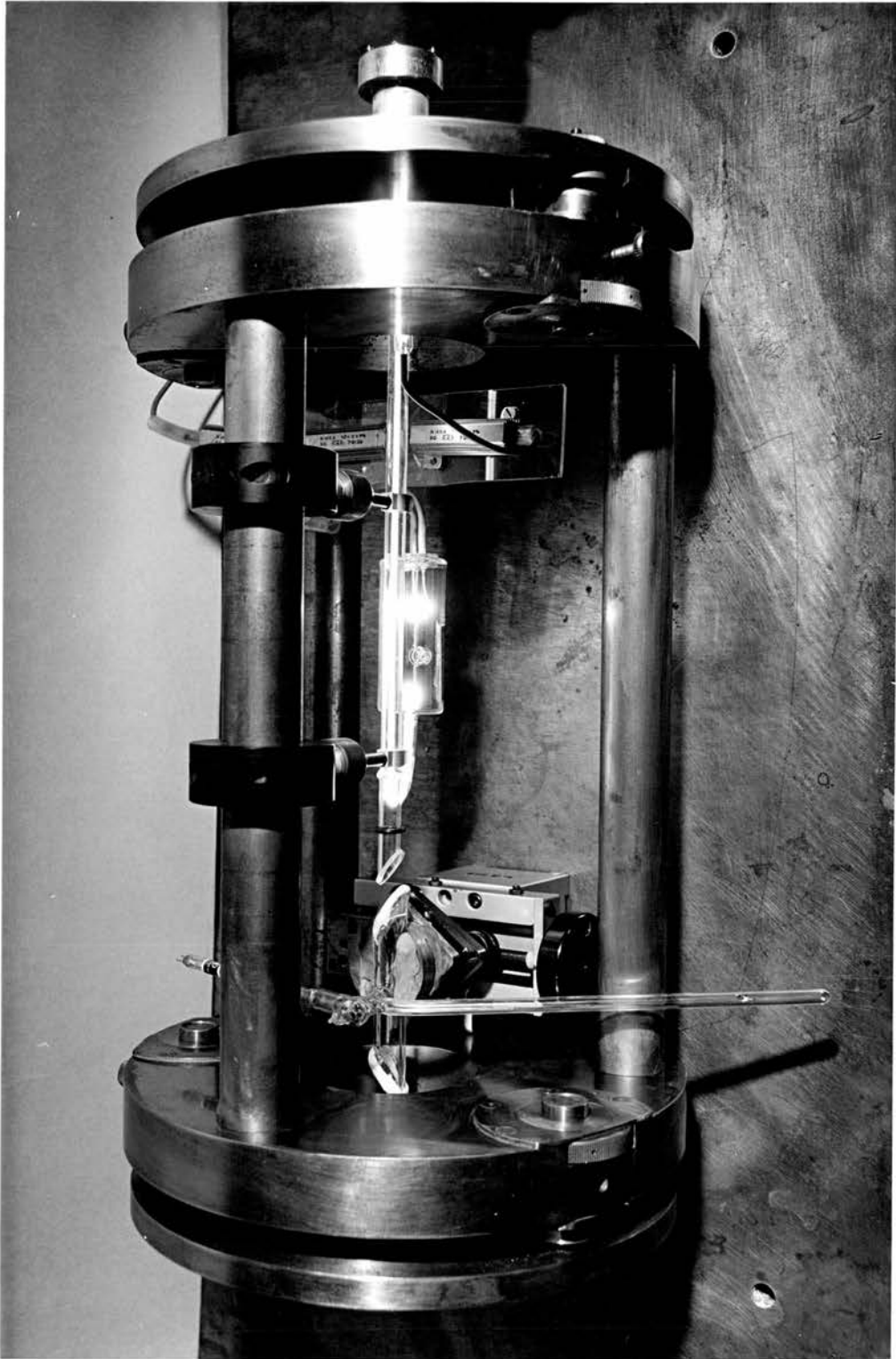


FIGURE 24
PLAN VIEW OF THE LASER

2.2. Laser Tube Construction

In several cases, it was possible to use commercially available laser tubes in these experiments. Tubes were supplied by Scientifica and Cook Electronics, Spectra Physics and Oriel Optics. Both the Scientifica and Cook and the Oriel tubes had hot cathodes while in the Spectra Physics tube a cold aluminium cathode was used.

The tungsten wire filament construction of Scientifica and Cook proved unreliable. The filament was operated from a 6 - 7 volt stabilized power supply at 1.25 amps and, in practice, tended to sputter as a result of ion bombardment. Moreover, the filaments were rather fragile and when, after some period of operation, the laser was moved, the wire tended to break. In operation the power supply voltage was increased or decreased gradually on switching on or off respectively. This eliminated large transients which might have overheated the wire.

The Oriel tubes were constructed with dull emitter electrodes and performed satisfactorily except for the heat generated (about 1 watt) inside the laser.

Spectra Physics cold cathodes proved more satisfactory, however. Constructed from an aluminium alloy, they are highly sputter resistant. The disadvantage is that, over long periods, the cathodes tend to clean up the helium and neon in the tube. Frequently one found that the helium and neon were absorbed into the aluminium. However, warming the cathode with heating tape was sufficient to restore full power to the laser.

For the 30 cm. Iodine stabilized lasers it was necessary to construct tubes (not available commercially) of a particular bore diameter and length. The practice of tube construction varies greatly from laboratory to laboratory. (36, 37, 38) Therefore a brief indication of that used in these experiments is necessary. Cold cathode tubes were constructed, as these were thought to be most reliable. In order to refill the lasers to different gas pressures, locally constructed tubes should be capable of reopening. Generally, the re-opening of a tube re-admits air and allows dust and dirt to settle on the inside of the tube windows. For this reason most of the tubes were constructed with windows sealed on to the tube using epoxy cements. After use, the windows could be removed, cleaned and re-sealed. Two particular cements were used: Torr Seal (Varian) and a flexible low vapour pressure Araldite (AY111 and HY111). The former was rapid setting and, on mixing, formed a thick paste which was easy to apply. It was, however, difficult to remove, being fairly resistant to the usual epoxy resin solvents. The Araldite product set in twentyfour hours

at room temperature or in about half an hour when heated to about 90°C in an oven. It was easily removed using De-Solv 8090 (Oxley Development Corporation). Both of these adhesives were used also on several absorption tube window assemblies.

The basic laser tube design was modified several times and a diagram of the final form is shown in Figure 2.5.

The capillary section was made of high bore tolerance fused silica. The anode A was a tungsten pin, as was the third processing electrode P. An aluminium cylinder (EHT 15, Approved Metal Co. Ltd.) which was machined to have an internal diameter of about an inch, formed the cathode. A nickel plate, on to which was welded a tungsten lead pin, was screwed into the back of the cathode. The important feature of the cathode envelope was the "funnel" which directed the discharge inside the cathode, rather than on to the outer surface. The latter situation tended to produce a noisy lasing output as the discharge flicked from point to point on the outside of the cathode and destroyed the power supply stabilization by making large and fast demands on the current regulation.

In practice, the glass funnel protruded about an inch into the cathode. The length of the cathode was determined by the discharge current at which the laser gave maximum power output. This, in turn, depended on the laser length and tube bore, and was typically 12 mA. for tubes about 30 cms. long and decreased as the lasers decreased in length. The dimensions of these cathodes have been investigated by several authors (39, 40, 41) and their results have been used in the present work. For the 30 cm. long lasers, the cathode dimensions were typically 1" I.D. and about 6" long.

A block diagram of the vacuum system used for evacuating and filling the tubes is shown in Figure 2.6. The vacuum system was constructed from Vacuum Generators Ltd. stainless steel components using copper gasket FC18 flanges. The backing pump was an Edwards ED 35, and the diffusion pump an oil pump. A triport filling facility existed and the required amounts of B.O.C. grade X gases were let into the system using needle valves. A large nitrogen trap above the diffusion pump was filled automatically from a dewar using a compressed air pump delivery system. The nitrogen level in the trap was controlled by a thermistor level controller system.

The laser tube was usually attached to a standard flexible bellows flange which was bolted on to the system. The pressure was measured on ion gauges and the tube filling pressures on calibrated Edwards Model 9 Pirani gauges. The final tube pressures could be relied upon to about 10%.

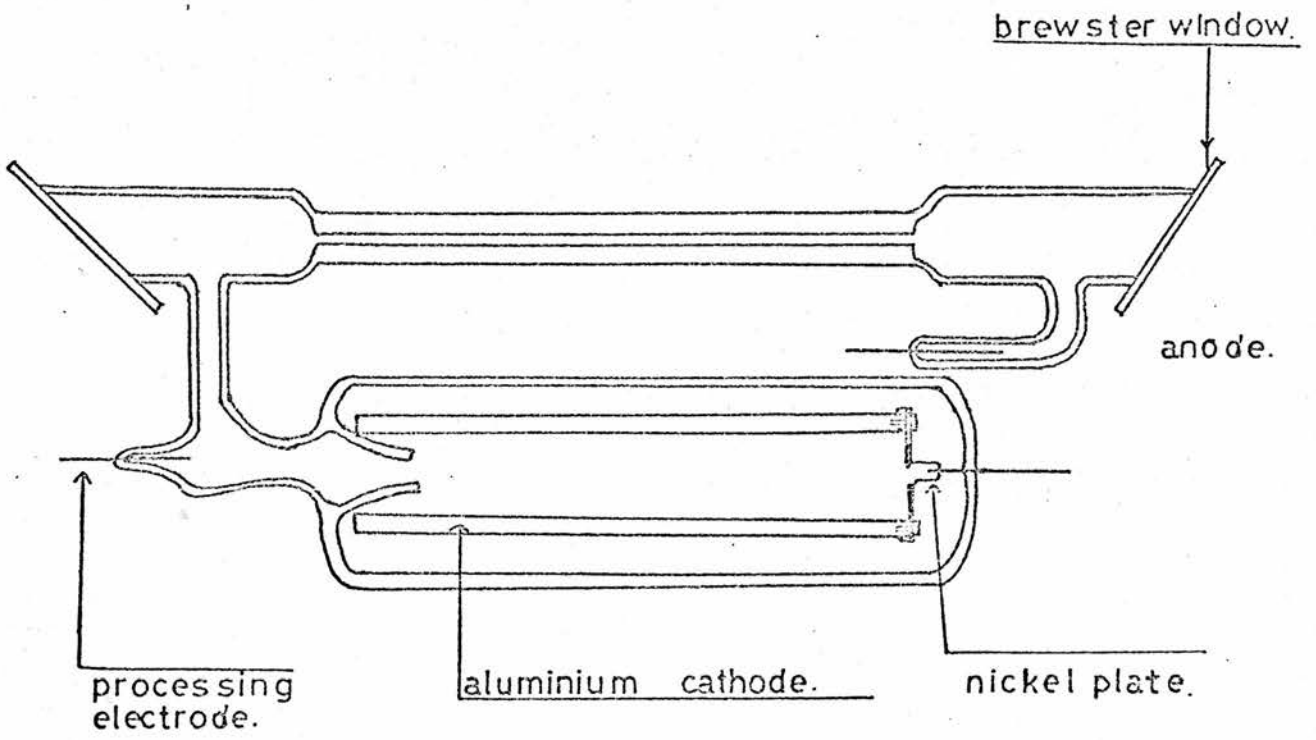


FIGURE 2.5

LASER TUBE DESIGN

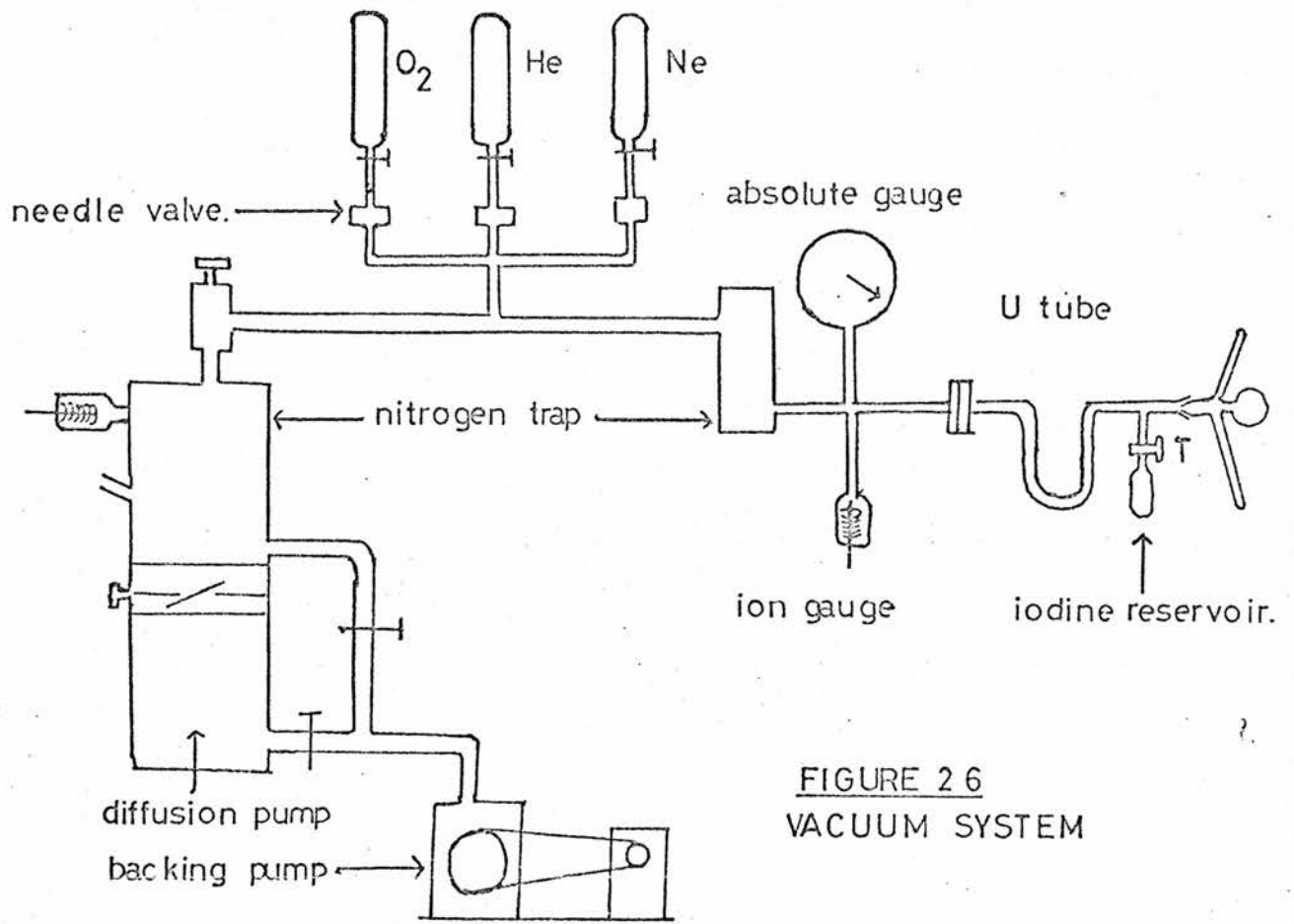
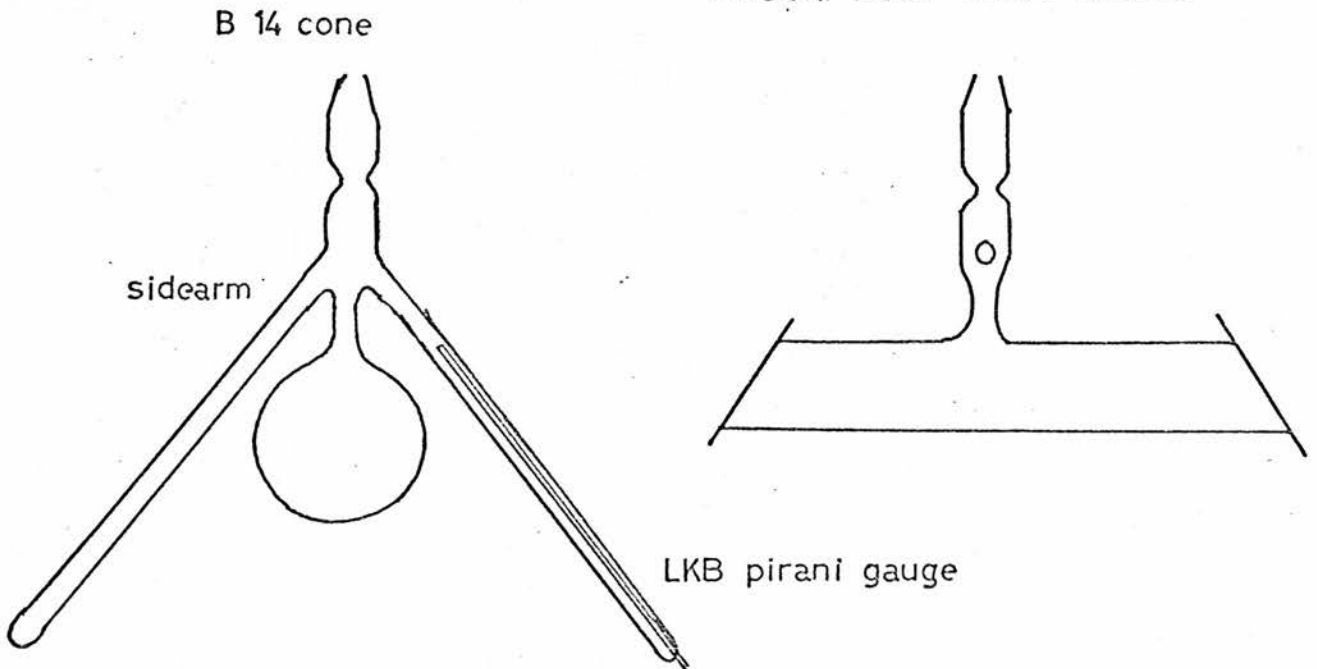


FIGURE 26
VACUUM SYSTEM

FIGURE 27
ABSORPTION TUBE DESIGN



The system regularly achieved base pressures of $8 - 9 \times 10^{-8}$ torr at the laser tube end. The procedure involved pumping down and outgassing the system, including laser tube, with heating tape at about 250°C until pressures of about 10^{-7} torr were achieved. The cathode processing was then carried out. The cold cathode is only effective and sputter resistant if a thin oxide coating is formed on the outside of the cathode. To effect this, discharges were run in a few torr of oxygen at about 40 mA for several hours with several fillings of oxygen. It was during this processing that the auxiliary electrode was used. Previously, processing discharges were run through the tube bore, but it was found that, in using this procedure, gases evolved by the cathode during the processing tended to settle on the cooler inside of the windows thus preventing lasing. All processing discharges were therefore run via the short discharge path, and with the nearest nitrogen trap kept full in order to gather the evolved gases. Initially the oxygen discharge would be very blue; after several oxygen flushes, the processing was judged to be complete when the discharge was colourless. On filling the tube to the required helium and neon pressures, a discharge was run under typical laser conditions for a few hours and then the tubes re-evacuated and refilled. A crude mirror system could be built up around the tube on the vacuum system. This would enable the tube to be tested for laser action before sealing and removing the tube from the vacuum system.

2.3. Absorption Tube design

A suitable absorption tube design gradually evolved during the experiments and the final form is shown in Figure 2.7. The side arm is used in the iodine tubes to cool the tube and therefore change the iodine vapour pressure inside. No side arm was used in the methane tubes. A L.K.B. type pirani gauge was incorporated so that checks could be made on the tubes periodically to ensure that they remained vacuum tight. This was particularly necessary when using epoxy window sealed tubes since water vapour is easily transmitted through epoxy glues. The tubes were attached to the vacuum system already described through a glass "U" tube nitrogen trap which prevented the iodine from travelling into the vacuum system from the reservoir. The glass joints were greased B14 cone and socket systems.

To fill the iodine tubes, the system was pumped out, with all nitrogen traps full including the iodine reservoir and then the tap T was closed. A nitrogen flask was held over the absorption tube side arm and the iodine was sucked into the tube. When a suitable amount was in the tube, the absorption tube could be sealed off at the constriction.

For all the preliminary experiments, epoxy sealed windows were used. These had the disadvantage that they tended to transmit water vapour and had a tendency to leak. Iodine also attacked both Torr-Seal and the Araldite window seal. A sealing technique using a Mylar film coated on both sides with epoxy resin was developed, particularly for the iodine tubes. Even though epoxy resins were used, the amount was smaller than if a complete epoxy seal were used and the majority of the seal was mylar (1/40 mm. x 3/40 mm. x 1/40 mm.) sandwiched between the end of the absorption tube and the window. The complete assembly was heated to about 90°C in an oven and pressed gently together while it was hot. This seal is, of course, not bakeable but the tube body may be baked with heating tape while keeping the ends away from the heating tape. Because of the flexible nature of the mylar and the epoxy film, it was easy to fill in any cracks or irregularities in the tube ends which therefore only required coarse polishing.

A much more satisfactory tube construction technique uses completely fused quartz assemblies, and, indeed, tubes made in this way were used in the final systems and are reliably leak proof. Quartz also has the feature of itself outgassing less than pyrex and so is a more suitable material to use in absorption tube assemblies. Such tubes had very low loss when inserted in the laser cavity and power losses of less than 5% were typical for empty iodine cells.

2.4. Cavity length modulators

Two types of modulators have been used, one a piezoelectric device and the second a magnetic type. Both will be discussed separately.

2.4.1. Piezoelectric length modulators

The extension of a piezoelectric material for a voltage V is given by

$$\Delta l = \frac{l}{t} d_{31} V \quad (2.1.)$$

in a direction normal to the applied voltage. Here l is the length of the material, t its thickness and d_{31} is the appropriate piezoelectric coefficient. To maximise the sensitivity ($\frac{\Delta l}{V}$) one requires long thin materials with a large d_{31} value. A useful arrangement for a laser length modulator is a thin cylinder with the mirror mounted on one end, the other end being fixed to the laser end plate. Alternatively three stacks of discs may be distributed around the mirror at 120° intervals. These may be arranged to give either a total length extension, when the three stacks are made to change length simultaneously, or two orthogonal tuning motions, when only one of the stacks is extended for each movement. The disadvantage of the three stack arrangement is that it is difficult to match the individual discs comprising the stacks to give the same sensitivity, in which case a

total length extension, obtained by applying the same voltage to the three stacks, would require retuning of the laser. This may be overcome by careful choice of the power supply sensitivities used to drive the stacks of discs. By connecting adjacent discs "back to back" the voltage needed for a given extension may be reduced. There are some considerable practical difficulties in cementing together small stacks to give a flat contact which is also electrically conducting. Frequently, thin copper or steel shim pieces are sandwiched between the discs to serve as solder tags. These difficulties resulted in the choice of cylinders $1/8$ " thick and $1\frac{1}{2}$ " to 2" long mounted as shown in Figure 2.8.a.

The ceramic material is produced by Brush Clevite (Venitron) in three grades having three different sensitivities PZT4 ($d_{31} = -123 \times 10^{-12}$ metres/volt) PZT5A ($d_{31} = -171 \times 10^{-12}$ metres/volt) and PZT5H ($d_{31} = -273 \times 10^{-12}$ metres/volt). However the dielectric constant increases with the more sensitive types (48 for PZT4 and 100 for PZT5H) and so the capacity of the tube increases as the sensitivity increases. This capacity increase decreases the maximum speed at which the piezoelectric works and may degrade the performance of the servosystem. It reduces the maximum frequency of the modulation on the cavity length thereby increasing the time constant needed on the phase sensitive detector and may also require operation of the electronics away from optimum low noise regions. The capability of the system for counteracting fast disturbances may also be impaired.

As a compromise between these features, PZT5A was used and for a $1\frac{1}{2}$ " tube, a DC sensitivity of about $2 \mu\text{m}$ for 1KV was obtained. This corresponds to about 7 orders of movement of the 30 cm long cavity. For a laser frequency stability of 1 MHz. in a 30 cm cavity ($\frac{c}{2L} = 500 \text{ MHz}$) the noise on the piezoelectric must be less than about 300 mV peak to peak. This is a figure well above that expected in practice.

The piezoelectric tube was fixed into a brass disc and cemented in place with Araldite (AY1111 + HY1111) or a cyanoacrylic adhesive to provide a rigid and electrically insulating joint. The outer electrode surface of the piezoelectric cylinder was kept at earth potential and the inner at high voltage. The electrical connections to a well stabilised power supply or a servo loop were made through a BNC socket the centre pin of which was joined to the inner electrode surface with a loop of wire passing through the brass disc and soldered with low melting point solder on to the inside of the cylinder. The light mirror mount was Araldited to the other end of the piezoelectric carefully ensuring that the two electrode surfaces were insulated from one another. The mirror, located on three ball bearings cemented inside the mount was held in position by three metal clips. The whole assembly was

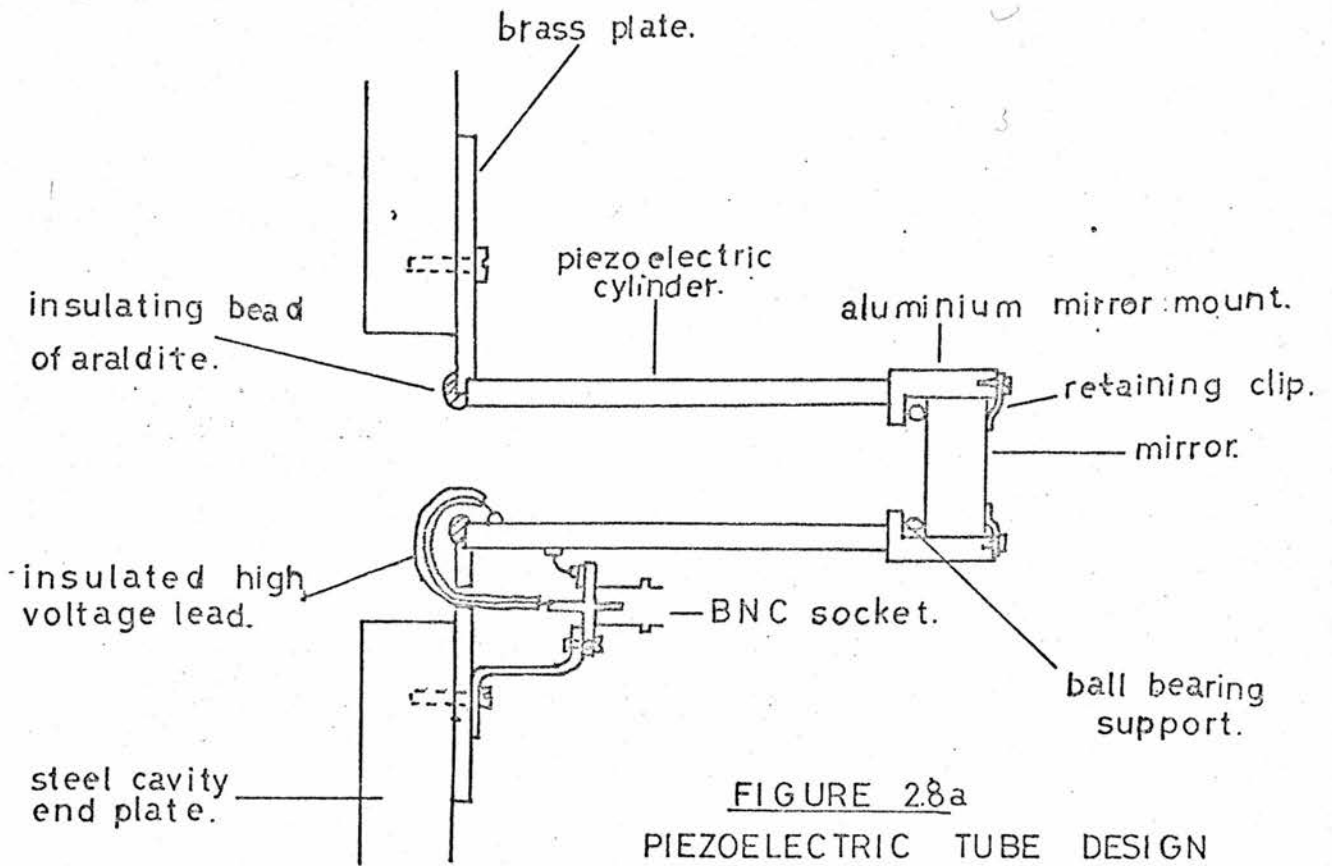
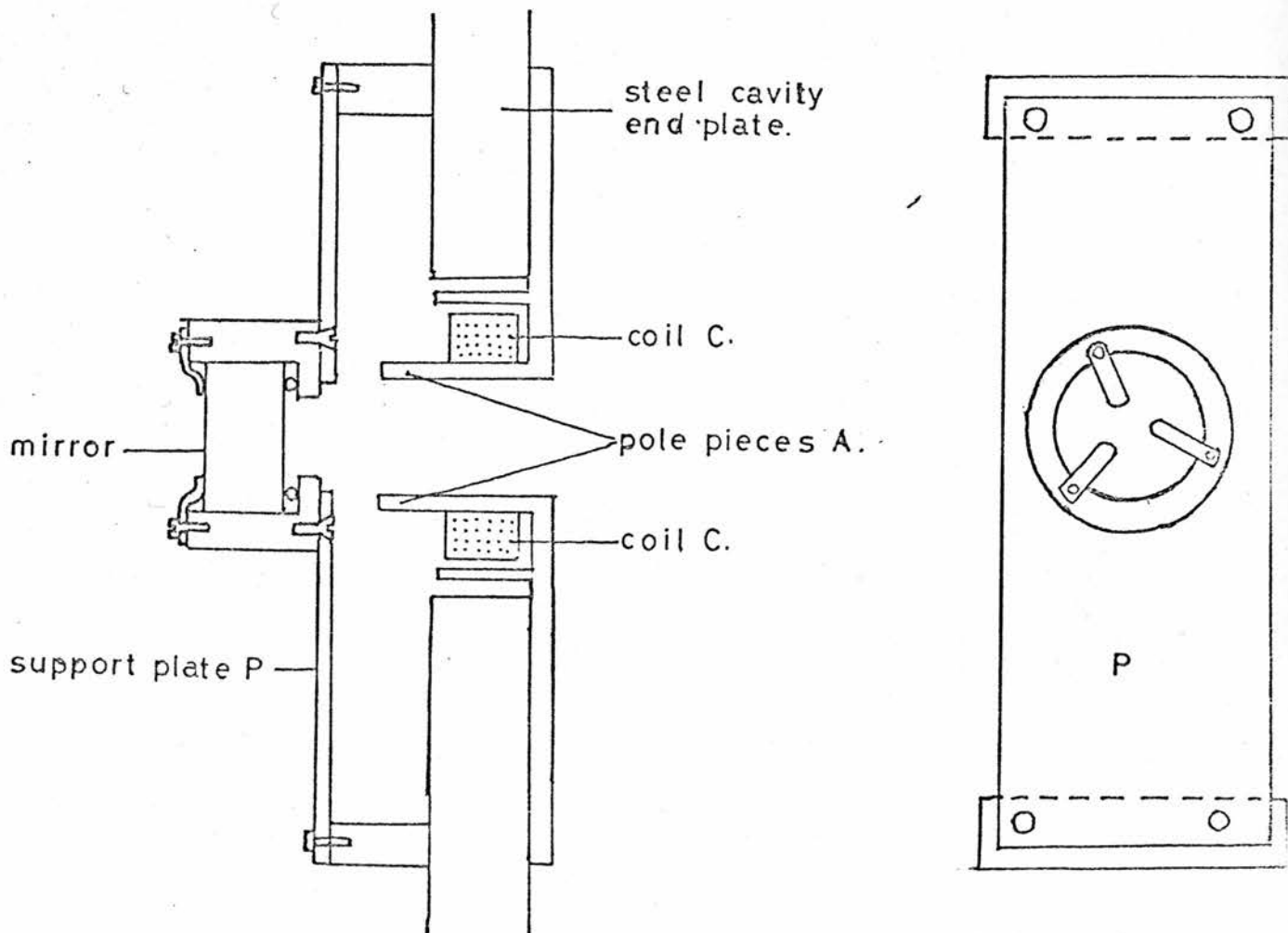


FIGURE 28b
MAGNETIC COIL DESIGN



bolted firmly on to the laser end plate. This allowed the easy interchange of mirrors without altering the cavity alignment.

2.4.2. Magnetic Length Modulators

The scanning coil arrangement is shown in Figure 2.8. b.

C are coils carrying a current supplied from an external stabilized voltage source. When a current flows through C the pole pieces AA attract the flexible steel plate carrying the mirror assembly. The plate P is rigidly fixed to the laser end plate at its ends, as shown in the plan view.

The advantage of this type of length changing mechanism is that the voltage sensitivity is far greater than the piezoelectric system and much lower voltages may be used. This gives the magnetic method a far greater dynamic range. The system is, however, microphonic, and has resonance frequencies around 600 Hz. It is also limited in speed but this depends on the amplitude of movement required and modulation frequencies up to 500 Hz may be used with optical modulation bandwidths of some tens of Megahertz.

2.4.3. AC Sensitivity of coil arrangement

The sensitivity of the coil, which had an impedance of 250 ohms, was measured for AC using a simple beat frequency experiment. In this experiment, the coil was again mounted in a laser cavity 800 mm long, having a free spectral range of 186 MHz. The TEM₀₀ mode laser output was mixed with the output from an Elliott HNL6 stabilized laser. This laser was a 15 cm long Lamb Dip stabilized laser, but the stabilization loop was not closed in these experiments. Under these conditions the laser was unmodulated and frequency drifts of a few MHz in several seconds were observed on an optical spectrum analyser.

The experimental arrangement, constructed on a vibration isolated table, is illustrated in figure 2.9. The laser output wavefronts were modified, using lenses L_1 and L_2 to give similar curvature, spot size and divergence and then were superimposed on the beam splitter BS. The beams were then detected on a fast Hewlett Packard 4220 PIN photodiode with a response time less than one nanosecond. The beat frequency spectrum from 0 - 100 MHz. was displayed on a Hewlett Packard Spectrum Analyser. The width of the beat frequency envelope with no modulation on either laser was less than 3 MHz.

When modulation from an oscillator was applied to the scanning coil the beat frequency envelope as observed on the analyser increased, and the peak to peak value of this width was taken to be the peak to peak frequency modulation applied to the laser. The beat frequency width for a fixed amplitude AC as a function of applied frequency for a DC bias of 8.85 volts is shown in figure 2.10. The curve shows a flat region around 300 Hz. and then

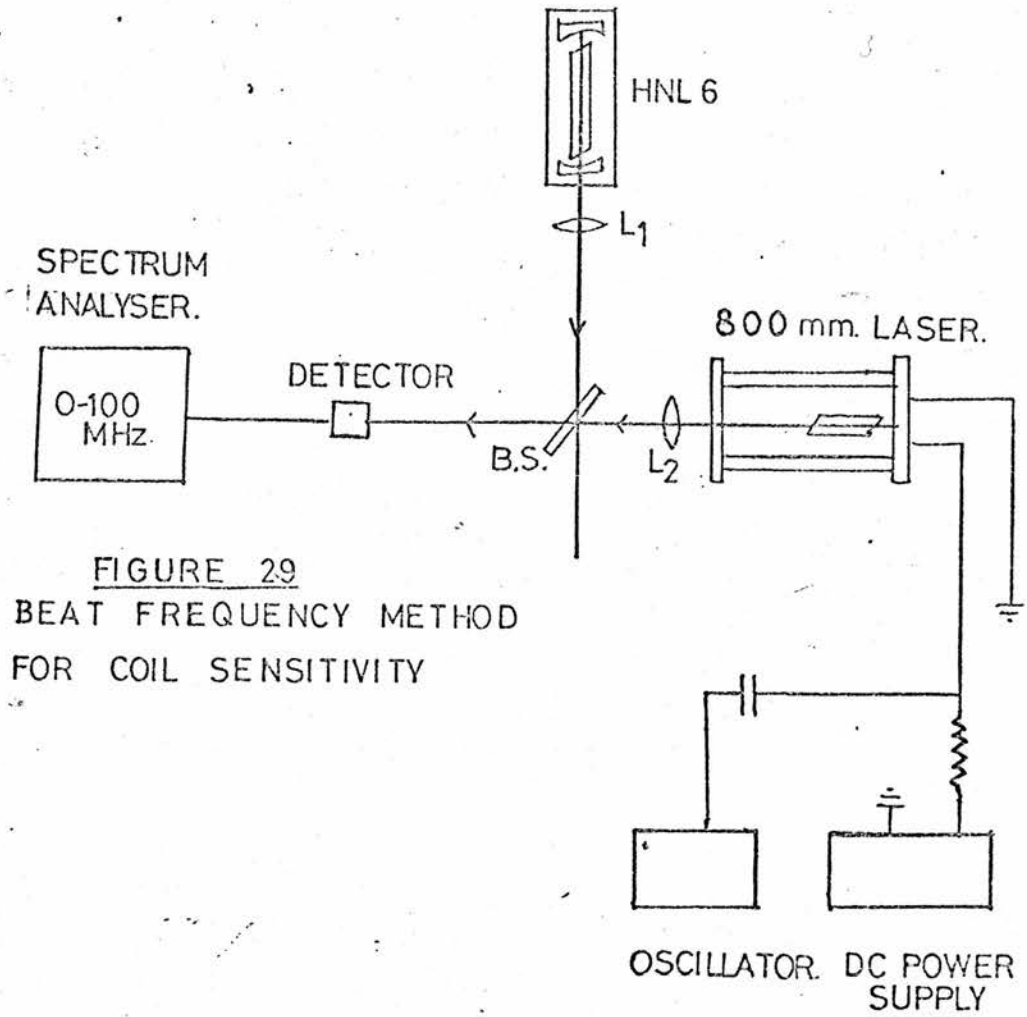


FIGURE 2.9
BEAT FREQUENCY METHOD
FOR COIL SENSITIVITY

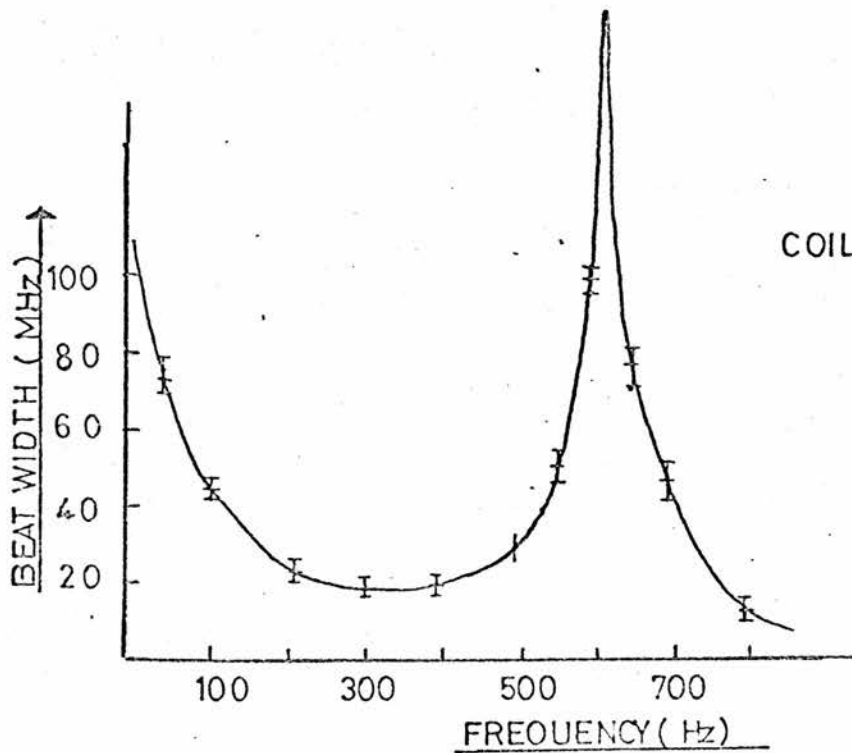


FIGURE 2.10
COIL SENSITIVITY PLOT

risers to a resonance at 600 Hz. This resonance is attributed to mechanical features of the mounting and is typical of scanning coil arrangements. The plateau is a suitable region for use in modulating the laser; frequency drifts in the oscillator have little effect on the resulting modulation width.

The AC sensitivity for a fixed DC bias and AC peak to peak amplitude was measured for several different frequencies and the results shown in Figure 2.11. The sensitivity appears to be linear over the voltage range investigated.

2.4.4. D.C. Sensitivity of the coil arrangement

The d.c. sensitivity of the scanning coil was measured using the optical spectrum analyser described in section 2.6. The output of the analyser was displayed on an oscilloscope, and the trace sensitivity calibrated to give a dispersion of one free spectral range of the analyser head (2GHz.) for ten divisions on the oscilloscope graticule. The scan coil was mounted in an 800 mm. long laser cavity which had a free spectral range of 186 MHz. and which was operated in the TEM_{00q} mode. It was possible, as Figure 2.9. shows, to apply both a d.c. bias and an a.c. modulation to the scanning coil. A change in d.c. voltage causes the cavity length to change and the mode display on the screen was observed to move. The d.c. sensitivity is plotted in Figure 2.12. in orders of movement of the cavity. If a voltage change causes the cavity to change in length by one half wavelength, the $(q + 1)$ th mode, as observed on the screen, moves in frequency to that of the q th mode. The voltage necessary to tune a particular mode to the position of its nearest neighbour was, therefore, that for a change in cavity length of one order. The curve of Figure 2.12 is seen to be linear after some 7 volts are applied to the coil, and it was with this level of d.c. bias that all a.c. modulation experiments were conducted. Clearly, operation of the scanning coil arrangement for d.c. bias levels lower than this value would lead to nonlinearities in the scan.

2.4.5. Piezoelectric Sensitivity measurements

A.C. sensitivity measurements for a $1\frac{1}{2}$ " tube of PZT 5A mounted on a 30 cm. long laser were made directly on an optical spectrum analyser display. The display had a calibrated dispersion of 5 MHz/cm.

The laser was subsequently used in the iodine saturated absorption measurements and was well shielded from atmospheric fluctuations and vibrations. It possessed a frequency stability of better than 1 MHz. over a few seconds thereby enabling these measurements to be made. The long laser used in the scanning coil experiments did not possess sufficiently good short term stability to permit an a.c. sensitivity measurement of this kind. An A.C. signal of 2.6V peak to peak amplitude from a tunable oscillator was fed directly on to the piezoelectric cylinder and the resulting frequency modulation, as

FIGURE 2.11
AC SENSITIVITY OF COIL

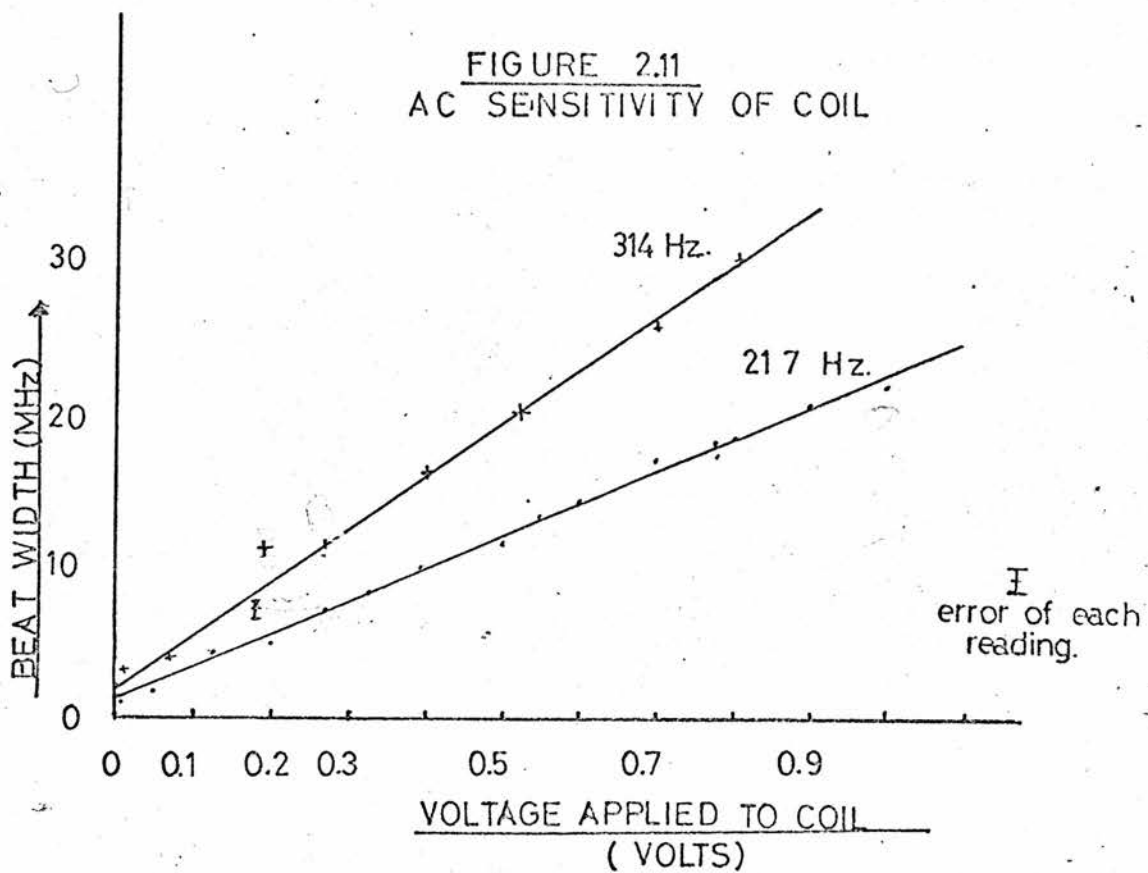
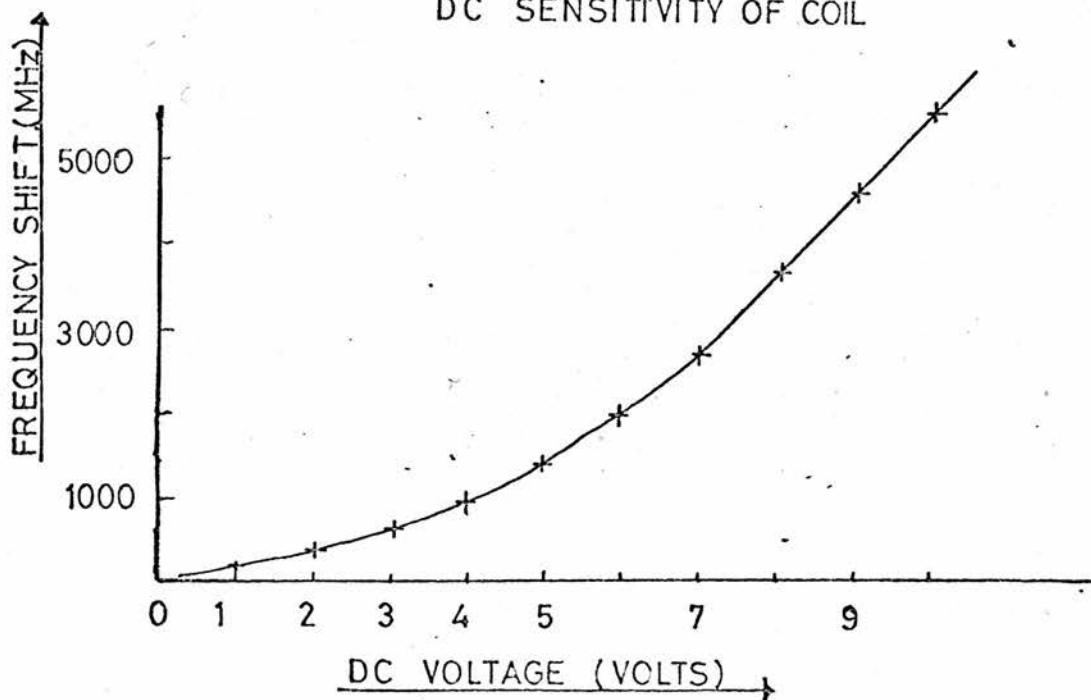


FIGURE 2.12
DC SENSITIVITY OF COIL



observed on the optical spectrum analyser display was plotted as a function of frequency (Figure 2.13) The Figure shows small fluctuations until mechanical resonances at 2.5 KHz. and 7KHz. are reached.

A typical piezoelectric has a measured capacity of 7 nanofarads. For frequencies over 10 KHz. the piezoelectric impedance drops. Current is drawn from the oscillator which distorts and reduces its output voltage. The series of resonances around 10 KHz. are typical of most measured mounted piezoelectric cylinders. The zero frequency intercept agrees well with the calculated d.c. sensitivity of PZT5A.

The variation of modulation bandwidth with a.c. peak to peak voltage was also measured for a series of frequencies near 1 KHz. The results showed a linear dependence of beat width upon a.c. voltage.

The DC sensitivity may be calculated from equation 2.1. and is 3.1 MHz/volt. This sensitivity was checked by applying known voltage steps to the piezoelectric and measuring the frequency change of the laser as observed on the optical spectrum analyser display.

Two possibilities exist when one is deciding upon the modulation frequency, which should be as high as possible to enable wide bandwidth servo loops to be designed (Section 2.8). One possibility is to modulate on a piezoelectric resonance. This produces a scan of displacement to applied voltage, more linear than that obtained by off-resonance modulation. However, the presence of steeply varying phase shifts around a resonance is detrimental and would lead to a reduction in signal to noise ratio of the stabilization discriminant. For this reason, off resonance working was preferred - particularly for the third harmonic techniques (49) as precise reference phase setting and stability was necessary to ensure good detection of the iodine absorption features.

In normal conditions, the laser was modulated near 1 KHz.

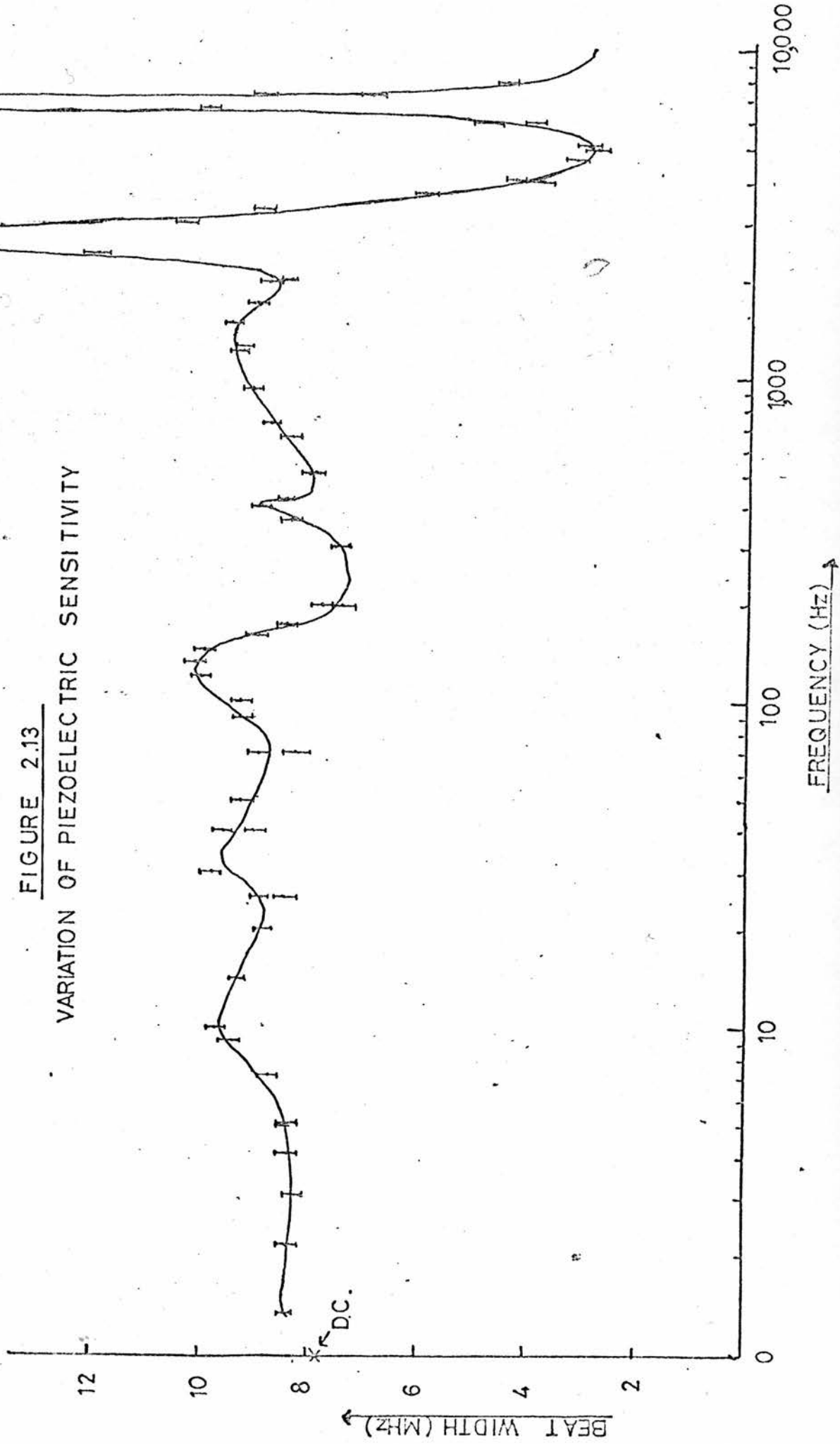
2.5. Antivibration Mountings and Temperature Control

All the experiments were carried out on an antivibration mounted table. This was a 6' x 4' steel table built on a large concrete plinth set into the foundations of the building. The table top was isolated from the plinth and table legs by a spring and damper arrangement and, as a result, the whole arrangement had a resonant frequency for vertical vibrations of a few Hz. The lasers were protected from draughts and acoustic noises by simple plastic screens and dust screens surrounding the space between the mirrors and laser windows.

The laboratory temperature was controlled by a system which maintained the room temperature at $22^{\circ}\text{C} \pm 0.1^{\circ}\text{C}$.

Section 4.5. discusses the effects of vibrational noise on the laser output.

FIGURE 2.13
VARIATION OF PIEZOELECTRIC SENSITIVITY



2.6. Optical Spectrum Analysis

A short confocal scanning Fabry-Perot spectrum analyser manufactured by Spectra Physics Ltd., was used to observe the frequency spectrum of the laser. The analyser head consisted of a piezoelectric ceramic tube with a high reflectivity mirror at each end. The free spectral range of the instrument was 2 GHz. and its instrumental linewidth 10 MHz. full width at half height. This results in a finesse of 200. The instrument was scanned using a sawtooth waveform of variable switched amplitude, corresponding to variable frequency scan width.

The same sawtooth of full amplitude was applied to the sweep input of an oscilloscope and hence the oscilloscope was scanned synchronously with the laser. The output of a photo-detector placed on the opposite side of the analyser head from the laser was suitably amplified and displayed on the vertical scale of the oscilloscope. When the laser and analyser were aligned, the Fabry Perot transmitted light each time its transmission resonance came into coincidence with a laser mode. The photodiode developed a voltage across its load resistor which was displayed as a vertical spike with the Lorentzian lineshape of the Fabry Perot transmission band. In this way the optical spectrum of the laser could be observed. Figure 2.14. illustrates typical spectra for a laser operating in the TEM₀₀ mode and one exhibiting off axis modes.

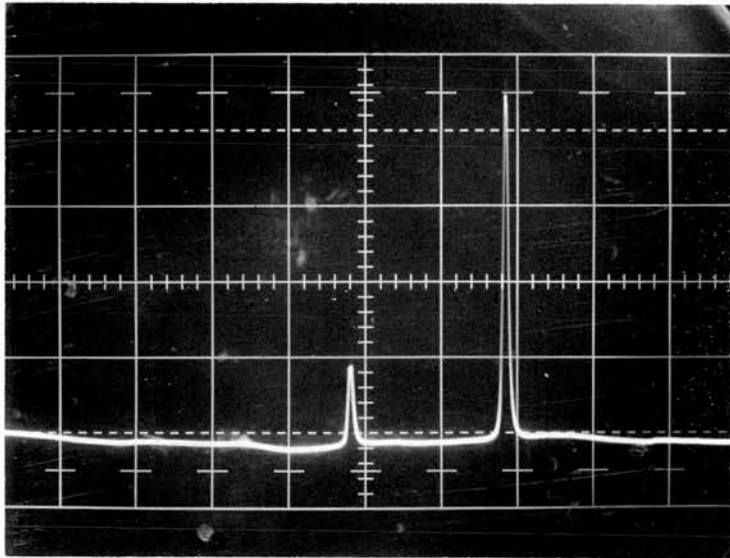
The scan amplitude to the analyser head may be switched in precalibrated steps thereby displaying sections of the total scan. A DC level control was also available on the analyser piezoelectric thereby enabling the analyser scan to be tuned to any region of the laser linewidth.

The confocal scanning interferometer has degenerate off axis and axial modes. No spurious resonances exist on the displayed spectrum, and alignment is easier than with non-confocal systems where the laser wavefront must be mode-matched to fit the fundamental mode of the interferometer.

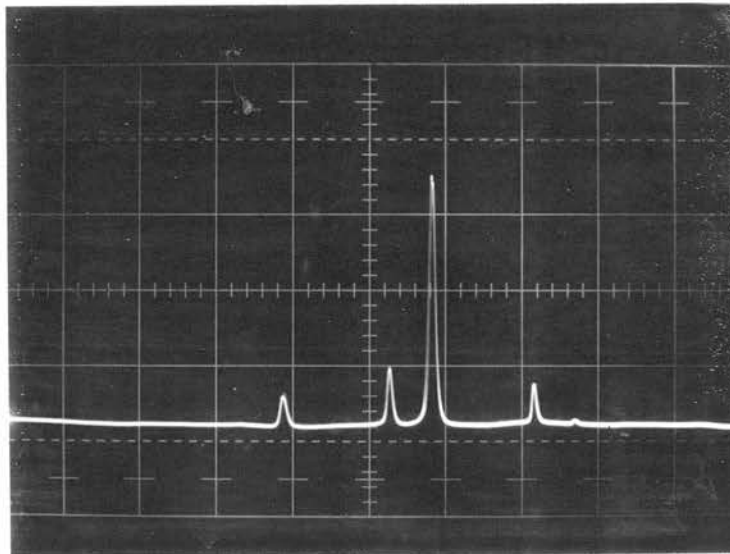
2.7. Beat Frequency Measurement

This technique enables careful measurements to be made on the performance of stabilized lasers. The outputs of two lasers under study are mixed together, generating both sum and difference frequency components. The sum frequency is also in the optical range, but the difference, for well stabilized lasers, falls into the radio or audio frequency range and therefore may be examined in a conventional frequency analyser system.

In practice, the arrangement shown in Figure 2.15. was used. The two lasers L1 and L2 are placed at right angles, thereby ensuring that each may be thought of as responding independently to mechanical or acoustic disturbances.



OPTICAL SPECTRUM ANALYSER DISPLAY OF A LASER OPERATING IN A TEM_{00q} MODE. THE DISPERSION IS 200 MHz. PER cm.



DISPLAY OF A LASER OPERATING WITH AN OFF AXIS MODE

FIGURE 2.14
OPTICAL SPECTRUM ANALYSER DISPLAYS.

The output wavefronts of the two lasers must be made equal in size and curvature at the mixer which is a beam splitter B. This criterion is necessary to enable maximum superposition of the beams which leads in turn to maximum interference or beat frequency signal. The output from one side of the beam splitter may be detected by a nanosecond response photodiode D_1 amplified, and then displayed from 0 - 100 MHz. on a Hewlett Packard model 8551 - R.F. Spectrum Analyser. The displayed beat frequency indicates the frequency difference between the two lasers; the width of the beat indicates the stability of the difference frequency over short time periods, and any movement of the centre frequency indicates the long term instability of the lasers.

The fundamental beat frequency arrangement was originally developed by D.C. Wilson and W.R.C. Rowley of N.P.L., to produce reversible beat frequency measurements. A reversible frequency counter displays the beat frequency at one second intervals with a one second integration time. An analogue output, linearly proportional to the beat frequency is also provided. Crucial to the system is a metallic coating on the beam splitter which produces phase quadrature beat frequency signals which are detected by diode D_2 thus enabling reversible counts to be made. This system has been extensively discussed in the literature. (42).

The reversible nature of the measurement, originally developed for fringe counting interferometry, is especially useful for lasers which are operating within a few MHz. of each other. The beat frequency from such well stabilized lasers makes excursions on either side of zero frequency; the lasers fluctuate relative to each other so that laser 1 is sometimes higher and sometimes lower in frequency than laser 2. Without a reversible system, study of this important aspect would not be possible. A logic unit provides information about this alternation in beat frequency and enables an analogue output to be derived which reverses polarity as the beat frequency passes through zero frequency. The analogue output then carries information to the counter which also indicates the polarity of the count.

A block diagram of the apparatus, together with its display features, is incorporated in Figure 2.15.

A typical beat frequency spectrum is shown in Figure 2.16. Two iodine stabilized lasers were separately locked to the adjacent components d and e, and the 13 MHz. beat frequency observed as described above. The peak at -4 on the horizontal scale is the zero frequency marker and the vertical sensitivity is 10 dB /division. The figure shows the spectrum at a dispersion of 2 MHz. per square indicating the beat centred on 13 MHz., with a

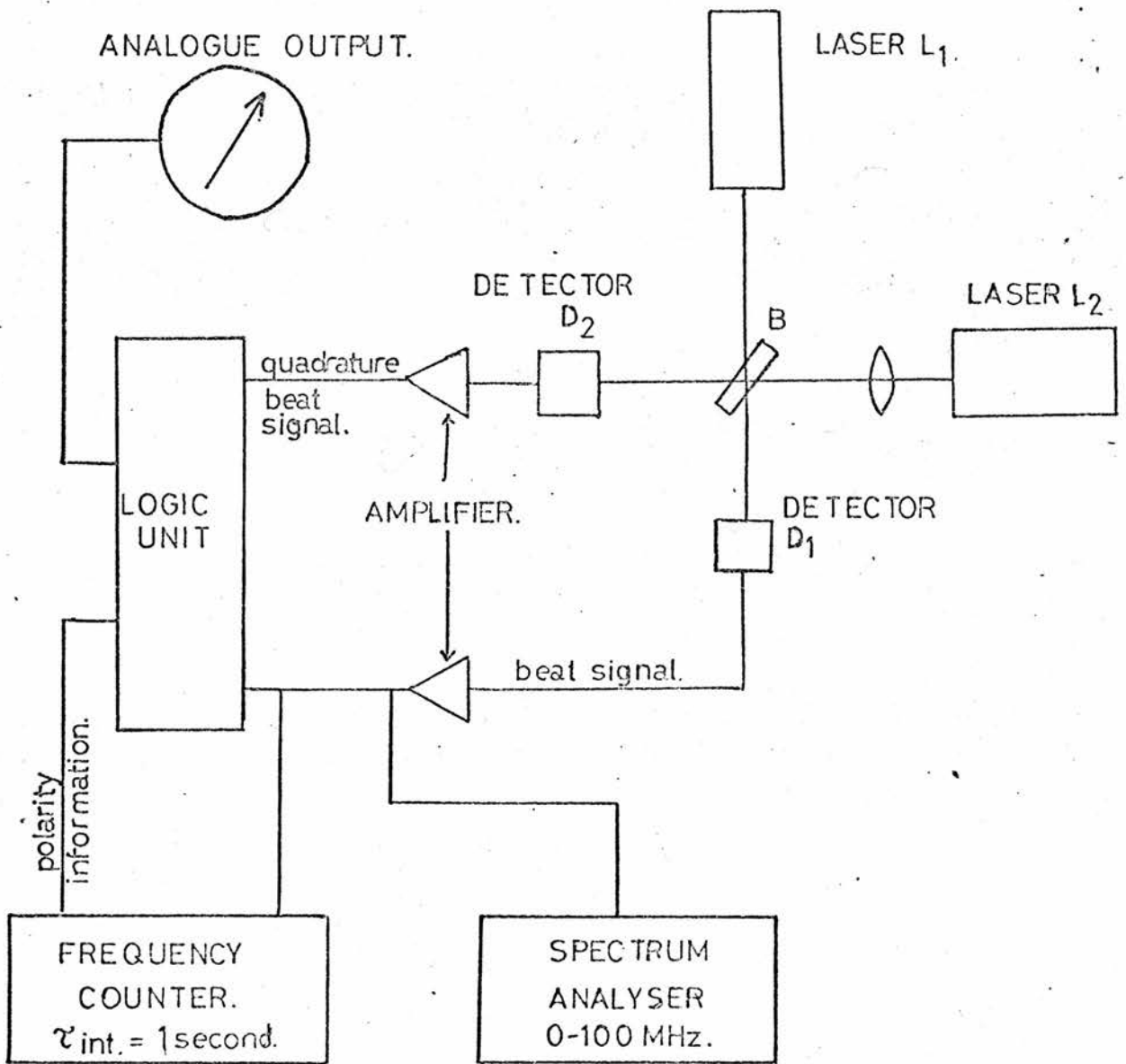


FIGURE 2.15
BEAT FREQUENCY APPARATUS.

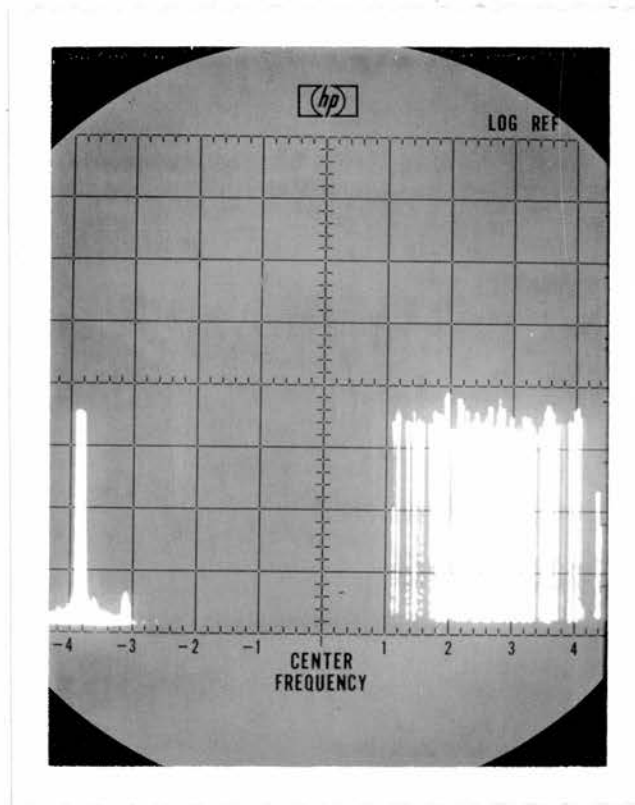


FIGURE 2-16

BEAT FREQUENCY DISPLAY OF A 13 MHz BEAT BETWEEN TWO LASERS. ZERO FREQUENCY IS AT -4 ON THE HORIZONTAL AXIS, WHICH HAS A DISPERSION OF 2MHz PER DIVISION.

width of some 3 MHz. This width is largely dominated by the frequency scan imposed on the lasers.

2.8.1. Servosystem Design

The basic concept of any servosystem embodies four features

1. An oscillator to be stabilized.
2. A reference frequency to which the oscillator may be constantly referred.
3. An electronic system which provides a voltage proportional to the offset between oscillator and reference frequencies.
4. A control element on the oscillator which changes a frequency sensitive parameter thereby retuning the oscillator to the reference.

Following the established principles of a feedback system in electronic amplifiers, the closed loop transfer function C of such a feedback system is:

$$C = \left[\frac{A}{1 + A} \right] R \quad (2.2.)$$

Where A is the open loop gain and R is the input signal.

The system error E is given by:

$$E = R - C = \frac{R}{1 + A} \quad (2.3.)$$

The object of a servosystem is to minimize E by making A extremely large, perhaps 10^3 or more over a large frequency range. Also, the phase shift introduced by A must not allow the system to oscillate, and so must be maintained below 180° for all values of A greater than or equal to 1.

In a laser control system R is the spectrum of environmental disturbances which perturbs the laser frequency, C is the servosystem response and E is the residual frequency instability of the laser due to the finite input R . In general, R is small at high frequencies, where acoustic effects are dominant and is large for low frequencies, where slow thermal drifts are important. Ideally the response of the system should be tailored to the environmental disturbance frequency spectrum.

The standard technique in deriving an error signal, or discriminant, (for lasers stabilized to some peak or dip feature in the power output tuning curve), involves modulating the laser at a frequency ω and detecting the resultant intensity modulation. This produces an A.C. signal which varies in amplitude as the laser frequency is tuned across the feature and which reverses in phase at the centre. Phase sensitive detection is then carried out on this intensity modulation at a reference frequency ω . The D.C. smoothed output of the phase sensitive detector (psd), as the laser frequency

is tuned over the frequency range of its discriminant, is shown in Figure 2.17. This shows an "S shaped" discriminant typical of laser stabilization systems which is positive on one side of the discriminant centre, is zero at the centre and is negative on the opposite side. If this voltage, representing a frequency detuning from line centre, is fed back to a length controlling element in the laser structure in the correct phase, then the laser will continually be returned to zero psd. output, that is to the centre of the peak or dip.

The stability of the resulting stabilized laser frequency may be affected by three classes of perturbation which are

- i) The laser frequency may be perturbed by electronic noise from the light detection system, usually a photocell, or from the input stage of the first amplifier. If the laser intensity fluctuates, then perturbations similar to these will occur.
- ii) The D.C. output stage of the final servosystem amplifier may drift and will lead to frequency instabilities
- iii) If the laser cavity drifts or is affected by vibrations the servosystem responds to this source of instability. A similar effect arises from voltage fluctuations on the piezoelectric length control element.

The performance of the laser servosystem will vary depending on which of the three noise sources perturbs the laser frequency. An analysis of a typical servosystem response to these fluctuation sources may be carried out using the circuit representation shown in Figure 2.18.(43)

We shall represent three noise sources by x , y , and z . The position of these in the servosystem indicates their origin: x refers to noise in the photocell and input amplifier, y represents the effects of amplifier D.C. drift, and z the effect of cavity length fluctuations. Voltages b , c , d , and e represent the total voltage measured at that point in the circuit. The amplifier gain $-A$ will be assumed to be independent of frequency. The simple R - C filter shown has the filter response function

$$d = \frac{c}{1 + i\omega\tau} \quad \text{where} \quad \tau = RC \quad (2.4)$$

The performance of the laser is specified by B which is the ratio of photocell output to applied PZT voltage. The laser output is proportional to the input and is not frequency dependent. Typical photocell output changes are a few millivolts for a change in PZT voltage of a volt, resulting in B values of about 10^{-3} .

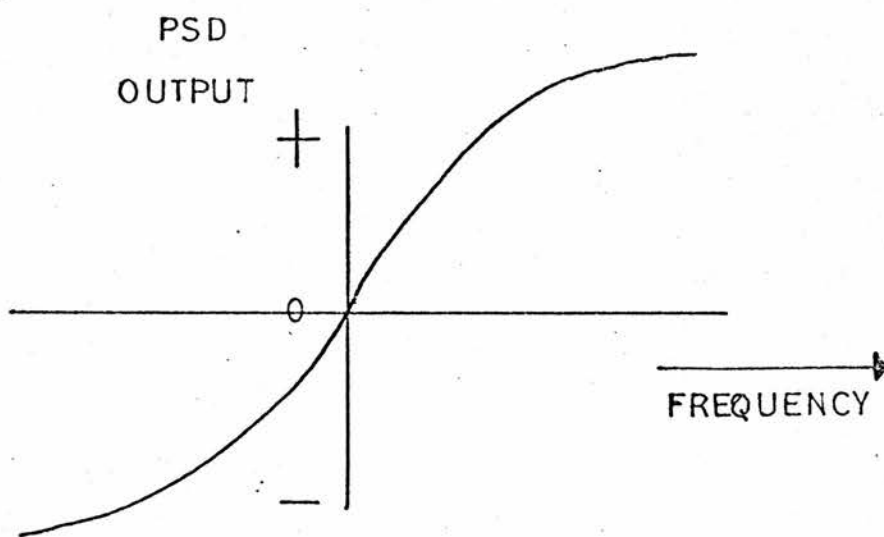
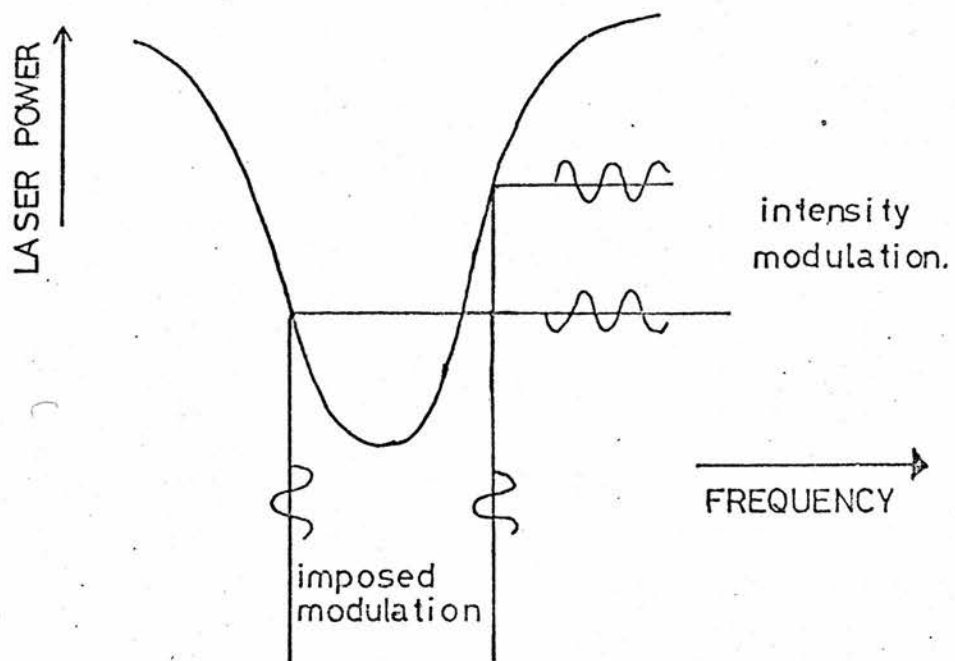


FIGURE 2.17

DISCRIMINANT FORMATION

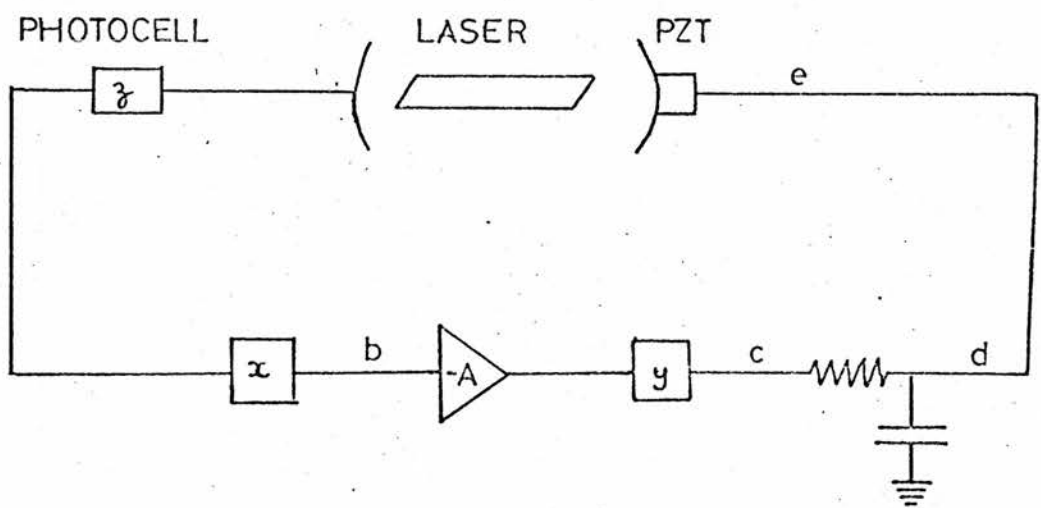


FIGURE 2.18

SERVO SYSTEM ANALYSIS.

The performance of the system with regard to the three noise sources indicated is as follows:

i) Photocell noise

This is characterised by $y = z = 0$ and a finite value of x . In this case, for closed loop operation we find that the voltage on the piezoelectric is:

$$|e| = \frac{x A}{K(1 + \frac{\omega^2 \tau^2}{K^2})^{\frac{1}{2}}} \quad (2.5)$$

Where $K = 1 + AB$ and is known as the stabilization factor and is much greater than 1.

For d.c. variations, therefore, $|e| \doteq \frac{x}{B}$ and the low frequency response is independent of amplifier gain. At higher frequencies, the behaviour depends on the time constant (τ/K) which appears small thereby extending the noise spectrum to higher frequencies. This indicates that the system bandwidth for noise is larger than might be expected on the basis of the R.C. filter time constant alone. There is an advantage, therefore, in using low-noise electronics.

The alternative approach is to reduce K , the system gain. This is only possible if servosystem compensation for frequency fluctuations is not demanding. The laser must therefore be a very mechanically stable system. High modulation frequencies of about 1 to 10 KHz. would have the beneficial effect of operating the electronics in a low noise region.

ii) Amplifier Drift

We may investigate this by setting x and z equal to zero and investigating the system performance for finite y . In this case, the modulation on the laser resulting from this noise source is:

$$|e| = \frac{y}{K(1 + \frac{\omega^2 \tau^2}{K^2})^{\frac{1}{2}}} \quad (2.6.)$$

This expression reduces to y/K for slow drifts which are minimised if A is increased.

iii) Cavity Variations

This fluctuation is represented by a finite z value, and zero x and y values. The residual PZT fluctuations are, in this case, given by

$$|e| = \frac{z(1 + \omega^2 \tau^2)^{\frac{1}{2}}}{K(1 + \frac{\omega^2 \tau^2}{K^2})^{\frac{1}{2}}} \quad (2.7.)$$

For slow variations, the effect is reduced by the stabilization factor K which therefore must be large for good long term stability. Higher frequency fluctuations, such as may be encountered as audio frequency airborne vibrations are less efficiently compensated since the response falls off, as dictated by the factor $(1 + \omega^2 \tau^2)^{\frac{1}{2}}$, with a roll off corresponding to the time constant τ . To ensure good mechanical compensation, a high gain system is required and τ must be small to enable compensation to be made for fast fluctuations.

As a measure of the effectiveness of various control systems to laser cavity fluctuations (type iii variation) figure 2.19 shows a plot of $\left[\frac{Z}{|e|} \right]^2$ against the frequency of a perturbing fluctuation. The figure shows, therefore, the response of the system to fluctuations ranging from d.c. to 1 KHz. for the values of stabilization ratio and time constant plotted. The behaviour of the systems again shows that short time constants and large gain values produce the most efficient compensation networks and indicates the range of frequencies over which the servosystem compensates for perturbations.

The time constant evidently plays an important part in servo design. It smooths the p.s.d. output so that the resulting ripple on the piezoelectric tube controlling the laser length does not modulate the laser sufficiently to cause oscillation. In other words, the system response must be less than unity at the modulation frequency. Ideally, the frequency response should then be a step function rising from zero at the modulation frequency and have large gain down to zero frequency. This behaviour is not obtainable from any single filter and various suitable designs will be discussed below. Full wave rectification of the p.s.d. output is advantageous as this produces smaller ripple than half wave rectification. The use of square waves in the p.s.d. system also minimises ripple. The Brookdeal coherent filter is such a device, (brookdeal Electronics Ltd.) and servo systems using this principle are at present being investigated by the Gas Laser Section at N.P.L. Experimentally, a factor of 10 reduction in ripple from a simple R - C filter by a coherent filter square wave device has been observed.

2.9.2. Filter design

The simple R - C filter has a response

$$V_{out} = \frac{V_{in}}{(1 + i\omega\tau)} \quad (2.8)$$

where V_{out} and V_{in} are the output and input voltages respectively.

The time constant τ is the product RC.

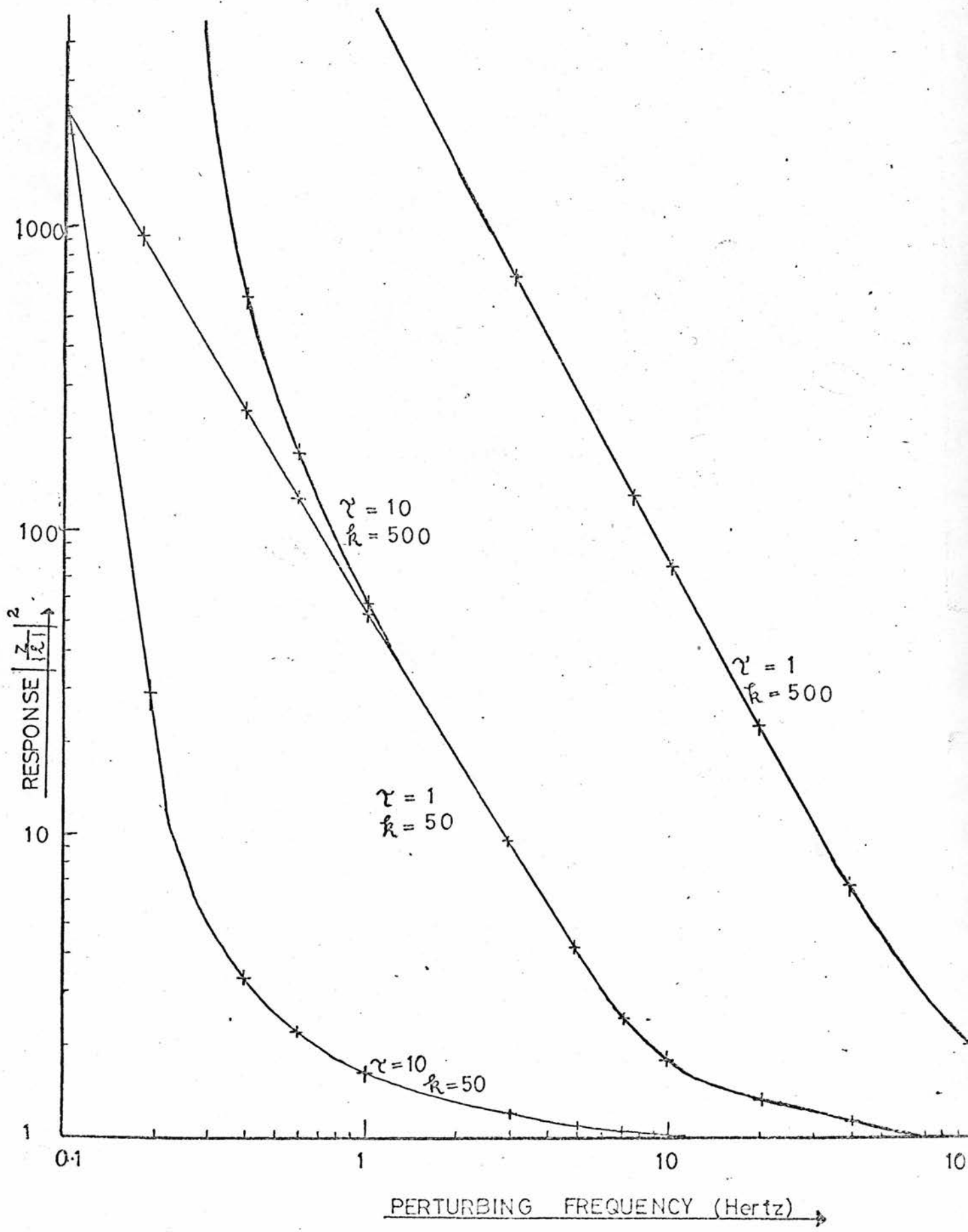


FIGURE 2.19

COMPUTED SERVOSYSTEM RESPONSE

The response of filters is characterised by a Bode Plot (44), where the gain of a filter in dB's is plotted on a logarithmic frequency scale. For an RC filter, this plot is level up to a value of $\omega\tau = 1$ and then rolls off at 6 dB per octave. The advantage of gain higher than the R - C filter may be achieved using the low pass circuit of Figure 2.20 which has the transfer characteristic:

$$V_{\text{out}} = -V_{\text{in}} \frac{R_2}{R_1} \frac{1}{(1 + i\omega\tau)} \quad \text{where} \quad \tau = CR_2 \quad (2.9)$$

Normally R_2 is much larger than R_1 . The low frequency gain is simply R_2/R_1 and at high frequencies, the roll off is that of a simple CR_2 filter. The filter has a low output impedance and so is largely unaffected by loading whereas the simple RC filter is affected by loading.

A more effective design still is that of the integrating filter. In essence it is similar to the low pass design discussed, but R_2 is vastly increased. The transfer function may be written:

$$V_{\text{out}} = \frac{V_{\text{in}}}{\left[\frac{R_1}{R_2} + i\omega\tau \right]} \quad \text{and} \quad \tau = CR_1 \quad (2.10)$$

Because R_2 is so large, the low frequency response of this type of filter is determined by the time constant CR_1 and not CR_2 as with the low pass filter. The performance, as described by a Bode plot, is shown in Figure 2.21. The integrating filter therefore has much larger low frequency response leading to small frequency offsets of a locked laser and a similar high frequency response to that of the low pass filter. Roll off is again at 6dB per octave.

It is possible to design filter systems employing integrator units with 9dB per octave high frequency roll off. These systems have the advantage of large d.c. gains and can extend the corner frequency typical of the low pass filter to higher frequencies, whilst still having a gain of less than unity at the modulation frequency. A servo system using an integrating filter is a type 1 servosystem; that with a simple RC filter is a type 0 system. For the type 0 system, the voltage driving the piezoelectric tube is proportional to the error signal voltage and the steady state error is finite for a step function input. The system cannot cope with a ramp input function, that is long term drifts. With a type 1 system, the voltage is proportional to the time integral of the error signal; the steady state error is identically zero for a step function but is finite for a ramp input. The best sort of

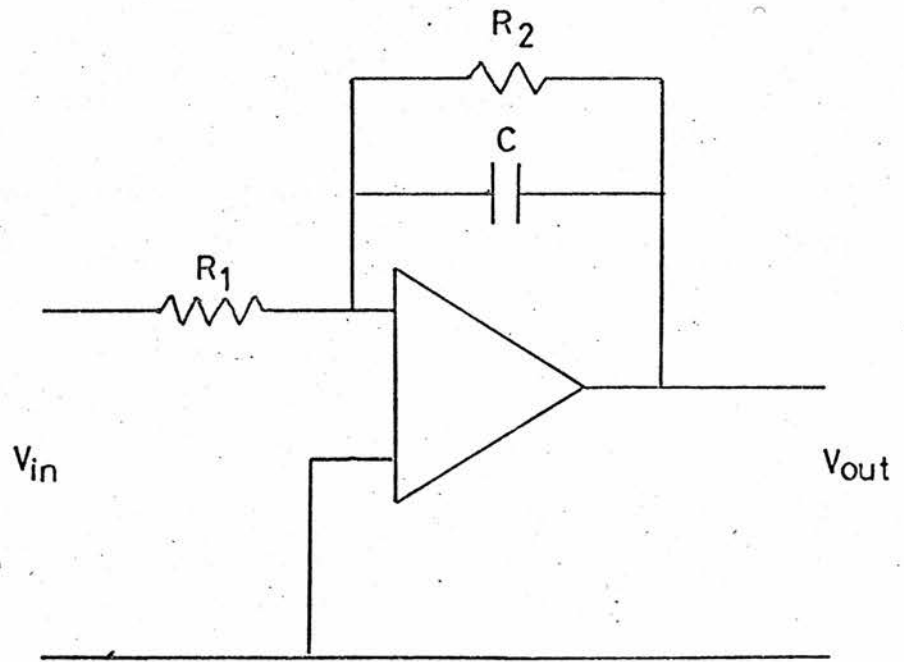


FIGURE 2.20
LOW PASS AND INTEGRATING FILTER.

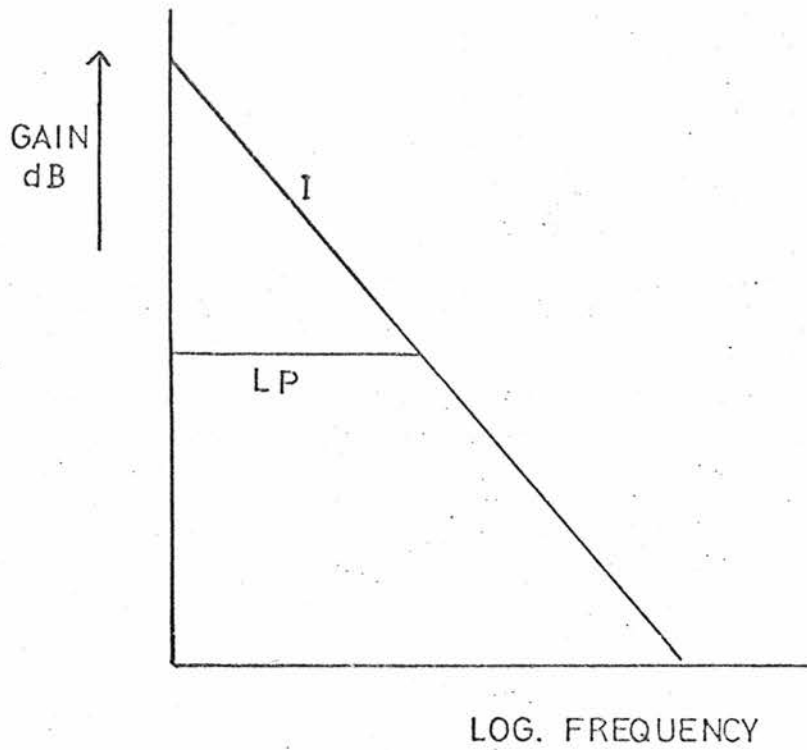


FIGURE 2.21

BODE PLOT FOR INTEGRATING (I) AND LOW PASS (LP) FILTERS.

servoloop, therefore, combines both of these features and has been incorporated in recent N.P.L. designs. Long time constant integrators are used to give large D.C. gains, with short time constant 9dB roll off filters to extend the variation compensation to higher frequencies which approach the modulation frequency.

CHAPTER 3SATURATED ABSORPTION THEORY3.1. Introduction

In this chapter, no attempts are made to formulate a theory for the saturated absorption effect, as this aspect of the work has been closely studied by other workers (45, 46, 47, 48). The early sections will set out a phenomenological description of the effect related to rather more well known phenomena such as the Lamb Dip and gain saturation.

Aspects of the saturated absorption technique which are discussed in greater detail are concerned with the widths of the features used for stabilization (section 1.1.) Ideally, the feature should be well formed and narrow. The first of these qualities enables the feature to be observed without a great deal of signal averaging. This leads to the use of short time constants in a servo loop, which enable fast perturbations on the laser frequency to be counteracted. The width of the feature determines the control range of the discriminant, or error sensing lineshape of the phase sensitive detector. This ensures a rapidly changing curvature near the line centre. A fast laser frequency movement therefore produces an immediate response with a large error signal from a small frequency shift.

These qualities impose two particular demands on the laser:

i) The laser intensity must be stable, in other words, the output should be noise free. The absorption features are small and frequently are lost in the laser noise. This implies that signal averaging is necessary to observe the feature, and to minimise this, a low noise laser system is desirable. In Chapter 1, the natures of various perturbations have been discussed, together with the steps taken to reduce them. Chapter 4 discusses a further noise source, that of instability due to plasma fluctuations. (Section 4.5)

ii) The frequency stability of the laser without any compensation is to be as low as possible to ease the demands on the control system; the free running fluctuations should not be more than the control width of the discriminant. Several workers have made considerable efforts to reduce these fluctuations (49, 50). The simple precautions discussed in Chapter 1 have been taken, but no sophisticated scheme was used here. Behind this was the philosophy that this development of an iodine stabilized laser was directed towards achieving the ultimate from a simple construction. This could be easily constructed by all research workers, and not just those in certain select national standards laboratories.

3.2. The Lamb Dip

As the frequency of a single mode single neon isotope helium-neon laser is tuned over the range of available oscillation frequencies a dip is observed at the centre of symmetrical power output curve. This is the Lamb Dip, a feature which was predicted theoretically by W.E. Lamb (4). The physics of this effect is well known: the dip is formed from the super-position at the centre of the gain curve, of the two Lorentzian shaped holes burned into the gain curve by the cavity electric field. Four points should be emphasised with reference to the Dip.

i) The hole width for some arbitrary detuning is, in the case of inhomogeneously broadened lasers, the natural width broadened by collisions, cross relaxation and power broadening effects. The width of the Lamb Dip is independent of Doppler Broadening effects and, in practical cases, is some 200 MHz. wide for 633 nm. He - Ne lasers.

ii) The dip width, as observed in the power output curve, is the homogeneous width of the transition and not twice it, as frequently and erroneously appears in published literature. The misconception arises from the idea that the convolution of two Lorentzian holes of width δ is also a Lorentzian of width 2δ . This is indeed true, but the crucial fact is that, as these two holes approach line centre, the apparent rate of approach doubles so that the observed power decrease has a width δ .

iii) The depth of the dip depends on the ease with which the gain medium may be saturated and may be characterised by a saturation parameter S . This, for inhomogeneously broadened media, is the power density at which the gain is reduced to $1/\sqrt{2}$ of its unsaturated value. A small value of S reflects the ease with which a laser medium may be saturated. For helium neon lasers, S has a value of about 2 watts per cm.² and the Lamb Dip is usually 5% - 10% of the total power. The value of S decreases with decreasing pressure, and so low pressure operation encourages a greater depth of saturation.

3.3. Saturated Absorption

Let us consider a cell of absorbing vapour placed inside a laser cavity. The absorption line width will be a sum of contributions from:

i) Doppler broadening due to the random motion of the absorber particles.
 ii) Collisional broadening due to collisions between absorbing particles which decrease the excited state lifetime.

iii) Power broadening, Stark and Zeeman Effects, and spontaneous or induced dissociation.

In normal circumstances encountered in typical absorbers, Doppler broadening is dominant; and for iodine vapour at room temperature, the line width is about 300 MHz.

Because of the standing wave nature of the strong electric field inside the laser, when a single frequency laser is tuned over the absorption profile the absorption saturates and a hole burning process in absorption occurs. At line centre, a Lamb Dip in absorption occurs and the width of this dip is determined by the homogeneous linewidth just as for a Lamb Dip in emission. Doppler broadening is eliminated, and we find that the line width of a saturated absorption Lamb Dip in iodine is about 4 MHz. This is about two orders of magnitude narrower than the emission Lamb Dip used in frequency control schemes.

In the case of absorption in the iodine molecule, the centres of several hyperfine components of the absorption band fall within the tunable range of the He - Ne laser. Each of these components, separately, produces a dip in absorption as the laser is tuned to the centre of the particular component, and each dip produces a corresponding increase in laser power at that point. It is to the centre of one of these peaks that the laser frequency is servo-controlled.

Several saturated absorption coincidences have now been discovered and are listed in Appendix I.

3.4. Linewidth of the saturated absorption features

In the above discussion, the width of these features was stated to be determined by the homogeneous width. In fact there are several contributions to the linewidth which are not usually encountered in this region of the spectrum and which are characteristic of saturated absorption effects.

3.4.1. Natural Linewidth

The natural linewidth of a transition may be thought of as arising from the finite time of the photon emission process between the two levels involved. The spectral linewidth of this radiation is Lorentzian in form and gives rise to the broadened linewidth described by:

$$I(\nu) = I_0 \frac{\gamma}{2\pi (\omega - \omega_0)^2 + \frac{\gamma^2}{4}} \quad (3.1)$$

Here I is the intensity of the line at an angular frequency ω from its centre frequency ω_0 where the intensity is I_0 .

The parameter γ is the halfwidth of the line at half intensity and is related to the lifetime τ by $\gamma = \frac{1}{\tau}$.

This last relationship may be obtained from quantum mechanical considerations by applying the Heisenberg Uncertainty Principle $\Delta E \Delta t \sim \hbar$ to a transition between two energy levels which has a lifetime τ .

$$\begin{aligned} \text{We write:} & \quad \Delta E \tau \sim \hbar, \\ \therefore & \quad \hbar \Delta \omega \tau \sim \hbar, \\ \therefore & \quad \Delta \omega \sim \frac{1}{\tau}. \end{aligned}$$

This lifetime is the reciprocal of the spontaneous transition probability.

In the case of the iodine lines investigated in this thesis, the lifetime of the upper level largely determines the linewidth of the absorption line as the lower level is the molecular ground state. The most recent measurements of the single ν' = 11 level of the B excited state indicate a lifetime of $410 \pm 15 \times 10^{-9}$ seconds giving a linewidth of 390 KHz. F.W.H.M. (69)

Other lifetime measurements have been made. (70, 71, 72)

The experiments of Sakurai (72) et al. involved the use of a tunable dye laser as a pumping source and it is likely that their results were for a blend of vibrational levels. They found a lifetime value of 1.5×10^{-6} seconds giving a F.W.H.M. of 105 KHz.

3.4.2. Interaction Linewidth

The molecules contributing to absorption at the Lamb Dip are those moving transversely to the laser axis, in other words, those with zero longitudinal velocity. During the interaction, a molecule moving with velocity V travels across the laser beam and spends a time t within it. If the width of the beam is $2a$ then $t = \frac{2a}{V}$. Because of this time spent in the beam, there is a contribution $\Delta\nu = \frac{V}{2\pi a}$ to be observed linewidth. For an order of magnitude calculation for iodine molecules, V may be taken as the thermal velocity which is about 25×10^2 cm. per second at room temperature. For a beam diameter of 2 mm. we therefore have an interaction linewidth of approximately 40 KHz. or 1 part in 10^{10} of the laser frequency. This linewidth may be reduced either by cooling the iodine or increasing the beam diameter. The first possibility reduces the absorption of the iodine and hence would require the use of a longer absorption cell therefore necessitating an increase in laser length with the associated problem of ensuring single mode operation. Methods for increasing the beam diameter fall into two groups. A simple approach to the problem is to choose the mirror curvature such that the mode shape is at its widest in the iodine cell. A suitable configuration for the 30 cm. long laser is a flat mirror at the gain tube end and a 60 cm. radius mirror at the absorption tube end. The beam spot size, w , at the flat mirror, is 0.05 mm. and at the 60 cm. mirror is 0.11 mm. This configuration, unfortunately, reduces the mode volume from the larger volume generated by two long radius mirrors and so reduces the laser power and the degree of saturation of the absorption. For two 1 metre radius mirrors, the spot size at the mirrors is about 0.09 mm. For this laser, then, the spot size varies only a small amount throughout both tubes; the waist of the mode, w_0 is 0.08 mm. Variations of mirror curvature do not, therefore, have a noticeable effect on the interaction linewidth. Changes in beam diameter of a factor in excess of two are really

needed to make a significant difference. This leaves two courses of action, both of which have been exploited experimentally.

With high power single mode lasers such as CO_2 around $10 \mu\text{m}$. or the $3.39 \mu\text{m}$. radiation from a He - Ne laser, saturated absorption may be observed in tubes external to the laser cavity by an arrangement which reflects back the light beam which has come from the laser. In these experiments the light from the laser is shone through an external cell then reflected back almost along the same path. The return beam is then reflected on to a photodiode. The almost parallel light beams both interact with the same zero longitudinal velocity molecules in the absorption cell. In this arrangement, a lens system may be used to expand the beam to any desired size and so reduce the interaction linewidth by more than a factor of 10. This method may only be used with lasers which have sufficient output power to saturate the absorption involved and is not suitable for the visible helium neon laser. (section 3.5.) Barger and Hall (73) have used an intracavity telescope arrangement with the very high gain $3.39 \mu\text{m}$. transition to provide an interaction linewidth of 40 KHz. They are interested in minimising this linewidth as it is the dominant broadening contribution. In normal operation, with infra-red beam diameters of about 1 mm. the light methane molecule has a higher thermal velocity than iodine and interaction linewidths for typical intracavity methane cells may be about 160 KHz. (or 1 part in 10^9 .)

3.4.3. Recoil Effect

The saturated absorption effect makes possible a resolving power in excess of that previously obtained in the visible part of the electromagnetic wave spectrum. This enables sensitive experiments to be carried out on phenomena which have not been observed in this region. In particular, the recoil effect characteristic of X-rays may now be a significant feature of saturated absorption linewidths.

During the interaction of the laser light and a ground state absorbing molecule of mass M , a photon is absorbed by the molecule which is excited to the Upper absorption level from which it decays by a variety of means and returns to the ground state. The photon carries with it a momentum $p = \hbar k$ where k is the photon wave vector and \hbar is Planck's Constant divided by 2π . The molecule absorbs this energy $\frac{\hbar^2 k^2}{2M}$. The photon must therefore have a total energy

$$(E_0 + (\hbar^2 k^2) / 2M) \quad (3.2)$$

where E_0 is the energy corresponding to the centre of the absorption transition.

This means that the laser frequency is shifted by an amount $E = \frac{\hbar^2 k^2}{2M}$ from the Bohr energy $E_0 = \hbar \omega_0$. Similarly emission of a photon also means that the molecule must recoil with the photon momentum. The absorption and emission lines are therefore shifted in frequency by $\delta\nu$ from an unperturbed value. The separation of these lines is therefore $\pm \delta\nu$ where:

$$\pm \delta\nu = \pm \frac{\hbar^2 k^2}{2M} \quad (3.3)$$

$$= \pm \frac{1.25 \times 10^6}{M \lambda^2} \text{ Hz.} \quad (3.4)$$

where M is the mass of the absorber and λ is the wavelength in microns.

Evaluating this for iodine ($\lambda = 0.633 \mu\text{m}$, $M = 254$)

we find that $\pm \delta\nu = \pm 12 \text{ KHz.}$ or 4 parts in 10^{10} and for methane ($\lambda = 3.39 \mu\text{m}$, $M = 16$), $\pm \delta\nu = \pm 70 \text{ KHz.}$ or 2 parts in 10^9 .

The importance of this effect is that the measured laser frequency may deviate from the unperturbed absorption centre frequency.

3.4.4. Wavefront Curvature Effects

In our discussions so far, we have assumed that the absorbing molecule interacts coherently with the laser wavefront over the whole period of the interaction. In practice, the laser wavefront is curved and this curvature gives rise to a line broadening effect. Figure 3.1. illustrates a molecule following a trajectory BA and a curved wavefront of radius of curvature R .

Let us assume that a molecule starts from B with a mean velocity V_m . At A, the molecule trajectory is tangential to the wavefront, but at B the velocity component tangential to the wavefront is $V_m \sin \alpha$ or $V_m \frac{a}{R}$ where $2a$ is the aperture of the beam. Now, $\nu' = \nu (1 \pm \frac{V}{C})$ (3.5) and so the frequency broadening may be written approximately as :

$$\Delta\nu = \nu' - \nu = \frac{\nu}{C} V_m \frac{a}{R} \quad (3.6)$$

Normally $V_m \sim 2 \times 10^2 \text{ cm. per second}$, $a \sim 0.1 \text{ mm.}$ and $R \sim 1 \text{ metre}$
So $\Delta\nu = 300 \text{ Hz.}$ or 1 part in 10^{12} .

This very small effect is practically eclipsed by the other line broadening and shifting processes observed.

3.4.5. Pressure Effects

These effects are quite complicated for saturated absorption phenomena, and, as a prelude, it is instructive to make two simple calculations.

The width of the saturated absorption resonance is small as the technique samples only those absorber molecules which move nearly perpendicular to the laser axis. A rough estimate of the angle to the normal or "acceptance angle" is:

$$\theta \doteq \frac{\Delta\nu_{\text{resonance}}}{\Delta\nu_{\text{Doppler}}} \quad (3.7)$$

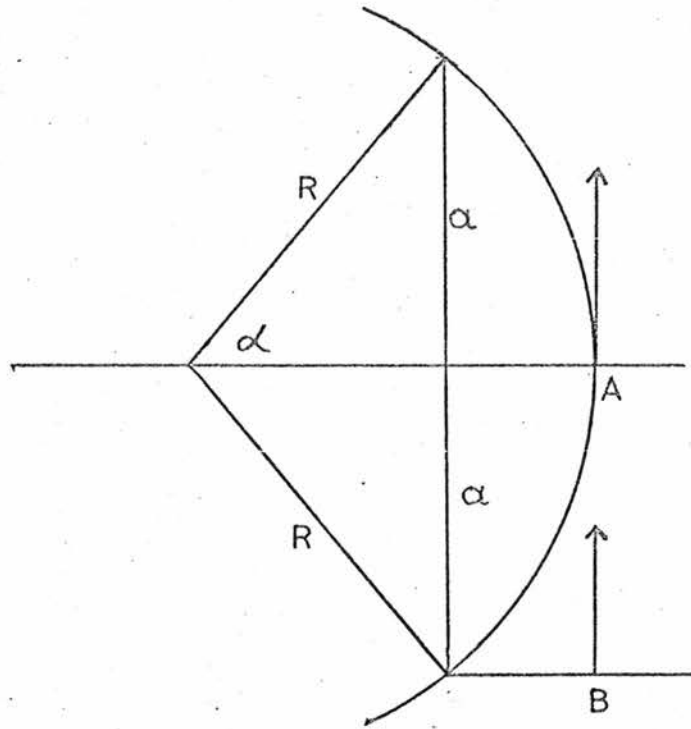


FIGURE 3.1

WAVEFRONT CURVATURE EFFECTS

$\Delta \nu_{\text{doppler}}$ for iodine molecules (400 MHz) reflects the width of the absorption linewidth of molecules moving with a Boltzman distribution at the temperature of the molecules. For a typical saturated absorption linewidth of 10 MHz., we have $\theta = (\pi/40)^c$ or 70 milliradians. Absorbers with trajectories which have an angle of greater than 70 milliradians to the normal do not contribute to the absorption peak signal. This is different from the normal situation in collisional physics when all interaction angles must be considered.

The mean free path, or distance between collisions, is also a feature of interest. For normal iodine pressures of about 100 microns, the particle density is about 30×10^{14} per c.c. and for a typical gas kinetic diameter of 10^{-15} cm^2 we have a mean free path of about 3 mm. This implies that many molecules traverse the laser beam, and interact with it, if they are within 70 milliradians of the normal, without suffering a collision. Moreover, if a particle does suffer a collision, a phase shift occurs in the laser field - absorber interaction and a longitudinal impulse along the laser axis is also imparted to the absorber molecule undergoing the interaction. This impulse gives a longitudinal velocity to the absorber and so shifts it out of the resonance. The saturated absorption phenomenon, therefore, preferentially selects not only molecules moving very closely in a particular direction but also those molecules which do not suffer a collision during the interaction. This results in collisional shifts and broadenings much smaller than those observed in non-saturated absorption experiments. This absence of strong collisional effects encourages the use of saturated absorption phenomena as reference frequencies.

More thorough consideration of these points is made by J.L. Hall in his treatment of the collision physics of the methane saturated absorption lines (46)

Studies have been made of the fluorescence of iodine vapour induced by laser sources (72) and self quenching coefficients arising from $\text{I}_2^* - \text{I}_2$ collisions in external cell experiments have been measured. Similar experiments have been carried out by Shotton and Chapman (69) where more care was taken to ensure excitation of a single vibrational level. From experimental Stern-volmer plots they have calculated a value for the self-quenching cross-section for $\text{I}_2^* - \text{I}_2$ collisions, σ^2 of $70 \frac{\text{cm}^2}{\text{A}}$. Using the results of Brewer et al (71) for the self quenching coefficient in the Stern-Volmer equation, we may write, for the lifetime τ of a collisionally broadened line from the $v' = 11$ level of the iodine B state.

$$\frac{1}{\gamma} = \frac{1}{\gamma_0} + 2.264 \times 10^5 \sigma^2 P \quad (3.8.)$$

where σ is in angstroms and P is the pressure in torr. Therefore:

$$\frac{1}{\gamma} = \frac{1}{\gamma_0} + (2.26 + 10^5) \times 70 P \quad (3.9.)$$

$$\frac{1}{\gamma} = \frac{1}{\gamma_0} + 90.4 P \times 10^6 \quad (3.10)$$

For $\gamma_0 = 410$ nsecs we have, for the zero pressure linewidth $\Delta\nu = 390$ KHz. FWHM. and a collisional broadening of 2.6 MHz. per torr. These measurements are for all angle collisions and molecules moving in all directions and will be referred to as linear experiments.

It is possible that other processes more complicated than the naive picture of collisional broadening discussed in this Section contribute to the observed linewidth. In the experiments of Barger and Hall (74) on saturated absorption in methane, the self-quenching coefficient decreases as the laser beam diameter in the methane cell is increased. This aperture dependence may be explained in terms of a critical collision diameter which is aperture dependent. In the iodine experiments, aperture, or interaction time broadening, is very much smaller than many other linewidth contributions. The methane linewidth is dominated by this consideration. As yet, the physics of line broadening in saturated absorption experiments is not clearly understood and more work under a variety of experimental conditions is necessary to investigate the possible experimental variation in observed pressure broadening.

Pressure shifts are also not well understood. The methane experiments to which we have already referred show shifts some ten times smaller than those observed in non-saturated absorption or linear experiments. This appears reasonable on the basis of the suggestions outlined at the beginning of this section: saturated absorption selects preferentially those absorbers which interact coherently throughout their passage through the laser beam. The Lindholm theory of pressure effects (75) states that at low pressures and for frequencies near the line centre, the shift and broadening are proportional to the perturber density N . Assuming we may characterise the forces between emitter and perturber by a Van der Waal's type interaction we find a

$$\text{Broadening } \Delta\nu = 2.71 C_6^{2/5} \nu^{3/5} N \quad (3.11)$$

$$\text{and a Shift } \delta\nu = 0.98 C_6^{2/5} \nu^{3/5} N \quad (3.12)$$

Where C_6 is the Van der Waal's Constant and ν is the average perturber velocity. The ratio of shift to broadening is 0.36. For methane, the observed broadening is 8 MHz. per torr and the shift 70 KHz. per torr giving a ratio of 0.009.

Thus, even if we take the conservative result of Lindholm theory, clearly not truly applicable in saturated absorption, then the expected pressure shift for iodine self broadening will be less than 0.9 MHz./torr. This assumes Chutjian's value of 2.6 MHz. per torr for linear broadenings (70). This estimate is certainly too large in the iodine case. Two iodine stabilized lasers operating under identical conditions except for the iodine tube temperatures of 20°C and 30°C respectively - a pressure difference of 0.35 torr - show no frequency shift larger than 20 KHz. This would indicate pressure shifts of less than 55 KHz./torr.

3.4.6. Power Broadening

It is well established that the width of the Lamb Dip $\Delta\nu$ observed in lasers depends on the laser power P: this dependence may be simply described by

$$\Delta\nu = \sqrt{\Delta\nu_0 + \alpha P} \quad (3.13)$$

where $\Delta\nu_0$ is the homogeneous width which is the sum of natural and collisional broadened linewidths.

The parameter α is proportional to the ratio of the dipole matrix element of the transition between the two laser levels and the sum of the radiative decay rates of these levels.

This situation may also be described by the interaction between the electric field inside the laser and the energy levels of the molecule which leads to saturated absorption. The broadening interaction is a process which shortens the lifetime and encourages stimulated radiative decay of atoms in the upper absorber level and is proportional to the field strength as indicated above. Physically the effect is to broaden the observed saturated absorption feature.

The results of this investigation for iodine saturated absorption are discussed in greater detail in Chapter 5 where equations pertinent to the experimental measurements will be developed.

3.4.7. Stark and Zeeman Shifts

We have so far considered most of the line broadening mechanisms common to saturated absorption experiments. There remain those broadening mechanisms, such as Stark and Zeeman shifts, which perturb the features. A major advantage of the saturated absorption technique is that for iodine and methane the ground state is populated thermally, therefore no pumping discharge is run in the absorption tube. This is not the case for saturated absorption in neon (7, 8) mentioned in Chapter 1 where the lower $2p_4$ laser

level must be populated in a discharge. In these active systems, Stark Effects from the electric field broaden and shift the energy levels involved, thereby perturbing the absorption frequency. Magnetic fields have a similar effect and broaden the absorption line. Furthermore, the discharge excites neighbouring spectral lines which have considerable effects on the refractive index of the plasma at the absorption frequency. Changes in these contributions arising from variations in the level populations and the discharge current have a marked frequency pulling on the centre of the absorption line in an active discharge. Arrathoon and Siegman report current shifting effects of 4 MHz. per mA. for the centre of the Lamb Dip in a gain cell (76)

Despite the lack of a discharge in the cell, the absorption lines may still suffer shifts from interaction of the molecular electric dipole moments of the molecule with electric fields. Insensitivity to these effects is aided by the choice of a symmetric molecule as an absorber, thereby ensuring an extremely small dipole moment. Iodine has a dipole moment of $\sim 10^{-1}$ debyes (Chapter 5) and methane 5.4×10^{-6} debyes (77). Dahlstrom and Hanes considered the effects of magnetic fields on the iodine saturated absorption peaks observed in their lasers (66). They found that the observed widths increased from some 4 MHz. by a maximum factor of two for 500 gauss field and their centres shifted less than 2 MHz. for 500 gauss. This measurement was limited by the accuracy of their reference laser which was locked by the first derivative technique (Chapter 4) but they conclude that perturbations of the earth's magnetic field of 5% would give wavelength shifts of less than 2×10^{-13} .

3.4.8. Additional relaxation mechanisms

In Chapter 5 we shall discuss a comparison between theory and experiment for the observed saturated absorption iodine linewidths. We shall find that there is a discrepancy of about 1 MHz. F.W.H.M. in an observed width of 3.75 MHz. It is possible that there is a substantial contribution to the upper state decay from predissociation, both spontaneous and collisionally induced. Chutjian and James (78) report that in their experiments, which also required additional relaxation mechanisms to explain observed lifetime variations, some 66% of molecules entering the B state spontaneously predissociate and only 34% radiate to the X ground state in the absence of collisions. For collisionally induced predissociation at 0.3 torr of iodine, some 20% predissociate, 10% radiate to the X state and 70% leave the B state by non-radiative or collisionally induced processes. From their measurements we conclude that some form of predissociation is also a strong relaxation mechanism for saturated absorption measurements. This has been confirmed by the magnetic predissociation experiments of Chapman (79).

Other evidence for predissociation lies in the shape of the iodine absorption coefficient curve of Figure 4.4. In that curve, the large rise at low frequencies is due to the P (33) line and the flatter region is the R (127) line hyperfine components of which have been observed in the experiments described in this thesis. The important feature to notice is the large continuum value. This cannot be attributed to the overlapping effects of the Doppler broadened lines of the absorption spectrum and so indicates the presence of some other mechanism which is likely to be predissociation.

Predissociation is particularly likely for the upper $v' = 11$ vibrational level involved in the R (127) line. There are crossings of the potential energy curve for the B state near $v' = 11$ by dissociative $A^3\Pi_{1u}$ and $^1\Pi_{1u}$ states leading to the formation of two $^2P_{3/2}$ state atoms. It is via this predissociation path that the upper level decays within its natural lifetime thereby increasing the observed saturated absorption linewidth.

The contributions to the linewidth are summarised in Table 3.2.

3.5. Power required to saturate the iodine absorption

Fundamentally, saturated absorption occurs when every absorbing molecule entering the laser field region in an energy state capable of absorbing a photon has a probability of one of absorbing that photon. In other words, the laser field must be sufficiently intense to ensure an absorption transition probability of one.

The quantum mechanical expression for the transition probability P between states p and q is well known (80, 81) and may be stated as:

$$P_{p-q} = f(b^2) \sin^2 \frac{1}{2} (t - t_0) \left[(\omega_0 - \omega)^2 + b^2 \right]^{-\frac{1}{2}} \quad (3.14)$$

$$\text{where } f(b^2) = \frac{(b)^2}{(\omega_0 - \omega)^2 + b^2} \quad (3.15)$$

where ω_0 is the centre frequency of the absorption lineshape, ω is the perturber frequency and b is the matrix element of the perturbation characterising the interaction between the laser electric field E and the iodine molecule. Since this is an electric dipole transition:

$$b = \frac{1}{\hbar} \langle p | E e \cdot r | q \rangle \quad (3.16)$$

where e is the electronic charge and r the separation of the energy states. The factor $(t - t_0)$ describes the time evolution of the energy states involved in the interaction.

On resonance when $\omega = \omega_0$ then:

$$P_{p-q} = 1 \quad \text{if} \quad \frac{1}{2} b (t - t_0) = \pi/2 \quad (3.17)$$

	$^{127}\text{I}_2 - 633\text{nm.}$	$\text{CH}_4 - 3.39\mu\text{m.}$
Frequency.	$5 \times 10^{14} \text{ Hz.}$	$1 \times 10^{14} \text{ Hz.}$
Natural Lifetime.	390 KHz. 2×10^9	100 Hz. 1×10^{12}
Pressure Broadening.	< 2.6 MHz/torr. 2×10^8	8 MHz/torr. 2×10^7
Pressure Shift	< 60 KHz/ torr. 8×10^9	< 75 KHz/ torr. 1×10^9
Interaction Time.	38 KHz. 1×10^{10}	160 KHz - 30KHz. $1 \times 10^9 - 3 \times 10^{10}$
Power Broadening.	60 KHz. (8×10^9) /mW./mm. ²	
Zee man Effect	0.5 KHz. /gauss. 1×10^{12}	
Recoil Effect	$\pm 12 \text{ KHz.}$ $\pm 4 \times 10^{10}$	$\pm 70 \text{ KHz.}$ 2×10^9
Wavefront Shape	300 Hz. 2×10^{12}	60Hz. 2×10^{10}

TABLE 3.2

SATURATED ABSORPTION WIDTH CONTRIBUTIONS.

So by writing $(t - t_0)$ as the mean lifetime of the excited state then for the $v' = 11, v'' = 5$ transition in the iodine molecule.

$$E = \frac{h}{\tau} \left[e \langle 11 | r | 5 \rangle \right]^{-1} \quad (3.18)$$

Chutjian and James (78) have evaluated $\langle p | r | q \rangle$ for several similar transitions giving a mean value of about 0.2 \AA which will be used in this calculation. For the B state lifetime of 410×10^{-9} seconds; equation 3.18 gives a value of $E \doteq 2 \text{ mW per mm}^2$ for saturation of the iodine absorption.

In practice, good saturated absorption signals have been observed at a minimum power level of 10 mW per mm^2 . Below this power, the absorption signals are lost in the detection system noise. Clearly, the calculation outlined above gives the correct order of magnitude of the field required for saturation, despite the assumptions made in deriving the formula which have not been justified in this case (80). Essentially these are that the states p and q are isolated states and E is a monoenergetic wave. In other words, this transition is the only one brought about by the perturbation, a double transition is not considered, nor is coupling to other states via spontaneous emission, collisional termination and predissociation.

In the experiments reported in this thesis, saturated absorption has been observed from power densities of 10 mW / mm^2 to 150 mW / mm^2 corresponding to laser output powers of $6 \mu\text{W}$ to $100 \mu\text{W}$ for an output mirror transmission of 0.3%. The upper power limit was simply the maximum power available from the gain tube.

3.6. Spectroscopy of the Iodine molecule

The particular absorptive transition studied in these experiments has been studied theoretically by Kroll (82). There are 21 hyperfine components of this line which has an odd J value (= 127) and only $\Delta F = \Delta J$ transitions will have appreciable intensity (83). The separations of these components have been discussed by Kroll and he has advanced a theory for the hyperfine splittings based on a nuclear electric quadruple interaction in both electronic states and a smaller magnetic hyperfine interaction for the excited state. His calculations indicate agreement between the theoretical results and the experimental results of Hanes and Dahlstrom (66) to which their experimental accuracy of 1 MHz. Chapter 5 discusses the agreement between the theory of Kroll and the experimental results obtained in this thesis.

Figure 3.3. shows the position of the fourteen components which lie under the Neon 20 laser gain curve together with the alphabetical notation originally given by Dahlstrom and Hanes (66) which is retained in this thesis. The measured frequency separations between the components are also shown relative to component i.

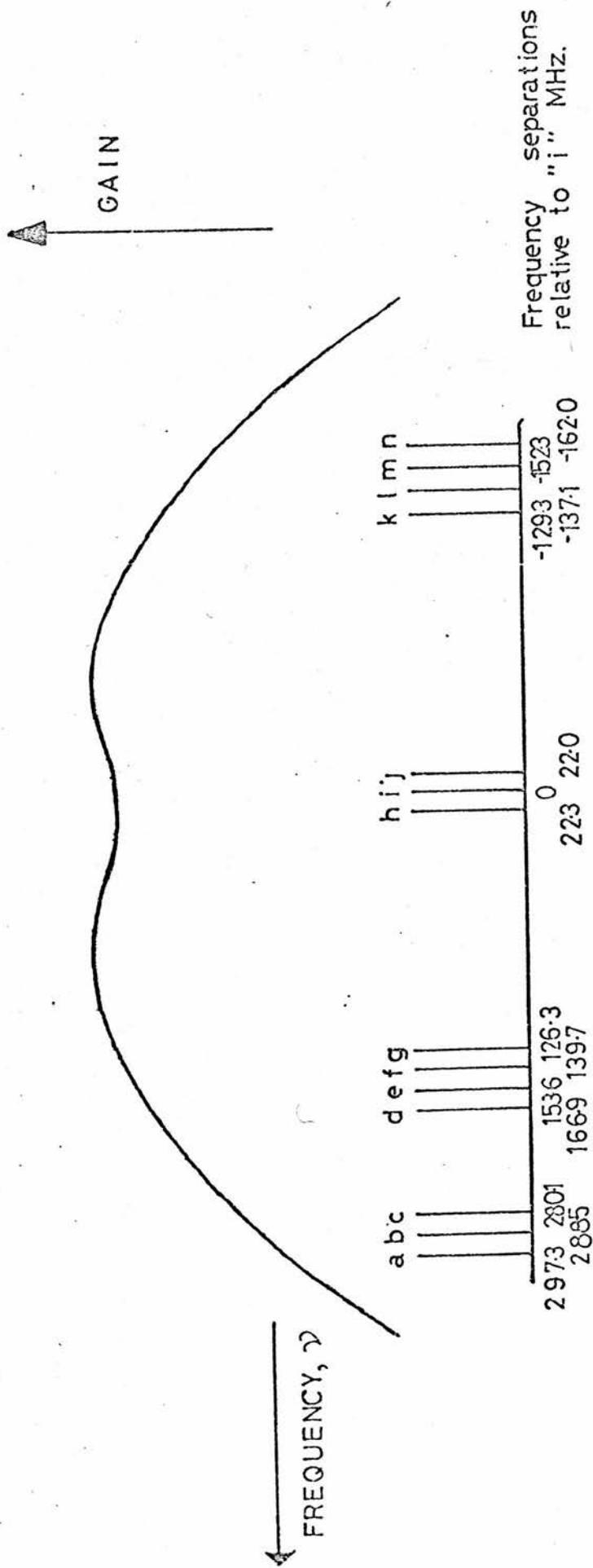


FIGURE 33

HYPERFINE COMPONENT POSITIONS UNDER
THE NEON 20 GAIN CURVE.

CHAPTER 4

INITIAL EXPERIMENTS WITH IODINE AND DEVELOPMENT OF THE
IODINE STABILIZED LASER SYSTEM.4.1. Choice of absorbing vapour, and laser design

The first stage in the development of a laser stabilized to a saturated absorption reference frequency was concerned with the choice of a suitable absorber. Table 4.1. lists several vapours with known absorption coincidences or possible coincidences within the neon line width. The suitable absorber should be easily handled, and should not require extreme conditions, for example, high temperatures in order to maintain it in an absorbing state. Of the short list in the table, and from other known materials having extensive absorption spectra in this region, it was decided to attempt an investigation with iodine 127 (Analar grade 99.9% pure). As a first step, a tube some 2 cm. in diameter and about 25 cm. long was constructed with flat ends on to which polished quartz windows were sealed with araldite.

This tube was filled in a similar manner to that described in section 2.2. It had a side arm which could be cooled and, after evacuating and filling with iodine, the iodine vapour pressure was altered by changing the temperature of this side arm.

This iodine tube was used in a single pass measurement of absorption coefficient for the assumed iodine vapour absorption. The experimental arrangement is shown in Figure 4.2. The laser used in this experiment was running multimode and was filled with a naturally occurring mixture of neon isotopes. The photodiode registered the laser power with the absorption cell empty (side arm immersed in liquid nitrogen) and with the side arm at room temperature. A change in laser power under these circumstances indicated iodine absorption within the composite neon 20 and neon 22 linewidth. The result of this simple experiment was that the laser power was reduced by some 5% indicating a value for the iodine absorption coefficient of 20% per metre averaged over the gain bandwidth of the laser.

4.2. Iodine absorption coefficient

As a result of these experiments, which demonstrated the presence of absorption of the laser light by a vapour pressure controlled tube of iodine vapour, consideration was given to the design of laser. As indicated in the introduction, several schemes for the selection of a single laser frequency were considered, and this led eventually to the choice of a short laser cavity. The rough absorption coefficient measurements showed that a 10 cm. tube containing iodine vapour at room temperature would give a single pass laser loss of some 2%. The single pass gain of the visible laser transition was known to be given by $G = 3 \times 10^{-4} \ell/d$, where ℓ is the length of the gain tube and

ABSORBER	STATE AT ROOM TEMPERATURE	REFERENCE.
IODINE 127	VAPOUR	66
IODINE 129	VAPOUR	67
POTASSIUM	SOLID	56 57
RUBIDIUM	SOLID	58
CESIUM	SOLID	58
DYES	IN SOLUTION	

TABLE 41

ABSORBING MATERIALS AT 633 nm.

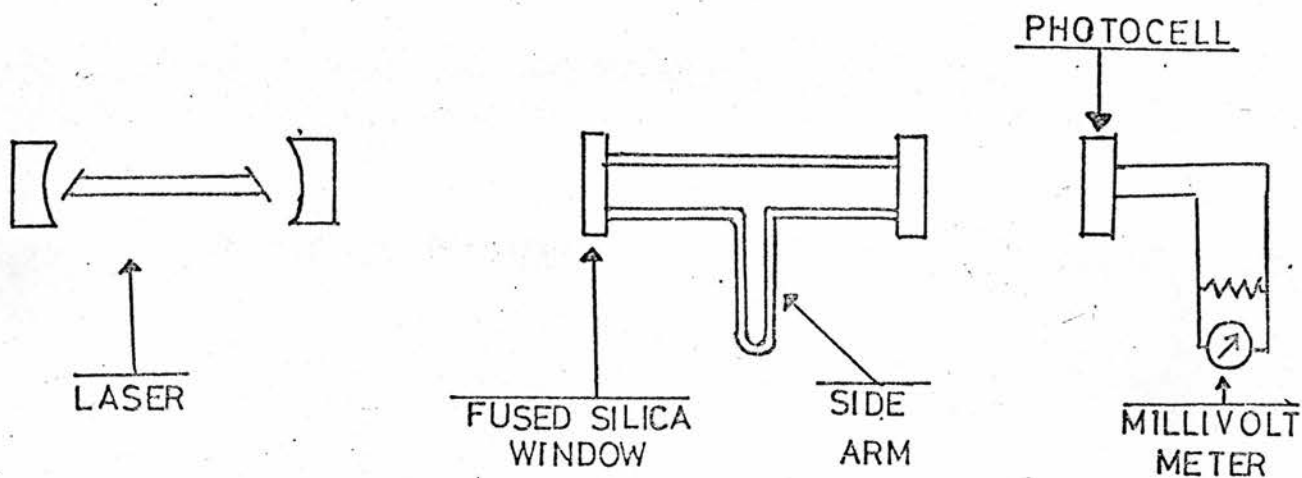
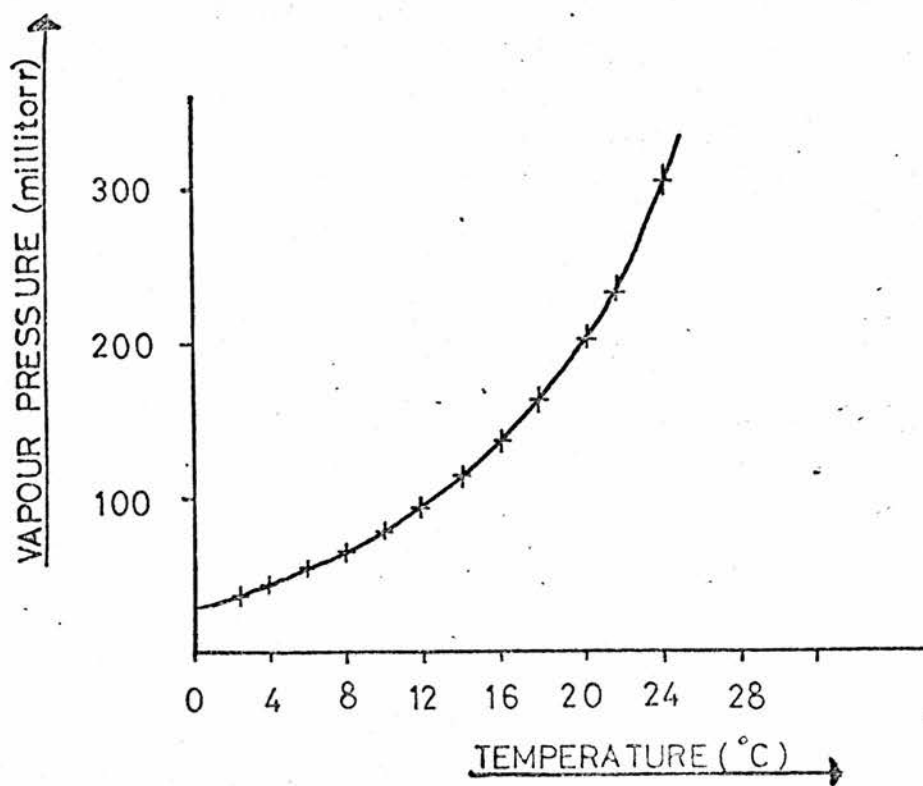


FIGURE 4.2
DEMONSTRATION OF IODINE ABSORPTION

FIGURE 4.3
IODINE VAPOUR PRESSURE VARIATION WITH TEMPERATURE



d its diameter. This gives a gain of 4% for a 20 cm. discharge length gain tube of bore diameter 1.5 mm. A laser constructed in this way would have a total cavity length of 30 cms. which is twice that necessary for single mode operation. However, the 2% extra loss introduced by the iodine vapour should provide the gain reduction necessary for single mode operation. Some adjustment of the loss factor may be necessary in practice and could be carried out by altering the iodine absorption via the iodine pressure. A plot of iodine vapour pressure against temperature is shown in Figure 4.3. The data points have been taken from values published in Kaye and Laby (92) and from measurements made on an iodine filled tube on to which an L.K.B. pirani gauge head was attached.

4.3. Iodine Absorption Coefficient Frequency Variation Measurements

Measurement of the absorption coefficient of iodine 127 and iodine 129 have been made by Knox and Yoh-Han-Pao (67) and of iodine 127 by Hanes et al. (66). The results for iodine 127 are summarised in Figure 4.4. where it can be seen that the 10 cm. tube of iodine used in these experiments has an absorption of approximately 1% over most of the neon 22 and 20 linewidths. The low frequency increase in absorption coefficient, rising to 50% per metre (at room temperature vapour pressure) is due to the P(33) line of the electronic spectrum. The approximate absorption coefficient measured in the experiment described earlier was an average value observed over the composite gain curve.

4.4. Laser Parameters in these Experiments

The laser cavity already discussed in Chapter 2, was 30 cms. long with a 17 cm. gain tube of 1.5 mm. bore and an absorption tube 10 cm. long and of 1 cm. bore.

The laser operated in a single longitudinal mode over some 450 MHz. with the iodine cell at room temperature, together with a small region of two mode operation. The regions of single mode operation were determined by observing the mode spectrum on a scanning spectrum analyser (section 2.6.) The beam diameter was about 0.3 mm. with the mirror configuration used. A variety of mirror radii were used, but reliable operation was obtained with a 60 cm. dielectric coated mirror of maximum reflectivity and a 100 cm. radius mirror of 99.5% reflectivity. The diameter of the laser beam in the iodine cell is an important parameter in evaluating the contribution of the interaction time contribution to the width of the saturated absorption features (section 3.4.) This could be changed for an intracavity absorption cell by substituting mirrors of different radii while maintaining only longitudinal mode operation. The laser had a maximum output power of 100 microwatts: typical powers were 50 microwatts.

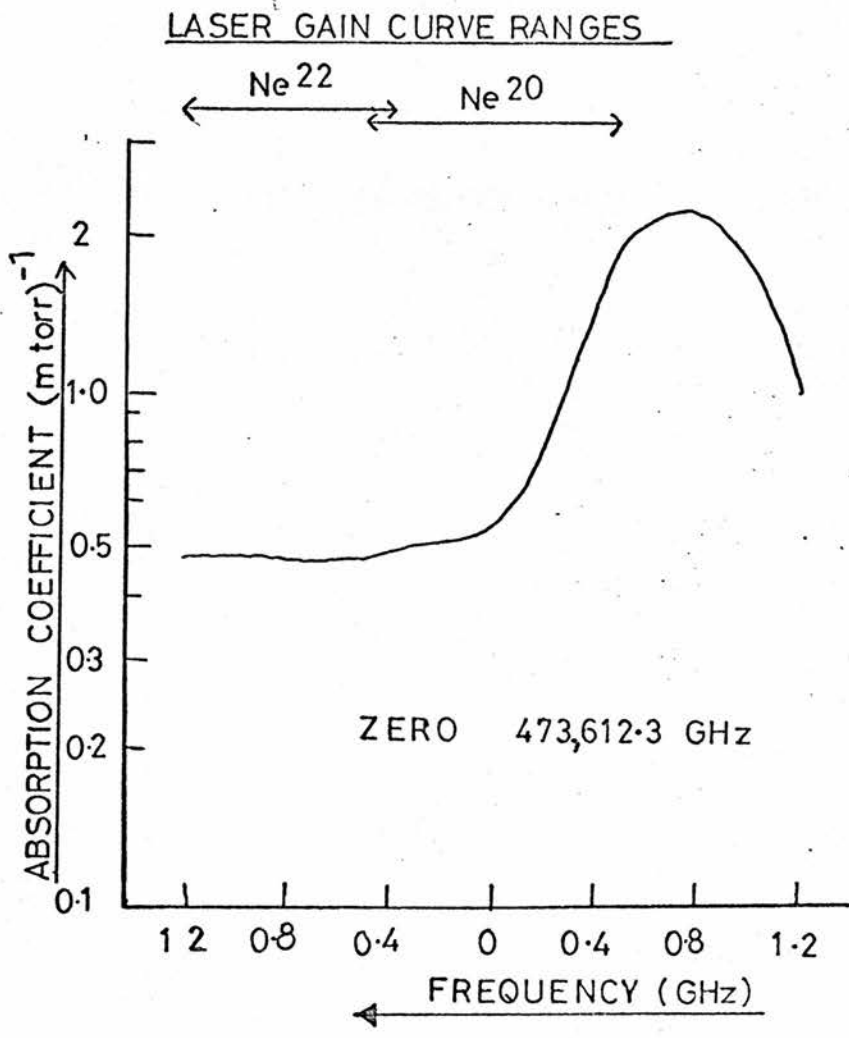


FIGURE 44
 FREQUENCY VARIATION OF IODINE ABSORPTION.

4.5. Laser Noise problems

As the saturated absorption features were expected to be small the construction of low noise laser tubes was necessary. Dahlstrom and Hanes (66) suggest that the peaks on the power output curve were only a few tenths of a per cent high and were lost in the laser noise. Experience with short iodine lasers agrees with this, and no direct observation of the iodine peaks on the laser power output has been made experimentally.

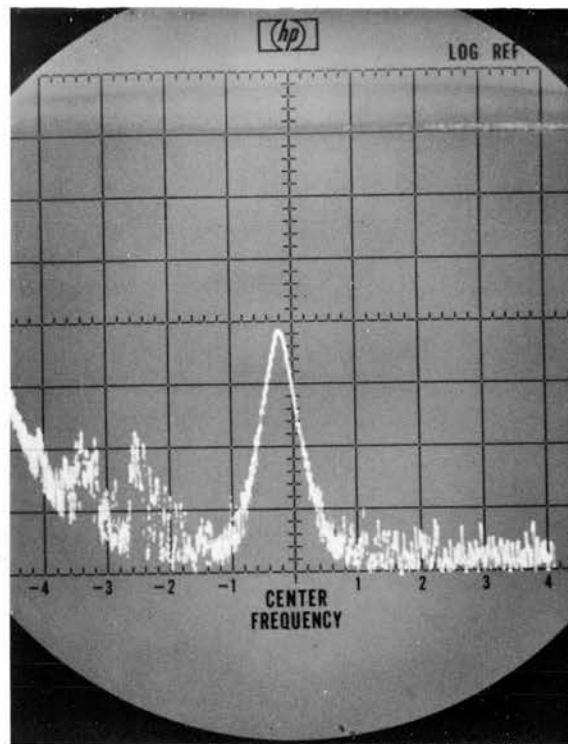
The noise observed on the output of a gas laser falls into several general classifications which are summarised below:

i) noise may be produced by laser length fluctuations due to mechanical vibrations and draughts. The effects of these perturbations are reduced by mounting the experiment on an isolation system as described in section 2.5., and placing a simple acetate sheet shield around the lasers. The noise frequency spectrum depends on the dominant noise source characteristics of the laboratory.

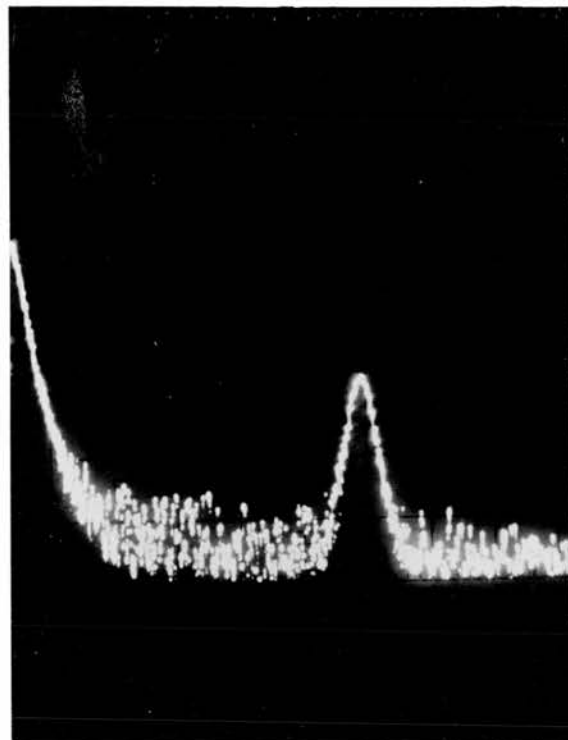
To investigate this effect, the laser power output, after photodiode detection, was viewed on an audio frequency spectrum analyser to establish the frequency of any perturbations. Figure 4.5.a. shows the spectrum with a horizontal dispersion of 200 Hz. per division with zero frequency at -5, just off the left of the picture. The vertical scale is 10 dB per division. The large spike near 1 KHz. is the result of modulation applied to the laser. The other observed frequency peaks are at 200 Hz., 400 Hz., and 600 Hz., all more than 20 dB down on the applied modulation. The slow increase in signal of low frequencies is the instrumental zero shape and is not representative of the laser noise. These spectra were taken with the laser on a poor vibration isolation system and without any draught shields. Figure 4.5.b. shows a similar spectrum taken with a good vibration isolation system and shielding, under identical display conditions. The improvements in the isolation systems have reduced all but the required 1 KHz. The magnitude of this signal, however, will depend on the position of the laser mode under the gain curve. A steeper sloping gain curve will give a greater intensity modulation than a flat gain curve region.

The noise observed on an oscilloscope was not more than 0.2% peak to peak of the total laser signal.

ii) Power supply fluctuations alter the discharge current and therefore the laser level populations. Power supply voltage or current stabilization is necessary to ensure a stable discharge current. Frequently, a large ballast resistor is used in the anode side of the laser tube to counteract the negative impedance of the discharge. If this is not done, the power supply circuit may oscillate at frequencies typically in the 10 KHz. region.



POOR NOISE ENVIRONMENT.



GOOD NOISE ENVIRONMENT.

FIGURE 4.5
 FREQUENCY SPECTRA OF A LASER OPERATING
 IN DIFFERENT NOISE ENVIRONMENTS.
 DISPERSION IS 200KHz/ HORIZONTAL DIVISION.

iii) Mode interactions occur between the oscillating cavity modes which are coupled via a nonlinear interaction with the gain medium. In particular, such interactions are observed in the presence of off axis modes and the effect of this situation is illustrated in Figure 1.3. This shows the mode spectra recorded on a scanning spectrum analyser together with the noise as observed on the photodiode detected laser output. The change from purely longitudinal mode operation to the multimode operation was accomplished by detuning the mirrors in a wide bore tube arrangement. This change resulted in a reduction of the observed high frequency noise by a factor of five from 1.25% of the total laser intensity to 0.25%.

iv) Much of the residual noise occurring in gas laser tubes arises from instabilities in the plasma which are not well understood. Such noise falls into two general areas:

1. The formation of a smooth stable discharge.
2. The presence of moving striations within the body of the plasma.

As discussed in Chapter 2, hot cathode tubes proved unreliable in practice and also were not commercially available with the required length. The cold cathode described in Chapter 2 was developed and ensured a sufficiently smooth discharge with low gas clean up rate. When the laser output was observed on an oscilloscope via a photodiode detector, random noise was observed to be less than 0.2% of the total power output.

The moving striation effect generates discrete oscillations in the plasma of frequencies generally above 10 KHz., and leads to oscillation noise on the laser light output. The origin of these striations is thought to occur in travelling regions of high metastable atom density which influence the laser level populations and also contribute to refractive index variations at the laser frequency.

These moving striations are most undesirable features of a wavelength standard laser and a study of the conditions likely to lead to the presence of moving striations and their nature in both hot and cold cathode tubes has been carried out. (16, 84). The subject of moving striations has been the object of study by several authors (85, 86, 87) and laser tubes have been designed to eliminate the striations (88, 89).

The presence of oscillations on the light output arising from moving striations also has a detrimental effect in beat frequency experiments between two lasers. When the laser beat is near zero frequency, the presence of an oscillation also in this region which may be 10 to 20 dB down on the beat signal gives rise to extra counts in the counter measuring the beat frequency.

In particular, when the beat is moving either side of zero frequency because the lasers are moving up and down relative to each other, the presence of a fixed oscillation frequency leads to bias in the reversible count to one side of zero. This may give rise to an apparent offset from zero beat frequency.

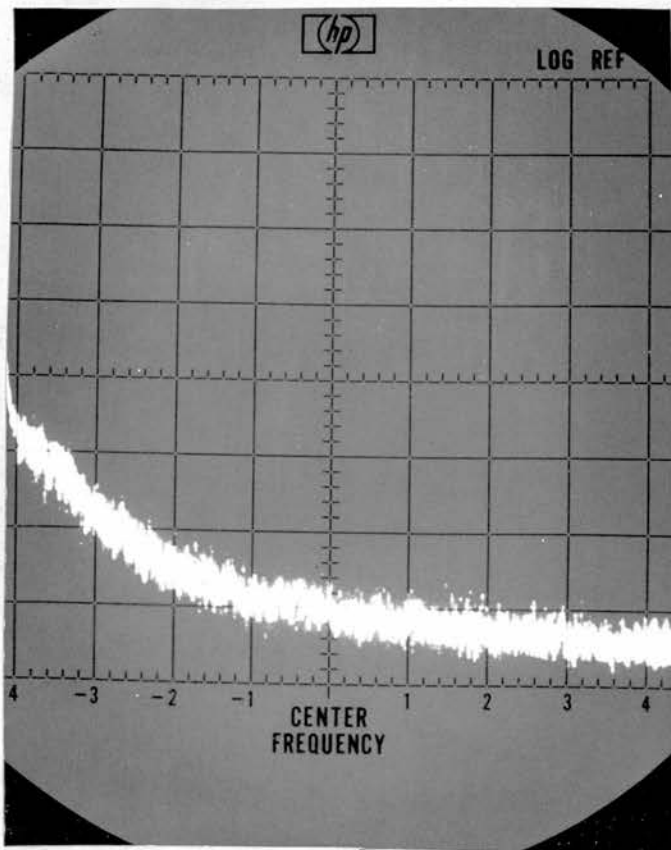
4.6. Experiments investigating moving striations.

4.6.1. Cold cathode tubes.

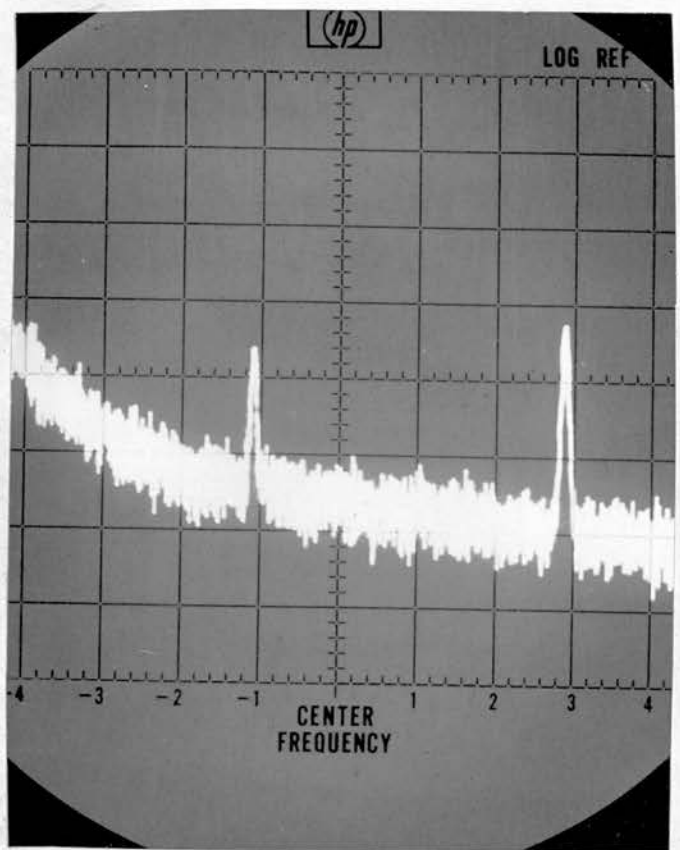
Experiments were carried out on three tubes: a short 17 cm. tube used in the iodine laser, a 30 cm. long cold cathode tube designed to compare the performance of a locally constructed tube with the Spectra Physics 130 tube, and the 130 tube itself. The frequency spectrum of the discharge current was observed by monitoring the laser current across a 100 Ω resistor on the cathode side of the laser tube. This voltage was analysed by a Hewlett Packard RF Spectrum Analyser.

The analyser dispersion and bandwidth could be set independently and figure 4.6. shows the observed spectrum for increasing discharge current in the 17 cm. tube. At currents less than 4 mA (which corresponded to maximum power output) no oscillations were observed and the laser noise was 10 dB above the spectrum analyser noise. As the current increased, discrete oscillations, at least some 20 dB above the background, were observed together with their harmonics. When the current reached values at which the laser has ceased to lase (about 8 mA) the spectrum had increased in complexity. The oscillations were very stable in amplitude and frequency, and Figure 4.7. shows one such oscillation at 100 KHz., with 50 Hz., sidebands. The observed bandwidth of the oscillation was less than 20 Hz., and was limited by the spectrum analyser, which, in this case, was a Textronix IL 5 oscilloscope plug in unit.

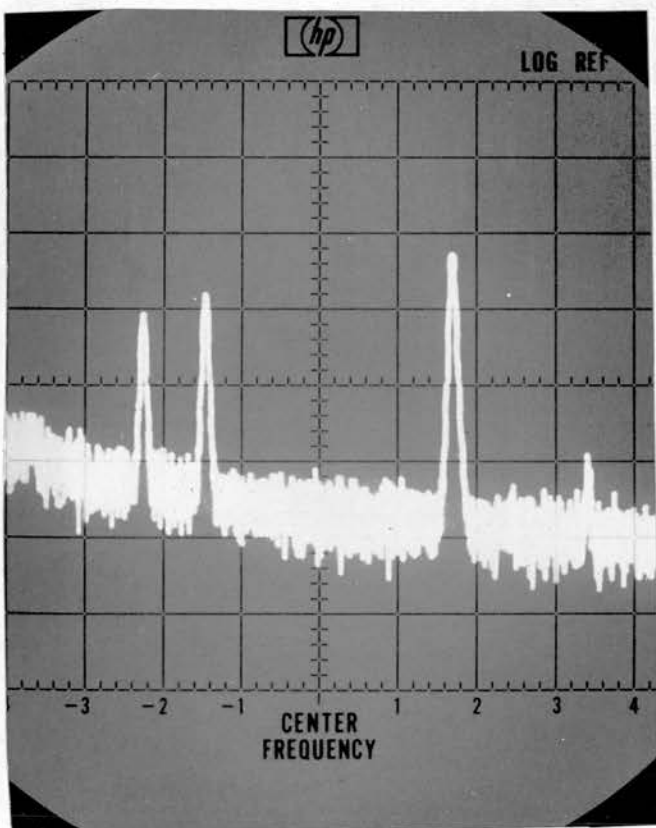
A similar series of observations on the 30 cm. tubes showed that similar oscillations occurred but these started at a higher threshold current than those observed for the 17 cm. tube. It was thought that the threshold current would depend on cathode geometry. It seems likely that the cathode space charge traps electrons in the negative glow region. The size of the cathode glow region is determined by the size of the cathode in these tubes. These "electron traps" lead to fast discharge current decreases which create voltage increases across the laser tube. Electrons in the positive column of the discharge are accelerated and so ionise more neon metastables. When this striation, moving from anode to cathode, reaches the negative glow area the trapped electrons are released and the process may reoccur at a characteristic frequency. Side light studies of the discharge intensity in the region of the cathode have shown the presence of moving striations which may reach 100% intensity



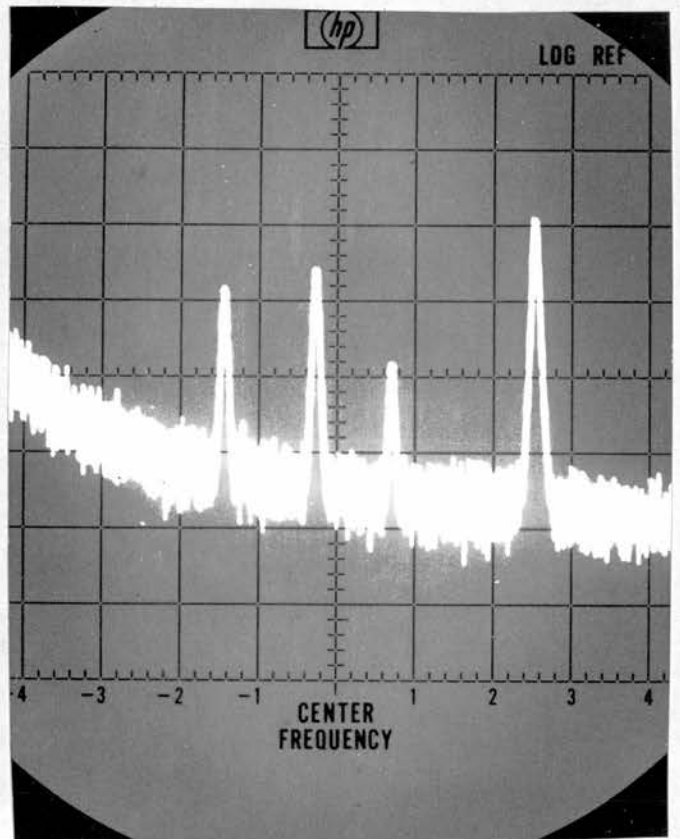
3mA



6m A



9 m A



12 mA

FIGURE 4-6
COLD CATHODE TUBE CURRENT SPECTRA OVER 0-200KHz. FOR
VARIOUS DISCHARGE CURRENTS.

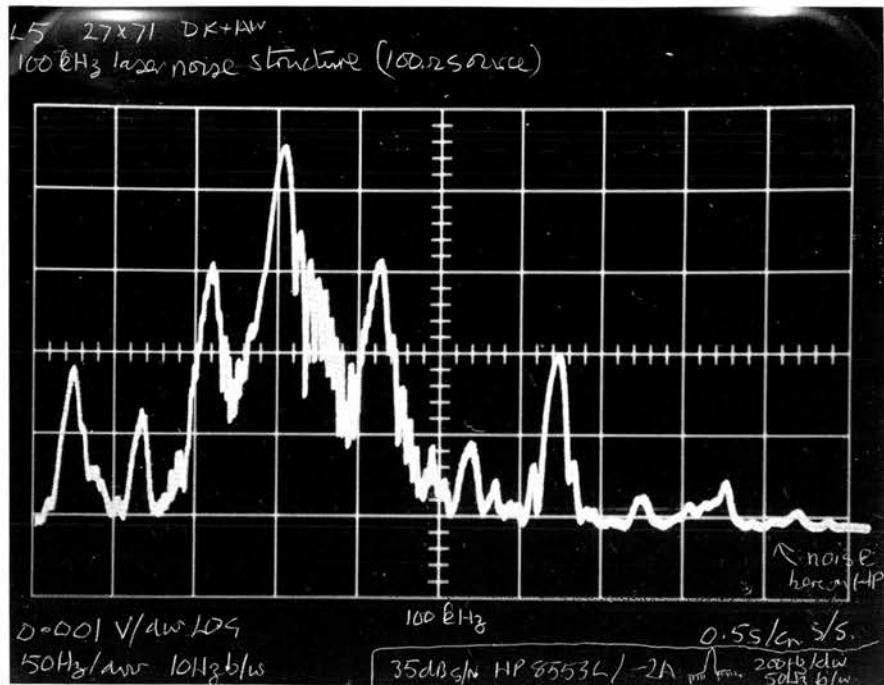


FIGURE 4.7

OSCILLATION NEAR 100 KHz. DUE TO A
 MOVING STRIATION. THE DISPERSION IS
 50 Hz PER DIVISION

modulation, and which have also been observed in infra-red molecular gas lasers (for example, HCN and I_2 lasers).

The oscillations in discharge current are reflected in the laser output and correlations between the discharge current and light output may be observed. The 30 cm. long cold cathode tube was operated at $3.39\mu\text{m.}$, and the light output was detected on an Indium Arsenide photodetector with a response up to 10 MHz. The light frequency spectrum was also observed on the Spectrum Analyser. In Figure 4.8., the discharge current spectrum is shown from 0 - 1 MHz., with a bandwidth of 1 KHz. Zero frequency is the large signal on the left; one large division of the vertical scale represents 10 dBs. The oscillation observed is at 600 KHz., some 30 dBs above background, and shows sidebands due to another oscillation at 60 KHz., here lost in the noise but which may be observed separately. These two oscillations couple to give the observed sidebands in a manner arising from the non linear nature of the plasma. In Figure 4.9 the light output spectrum is shown on a 0 - 2 MHz. scale, and demonstrates the same 600 KHz. oscillation, and also the lower frequency modulation at about 60 KHz. just visible near the zero frequency mark. This correlation has also been observed in the visible region of the spectrum.

Several workers have published (88, 89) laser tube designs which contain short capillary sections which break up any moving striations, but it is clear from this investigation that the cathode in the 17 cm. iodine laser system does not exhibit any oscillation at the currents normally used and is therefore eminently suitable for use in the stabilized laser system.

4.6.2. Hot cathode tubes

Observations were carried out on a 30 cm. long hot cathode laser tube (Scientifica and Cook type) which was compared with a similar length cold cathode tube.

Figure 4.10. shows the laser current spectra at typical operating currents (11 mA) over 10 - 200 KHz., and must be compared with Figure 4.6. Evidently the cold cathode tube shows little sign of the oscillation peaks at normal operating currents, in contrast with the hot cathode which does. The general noise levels for the two tubes show, however, that the cold cathode tube is some 10 dB noisier than a similar hot cathode tube.

Experiments on all the hot cathode tubes available showed oscillation peaks at maximum laser output power. The cold cathode tubes, because of their larger cathode area, seemed less susceptible to moving striations and none have been observed for maximum power output currents on the current spectra of tubes available.

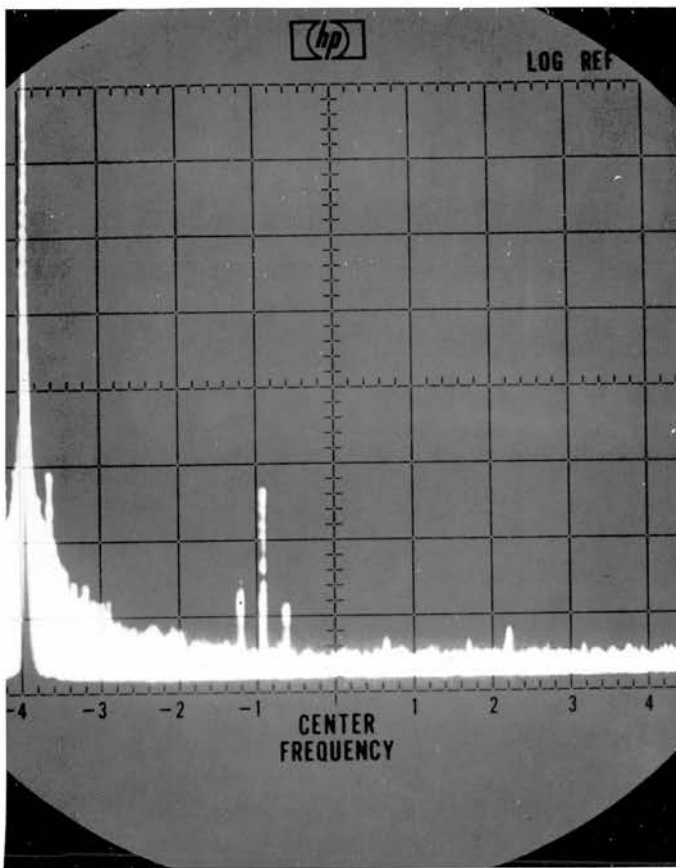


FIGURE 4.9
 LIGHT OUTPUT , $3.39 \mu\text{m}$
 0-2MHz :1KHz BANDWIDTH
 14.5mA DISCHARGE
 CURRENT
 30cm COLD CATHODE TUBE.

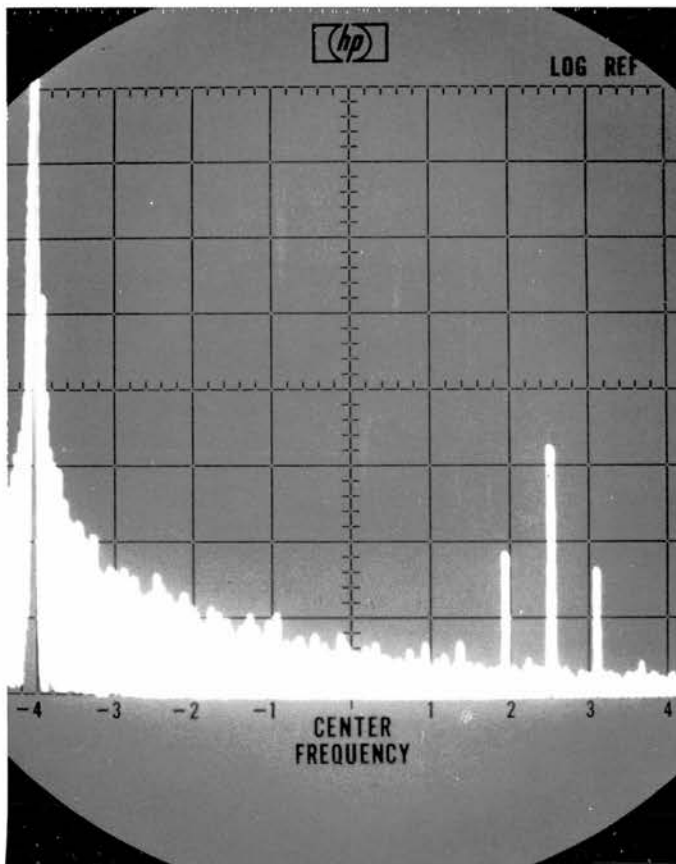


FIGURE 4.8
 CURRENT SPECTRUM
 0-1MHz :1KHz BANDWIDTH.

FIGURES 4.8 and 4.9
 FREQUENCY SPECTRA OF LIGHT OUTPUT AND DISCHARGE
 CURRENT ILLUSTRATING THE OSCILLATIONS PRESENT.

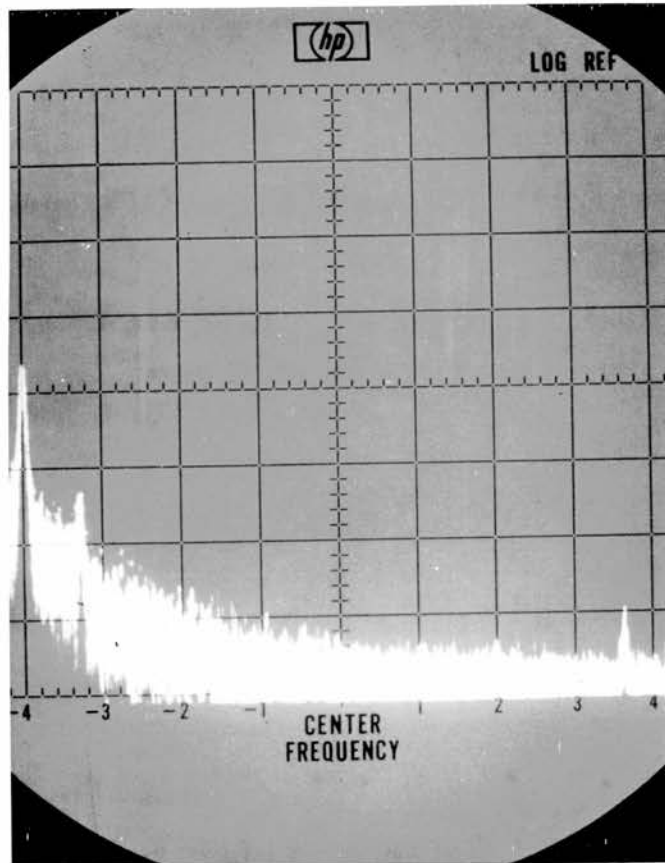


FIGURE 4.10
DISCHARGE CURRENT SPECTRUM OVER 0-200 KHz.
FOR A 30cm LONG HOT CATHODE TUBE SHOWING
OSCILLATIONS AT 200KHz AND 350KHz. THE
CURRENT CORRESPONDS TO MAXIMUM OUTPUT
POWER OF THE LASER.

ZERO FREQUENCY IS AT -5

Observations of the spectra over a higher frequency range, 1 - 10 MHz., are shown in Figure 4.11. for 30 cm. long hot and cold cathode tubes. The results indicate that the hot cathode tube is far noisier in the 5 - 10 MHz. region. The envelope shape of the oscillations for the cold cathode tube was found to be typical of all cold cathode tubes.

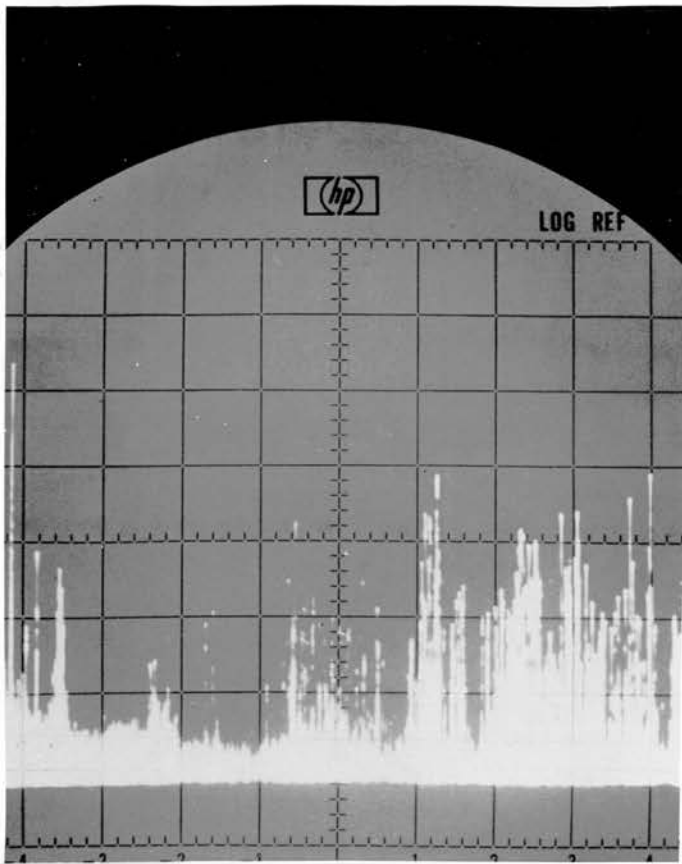
A summary of the observations made would indicate that:

1. Hot cathode tubes are less noisy than cold cathode tubes at low frequencies (0 - 1 MHz.) but are more noisy at higher frequencies.
2. There is a frequency correlation between the oscillations on the laser current and the light output.
3. There is a threshold for onset of these oscillations which may well depend on cathode geometry in the case of cold cathodes.
4. Hot cathode tubes are more likely to have current oscillation in the low frequency range than are cold cathodes.
5. The 17 cm. tube design used in the iodine laser system is free from any oscillations in the region corresponding to maximum power output.

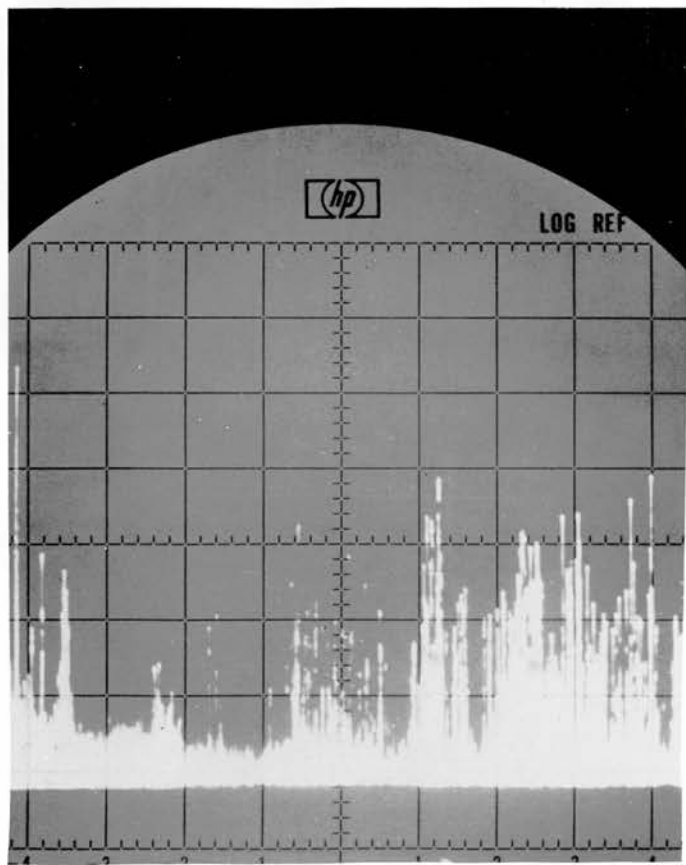
The consensus of these results is that the short cold cathode tube was thought to be suitable for use in the iodine stabilized laser because of the absence of any oscillation peaks and because of its proven reliability. A cold cathode tube of the type described has been in operation for over 1,000 hours with no decrease in output power.

4.7. Observation of Saturated iodine peaks

The laser cavity used in these experiments was 30 cm. long with both piezoelectric ($1\frac{1}{2}$ " PZT 5A) and magnetic type length scanning facilities. The gain tube was 17 cm. long with a 1.5 mm. bore diameter filled to 3 torr of a naturally occurring isotopic neon/helium mixture in a 1 : 5 partial pressure ratio. This pressure was found to be optimum for power output at a 4 mA discharge current. The fused silica iodine tube assembly was 10 cm. long with a 1 cm. inside bore. One mirror had a 60 cm. radius of curvature and maximum reflectivity, and the second mirror was 99.5% reflective with a 1 metre radius of curvature. The general constructional details have already been discussed. The free running stability of the single frequency laser was observed on an optical spectrum analyser, and was estimated to drift not more than 2 MHz. per second under average conditions. Single frequency oscillation was maintained over most of one cavity order, with two modes oscillating over a small range of frequencies. When two frequency operation was observed, one mode was nearing one extreme of the gain bandwidth, and



HOT CATHODE



COLD CATHODE.

FIGURE 4-11
CURRENT SPECTRA OVER 0-10 MHz FOR SIMILAR
HOT AND COLD CATHODE TUBES.

another mode would appear at the opposite end. Single frequency operation over the entire gain bandwidth could be obtained by reducing laser current or detuning slightly one of the mirrors. In a final design the mirror transmission was optimized to give an increase in output power with single mode operation over one order of the cavity.

A length modulation at 1 KHz. over 2 MHz. optical bandwidth was applied to the PZT cylinder from a sine wave oscillator, and the resultant light intensity modulation was detected on a MS5B Ferranti solar cell. The detector was constructed inside a screened box which shielded it both from room lights and also stray pick up. The signal was fed to an AIM phase sensitive detector system with a time constant of 10 milliseconds, the output of which was observed on an oscilloscope. The laser was scanned over a complete order by a ramp voltage derived from the oscilloscope sweep which was suitably reduced and then was supplied to the magnetic scanning coil. A D.C. bias was also supplied to the magnetic coil from a stabilized low voltage power supply. This ensured a reasonably linear frequency scan (section 2.4.) The experimental arrangement is shown in Figure 4.12. and typical results for a scan over one order in Figure 4.13. The oscilloscope was scanned at a display rate of 1 cm. per second which corresponds to 500 KHz. scan in 10 milliseconds (one p.s.d. time constant) to allow complete resolution of the peaks.

The scan shows seven saturated iodine peaks superimposed upon a large background slope signal. The background is due to the general shape of the gain curve modified by the iodine absorption. The observed peaks are the d e f g h i and j components already referred to (Section 3.6.). The iodine curve shapes are the expected "S" shaped features and measurements of the frequency separation of the maximum and minimum show the components to have a full width at half maximum intensity of less than 5 MHz. The set of four peaks, d e f g have a line centre spacing of about 13 MHz. and the h i j curves about 22 MHz. More accurate width or separation measurements were not possible due to nonlinearities in the scan and uncertainty in the dispersion. This could have been overcome, but more accurate methods of performing these measurements will be discussed later. (Section 5.8.)

The curve shown in Figure 4.13. would only be suitable for servo control to the frequency of the absorption feature when a zero p.s.d. voltage crossing occurs. This is because a servosystem would control the laser to zero p.s.d. voltage (Section 2.8). Control of the laser frequency to any other feature would only be possible if a signal were added to the p.s.d. output to offset the zero. The magnitude of this voltage would depend critically on the laser power and the parameters of the detection system, and must also be insensitive to drifts. If this were the case, some arbitrary criterion would be necessary in order to identify a centre of the feature, to which the p.s.d. zero is offset.

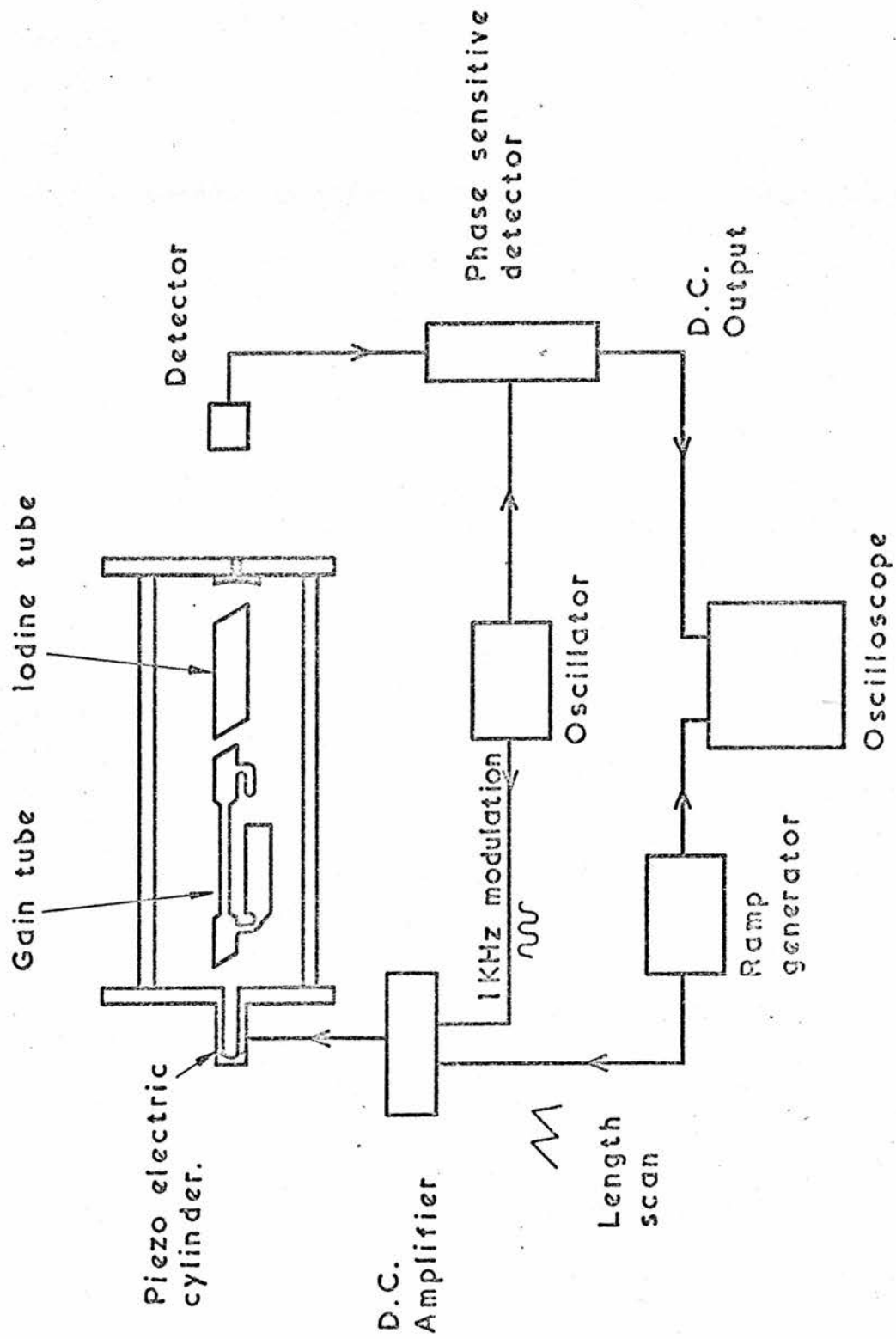
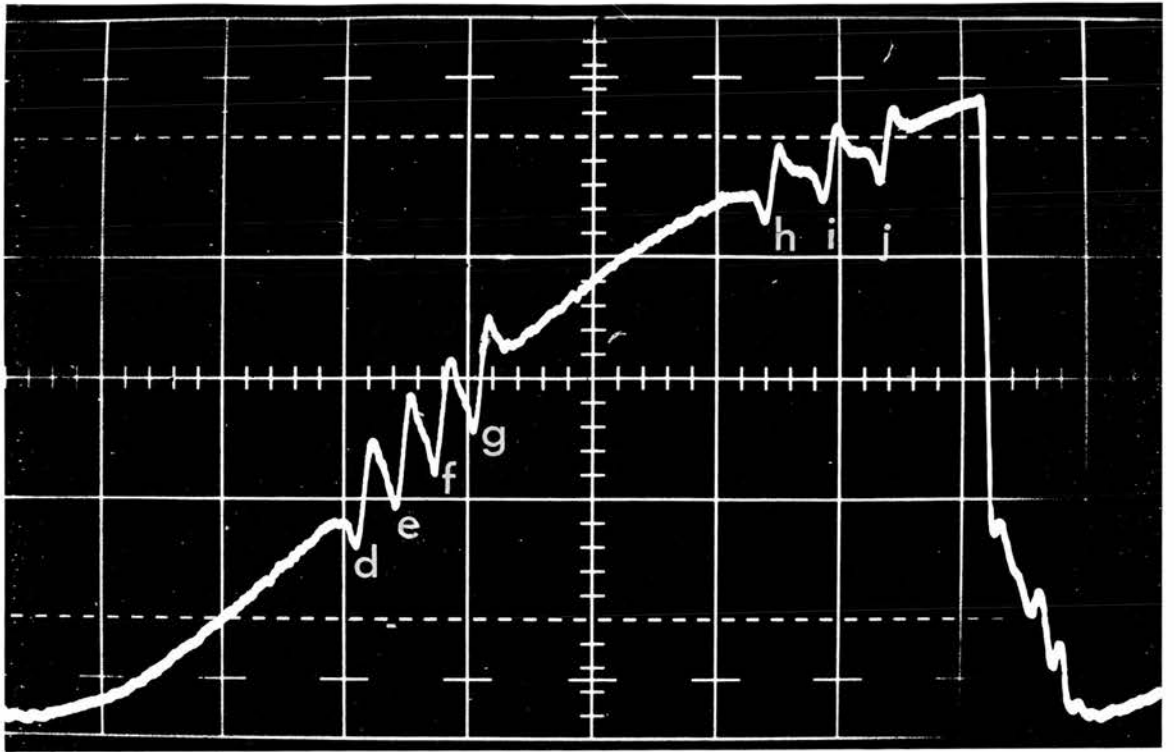


Figure 4.12

THIRD DERIVATIVE DETECTION SYSTEM.



← FREQUENCY

FIGURE 4:13

FIRST DERIVATIVE OBSERVATION OF SATURATED
ABSORPTION IODINE FEATURES.

Such a laser would not be reliably controlled to the true centre of the iodine hyperfine component and the potential high reproducibility of the feature is lost.

Earlier workers (66) found that in their particular laser, component i was fortunately placed in a flat portion of the gain curve and so had a zero voltage crossing to which the laser was controlled. Figure 4.13. shows that a zero offset would be necessary if this short laser were to be servo controlled to component i. The uncertainty in the frequency of the two differently constructed lasers would be a severe disadvantage in the use of these lasers as wavelength standards should the physical properties of the laser be so important. The wavelength of component i was measured by Baird and Hanes (90) and a vacuum wavelength of 632.99139 ± 0.0002 nm. was reported.

More difficulties arise when consideration is given to different laser designs and it will be seen that the position of any set of components relative to the maximum of the gain profile and hence the major zero crossing, depends on the laser tube filling pressures. In the experiments of Hanes and Dahlstrom, (66) a Fox-Smith mode selector was used with a 2 metre long laser to give single frequency operation over the entire gain profile. The laser tube had a bore diameter of 3.3 mm., and so has a total gas pressure of about 1 torr. Moreover the neon used in their experiments was single isotope, neon 20. This means that there are four major differences between the laser of Dahlstrom and Hanes and the short lasers described in this thesis.

- i) The use of differing isotopes leads to totally different gain curve shapes. That of the single isotope is symmetric while naturally occurring neon results in an asymmetric shape.
- ii) The shorter laser has approximately 3 torr more helium than the longer device. This means that the centre of the gain curve would be shifted some 60 MHz. to higher frequency because of the Helium pressure shift of 20 MHz. per torr. (20)
- iii) The pressure shift moves the laser gain curve relative to the iodine line centre features. This means that any given set of peaks will not be near the gain curve centre (and the possible flatter background of the Lamb Dip in a neon 20 laser) for lasers with different gain tube pressures.
- iv) The iodine absorption coefficient varies by a factor of about two over the neon 20 and neon 22 linewidths. This also gives rise to differing gain curve shapes for neon 20 and neon 20/22 mixture lasers.

4.8. Effect of the gain curve shape on the centre of the component

A fuller account of the effects of the background slope on the saturated absorption feature is presented in this Section.

Let us consider a Lorentzian absorption feature superimposed on a sloping background curve. Figure 4.14. shows the first derivative of this Lorentzian plus the derivative of the curved background which is approximated as a straight line over the narrow region of the absorption curve. The Figure shows the effects of three different slopes on the same shaped Lorentzian; situations which would occur if, because of isotope and pressure effects, a component were to fall on different slope regions of the gain curve.

The Figure shows:

- i) The X axis crossing point is not at the centre of the absorption line. This crossing represents the control zero of the p.s.d. system.
- ii) The resulting curve is asymmetric and the apparent width defined by the separation of the maximum and minimum, is not that of the original derivative.
- iii) A steep slope obscures the shape of the derivative shape.
- iv) The mean signal between the two peaks (a possible centre sensing technique) would be different should the slope around a particular control feature vary.

In particular, as mentioned earlier, where the absorption features occur away from a natural zero voltage crossing level, the p.s.d. zero must be offset to realise this situation and allow locking of the laser frequency to this feature. Where zero offsets are required, the reproducibility of the setting point is open to question.

As a method of eliminating the effects of the sloping background, a further differentiation could be carried out. The gradual changing slope of Figure 4.13. would be reduced almost to zero. However, the second derivative of a Lorentzian is a symmetric function and so a servosystem operating in the normal locking mode would be unable to sense the direction of any frequency change of the laser with respect to the centre of the absorption line. The third derivative, however, is asymmetrical and provides a suitably shaped discriminant to which a laser may be locked. The centre of the absorption feature is much more precisely identified as the point of maximum rate of change of curvature of the absorption peak on the gain curve. This implies that observation of the third derivative of the gain-frequency curve, rather than the first derivative, would result in a zero p.s.d. voltage at the true centre of the absorption line.

The shapes of the fundamental, first and third derivatives are plotted in Figure 4.15. for a Lorentzian $I = \frac{3}{1+\nu^2}$ It will be observed that:

- i) the third derivative is smaller than the first derivative;
- ii) the separation of the peaks $\Delta\nu$ is smaller for the first derivative than for the third. For the first derivative $\Delta\nu = 2\sqrt{3} = 1.165\sqrt{3}$

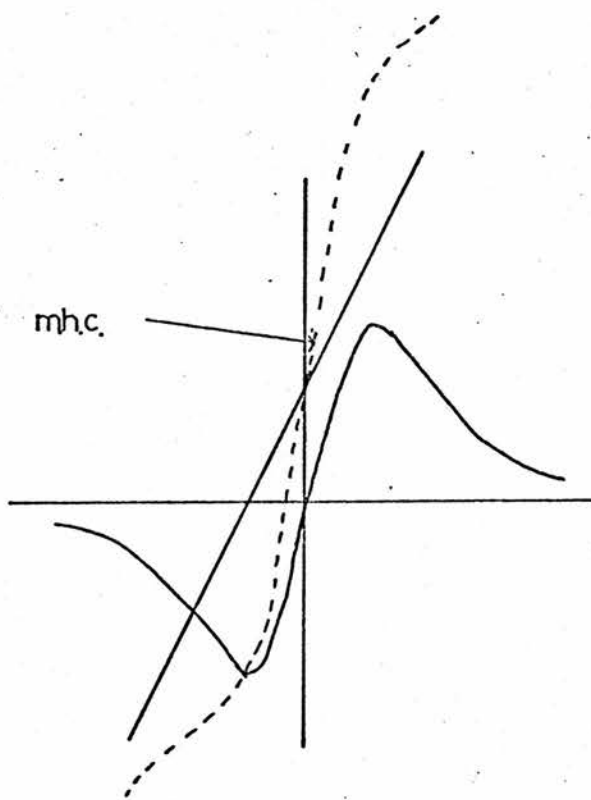
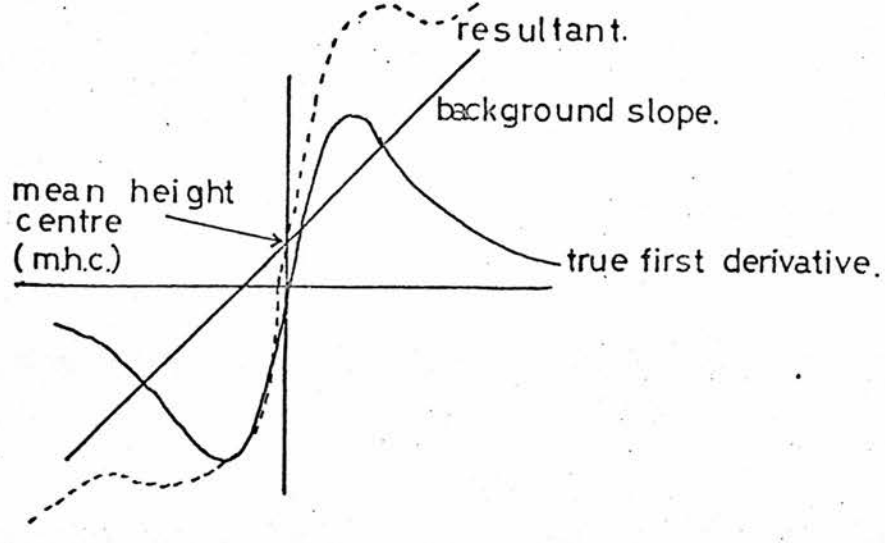
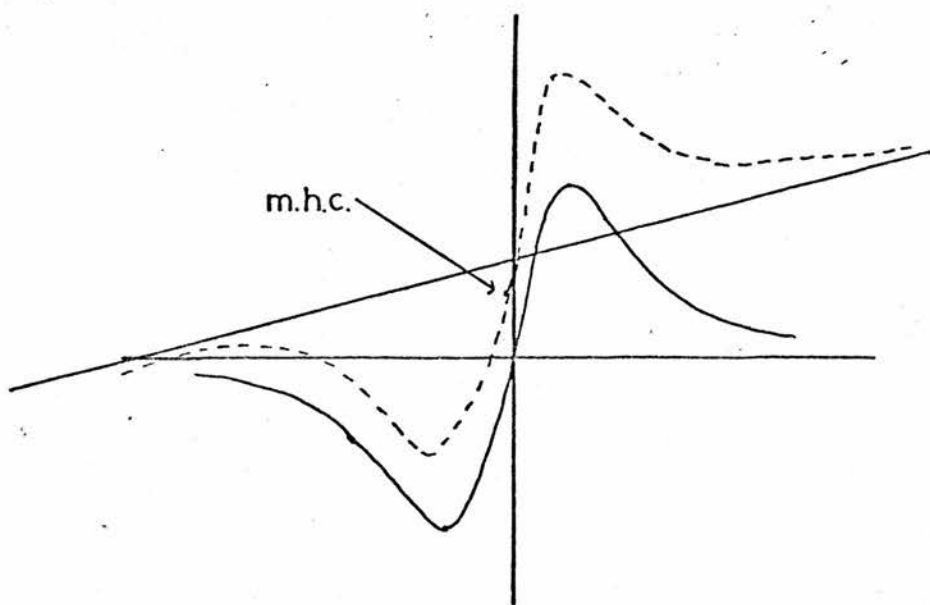


FIGURE 4.14
EFFECTS OF A BACKGROUND
SLOPE ON THE FIRST
DERIVATIVE OF A
LORENTZIAN FUNCTION.



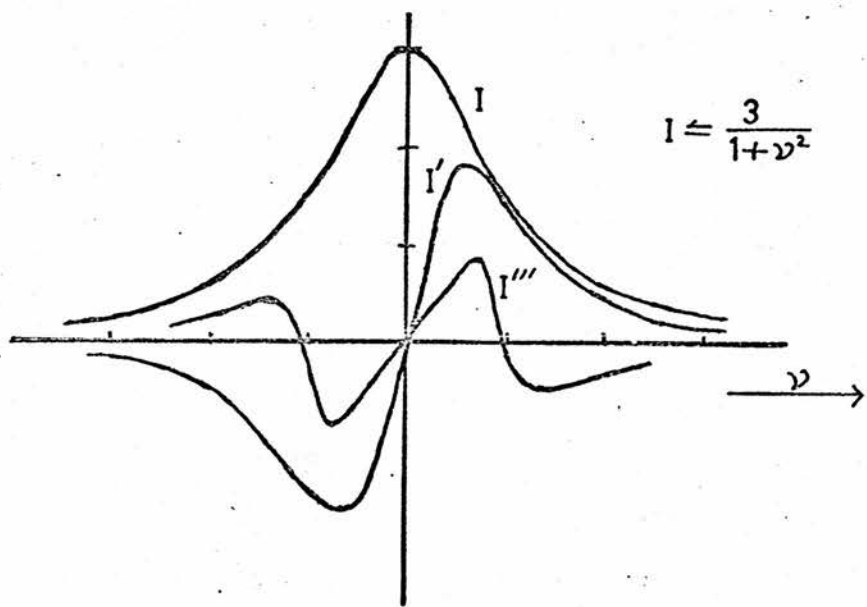


FIGURE 4.15
THE FUNDAMENTAL FIRST AND THIRD
DERIVATIVES OF A LORENTZIAN FUNCTION

where γ is the HWHM of the Lorentzian line shape and for the third derivative $\Delta\nu = 1.53$.

This means that the first derivative has intrinsically a narrower control range.

iii) The "sensitivity" defined by $\frac{dI}{d\nu}$ is lower for the third derivative than the first derivative around the centre.

4.9. Third derivative locking

Let us consider the technique used in locking a laser to any feature (91). A single frequency laser is modulated to produce frequency modulation around a mean frequency. The laser intensity I is a function of laser frequency, and we shall also include in this function a term representing the frequency modulation imposed on the laser. The amplitude of this modulation is k and the frequency is ω . Then:

$$I = F(\nu_0 + k \sin \omega t) \quad (4.1.)$$

where ν_0 is the mean frequency of oscillation. This is expanded in a Taylor's series which is valid for small values of k and, after some manipulation, we arrive at

$$I = F(\nu_0) + (k \sin \omega t) F'(\nu_0) + \frac{k^2}{2!} (\sin^2 \omega t) F''(\nu_0) + \frac{k^3}{3!} (\sin^3 \omega t) F'''(\nu_0) \quad (4.2.)$$

where $F^n(\nu_0)$ is the n^{th} derivative of $F(\nu_0)$.

Gathering terms in $\sin \omega t$, $\sin 2\omega t$, $\sin 3\omega t$, we have for the coefficients of:

$$\sin \omega t : k F'(\nu_0) + \frac{k^2}{8} F''(\nu_0) + \frac{2k^3}{960} F'''(\nu_0) + \dots \quad (4.3.)$$

$$\sin 2\omega t : \frac{-k^2}{4} F''(\nu_0) - \frac{1k^4}{96} F''''(\nu_0) \dots \quad (4.4.)$$

$$\sin 3\omega t : \frac{-k^3}{24} F'''(\nu_0) - \frac{3k^5}{2120} F''''''(\nu_0) \dots \quad (4.5.)$$

The leading term in the coefficient of $\sin n\omega t$ is proportional to $k^n F^n(\nu_0)$.

This tells us that observation of the n^{th} harmonic of the fundamental frequency modulation carries information about the n^{th} derivative of the gain curve shape.

We now need to specify F in the region of an absorption line, of width $2a$, and the above equations show that if F is of the form

$$F(\nu) = \frac{\gamma}{\gamma^2 + \nu^2} + B\nu^2 + C\nu + D \quad (4.6.)$$

The second and subsequent terms describe the gain curve as being quadratic in form.

The first differential, corresponding to phase sensitive detection at the fundamental modulation frequency as described in Section 4.7., shows that the gain curve shape gives rise to a straight line first differential of the form $2B\nu + C$. This representation seems justified by the observed differential curves (Figure 4.13.) Observation at 2ω gives a D.C. offset $2B$.

Observation at ω , however, reduces the effect of the background to zero. This gives a zero p.s.d. output voltage crossing for the true centre of each saturated absorption component and so will produce a more reliable control point.

4.10. Shape of the saturated absorption features

Let us again consider a Lorentzian shaped feature of width 2γ

$$I = \frac{\gamma^2}{\gamma^2 + \nu^2} \quad (4.7.)$$

and then:

$$I' = \frac{-2\nu\gamma^2}{(\nu^2 + \gamma^2)^2} \quad (4.8.)$$

$$I'' = \frac{6\nu^2\gamma^2 - 2\gamma^4}{(\nu^2 + \gamma^2)^3} \quad (4.9.)$$

$$I''' = \frac{24\nu\gamma^4 - 24\nu^3\gamma^2}{(\nu^2 + \gamma^2)^4} \quad (4.10.)$$

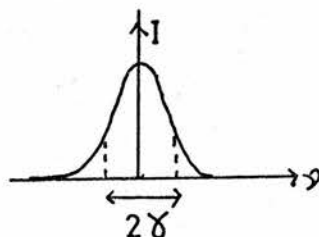
These curve shapes are reproduced in Figure 4.16. together with the separations of their maxima and minima. The first derivative has a peak spacing of $2\gamma / \sqrt{3}$ and the third 1.6γ . The second derivative is unsuitable as a frequency lock feature since it is symmetrical around $\nu = 0$ which would mean that a discriminant of this form would not be capable of indicating to which side of $\nu = 0$ the laser had drifted.

The choice of the third derivative feature therefore eliminates the effect of a quadratic gain curve shape and gives a suitable discriminant of "width" 1.6γ Figure 4.15. plots the first and third derivative of a function $F = \frac{\gamma}{1 + \nu^2}$ together with F, that is a Lorentzian of height γ and full width 2 . The Figure indicates that the slope of the first derivative is steeper near zero frequency than the third derivative slope. This means that the sensitivity of the third derivative discriminant would be less than the first for a given frequency shift from the centre.

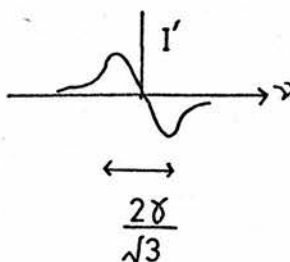
However, we see from equations 4.3, 4.4, and 4.5., that the leading term in the expression for the n^{th} harmonic is of the form (k^n / γ^{n+1}) . The magnitude of the n^{th} harmonic signal will increase as the modulation bandwidth increases but increases far more rapidly for the third harmonic than for the first harmonic. The use of larger modulation bandwidths, therefore, should increase the magnitude of the third harmonic signal. This is observed in practice, and the size of the third derivative detected curves is optimum for frequency scans of some 6 MHz. peak to peak whilst 2 MHz. peak to peak is optimum for observation of the first derivative features. The observed

FIGURE 4.16
 LINESHAPE PARAMETERS OF LORENTZIAN DERIVATIVES

$$I = \frac{\gamma^2}{\nu^2 + \gamma^2}$$



$$I' = \frac{2\nu\gamma^2}{(\nu^2 + \gamma^2)^2}$$

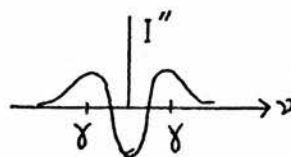


$$I'' = \frac{6\nu^2\gamma^2 - 2\gamma^4}{(\nu^2 + \gamma^2)^3}$$

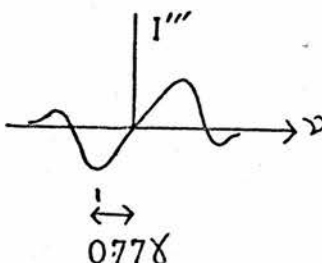
= 0 when

$$\nu = \frac{\gamma}{\sqrt{3}}$$

= 0.58\gamma



$$I''' = \frac{24\nu\gamma^4 - 24\nu^3\gamma^2}{(\nu^2 + \gamma^2)^4}$$



$$I = \frac{1}{(\nu^2 + \gamma^2)^5} \left(\left\{ \nu^2 + \gamma^2 \right\} \left\{ 24\gamma^4 - 72\nu^2\gamma^2 \right\} - 8\nu \left\{ 24\nu\gamma^4 - 24\nu^3\gamma^2 \right\} \right)$$

= 0 when

$$\nu = \pm \gamma \left(1 \pm \frac{1}{2} \sqrt{\frac{1}{5}} \right)$$

= 0.767\gamma \quad \text{and} \quad 1.223\gamma

third derivative signals are of similar size to the first derivative signals if the optimum scan widths are used. If the modulation is increased so that k becomes comparable with the peak separations of the feature, then the shape becomes obscured and sensitivity is again lost.

4.11. Third Derivative Observation of Saturated Absorption Features

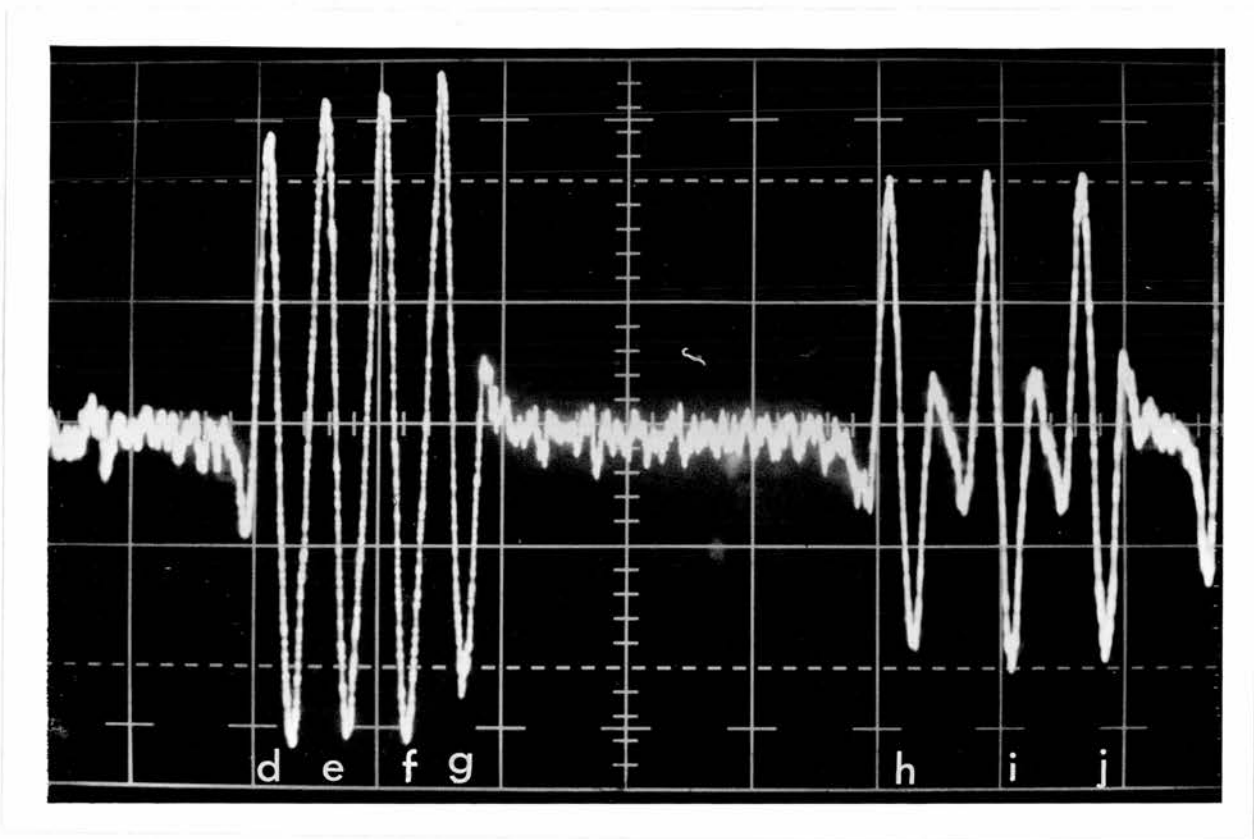
The third derivative curves are observed in much the same way as the first except that the phase sensitive detector is adjusted to detect at three times the modulation frequency. This presents three practical requirements.

- i) A third harmonic reference signal locked in phase to the fundamental must be generated.
- ii) This third harmonic signal must be free from first harmonic breakthrough otherwise the p.s.d. output will contain a signal corresponding to first derivative.
- iii) The modulation frequency on the laser must be a pure sine wave free from harmonics, otherwise the p.s.d. detects an amplitude modulation at 3ω which is not due to the nonlinear curve shape. If the gain curve were a pure straight line, only fundamental frequency amplitude modulation would be generated.

These conditions were satisfied and the results for a scan over one order are shown in Figure 4.17. for a modulation of 6 MHz. peak to peak and a p.s.d. time constant of 0.1 secs. The dispersion is about 20 MHz. per cm., the scan was such that a 1 cm. display was covered in 2 seconds and zero p.s.d. voltage occurs at the centre of the vertical scale. The figure shows excellent resolution of h.i.j. components, whilst d.e.f.g., being closer together are not so well resolved. This latter fact is due both to the small separation of d.e.f.g. and to the p.s.d. time constant. Complete resolution is observed if the laser is scanned more slowly, the time constant reduced, or the modulation bandwidth reduced, in which case, the size of the signal decreases.

In these experiments all length variations on the laser were made using the piezoelectric cylinder alone, in other words, the magnetic scan coil was not used.

The signal to noise ratio on these curves is extremely good, with elimination of the detrimental background effects observed in first derivative scans. Frequency locking to any of the d.e.f.g.h.i.j. features is quite possible and will be described in the next chapter.



← FREQUENCY.

FIGURE 4.17

THIRD DERIVATIVE OBSERVATION OF SATURATED
ABSORPTION IODINE FEATURES.

CHAPTER 5

EXPERIMENTAL RESULTS

In this chapter the results of preliminary experiments on two iodine stabilized lasers over a variety of experimental conditions will be presented. These experiments were directed towards measuring the frequency stability, reproducibility and performance of the lasers from day to day. The ultimate reproducibility of the iodine line is indicated from measurements of the Allan Variance. These measurements show that the existing systems may be improved, and new lasers of improved construction are currently under development.

The performance of the laser when subjected to variations in iodine pressure, laser power, and scan width is of vital importance in assessing the suitability of the laser as a length standard. Preliminary measurements of these variations have been made. They indicate the path towards greater understanding of saturated absorption phenomena and show the need for further experiments to complete the investigation of the laser system.

The various experiments will be discussed separately, and then the situation summarised.

5.1. Summary of known data concerning the iodine absorption lines prior to this work

- i) At 1 torr pressure, the iodine saturated absorption linewidths, observed by a first derivative method, are broadened by a factor of two. (66)
- ii) Pressure broadening may be expected to be less than some 2.6 MHz. per torr. (70)
- iii) Magnetic fields of 500 gauss broaden the d e f g lines by less than 1 MHz., and h i j broadenings were not observed. (66)
- iv) Wavelength shifts were less than 2 MHz. for a magnetic field of 500 gauss. The frequency perturbations from a variation of 5% in the earth's field would therefore be less than 2 parts in 10^{-13} (66)
- v) When the iodine pressure was raised from 40 millitorr to 1 torr, no wavelength shift greater than 2 MHz. was observed. (66)

5.2. Effects of the Finite Scan Width

5.2.1. Broadening by the Scan - Third Derivative Detection

In the theoretical discussion of Chapter 4.9, it was emphasised that the Taylor expansion treatment was valid only for small modulation amplitudes k . In practice k is some 6 MHz., and is comparable with the width of the absorption features for optimum observation of third derivative signals. The effects of such a wide scan are not easily evaluated by the method of Section 4.9 and a different approach is necessary.

We wish to calculate the third harmonic lineshape of a Lorentz lineshape

$\frac{1}{1 + \nu^2}$ which has a F.W.H.M. of 2 units and a height of 1 unit, and evaluate

and evaluate this lineshape for a variety of values of k .

Figure 5.1. illustrates the experimental situation for such a curve with an applied modulation at a frequency ω and a width k at an optical frequency α from line centre.

We know from Fourier Theory, that any periodic function $f(t)$ may be expanded as a series

$$f(t) = \frac{1}{2} a_0 + \sum_{n=1}^{\infty} a_n \cos nt + \sum_{n=1}^{\infty} b_n \sin nt \quad (5.1.)$$

where $a_0 = \frac{1}{2\pi} \int_{-\pi}^{\pi} f(t) dt \quad (5.2)$

$$a_n = \frac{1}{\pi} \int_{-\pi}^{\pi} f(t) \cos nt dt \quad (5.3.)$$

and $b_n = \frac{1}{\pi} \int_{-\pi}^{\pi} f(t) \sin nt dt \quad (5.4.)$

In our experimental situation, we are interested in extracting the Fourier coefficients corresponding to the third harmonic of the modulation frequency, and so must evaluate a_3 and b_3 .

Applying the theorem to our function we have, since the $\sin 3\omega t$ terms all vanish:

$$a_3 = \frac{1}{\pi} \int_{-\pi}^{\pi} \frac{\cos 3\omega t \cdot d(\omega t)}{(a + k \cos \omega t)^2 + 1} \quad (5.5.)$$

This integral may be solved by complex integration using the residue method and evaluated numerically using a computer. The results are indicated in Figure 5.2. which shows part of the third harmonic curve for a variety of modulation amplitudes, k . The figure shows the amplitude of the coefficient a_3 . This must be multiplied by a scale factor of k^3 if the true magnitude of the third derivative signal is to be found. This signal will therefore decrease for small values of the applied modulation, and an optimum value exists which ensures satisfactory detection of the third derivative signals. Experimentally, a scan of some 6 MHz. is required to give a good signal to noise ratio: for both larger and smaller scans the observed signal decreases. The importance of figure 5.2. lies in the fact that it predicts the scan broadening of a Lorentzian of width 2; no significance should be attached to the magnitude of the curves. Clearly, the separation of the maxima and minima increases as the scan width increases.

This theoretical prediction was investigated experimentally using the beat frequency apparatus discussed in section 2.7. One of the two lasers was locked to a chosen hyperfine component of the d e f g group (Figure 3.2.) and the second laser was scanned over a small range, typically 70 MHz, around zero beat frequency, therefore encompassing the d e f g features of the frequency scan of this laser. Both lasers were operated using third derivative detection techniques.

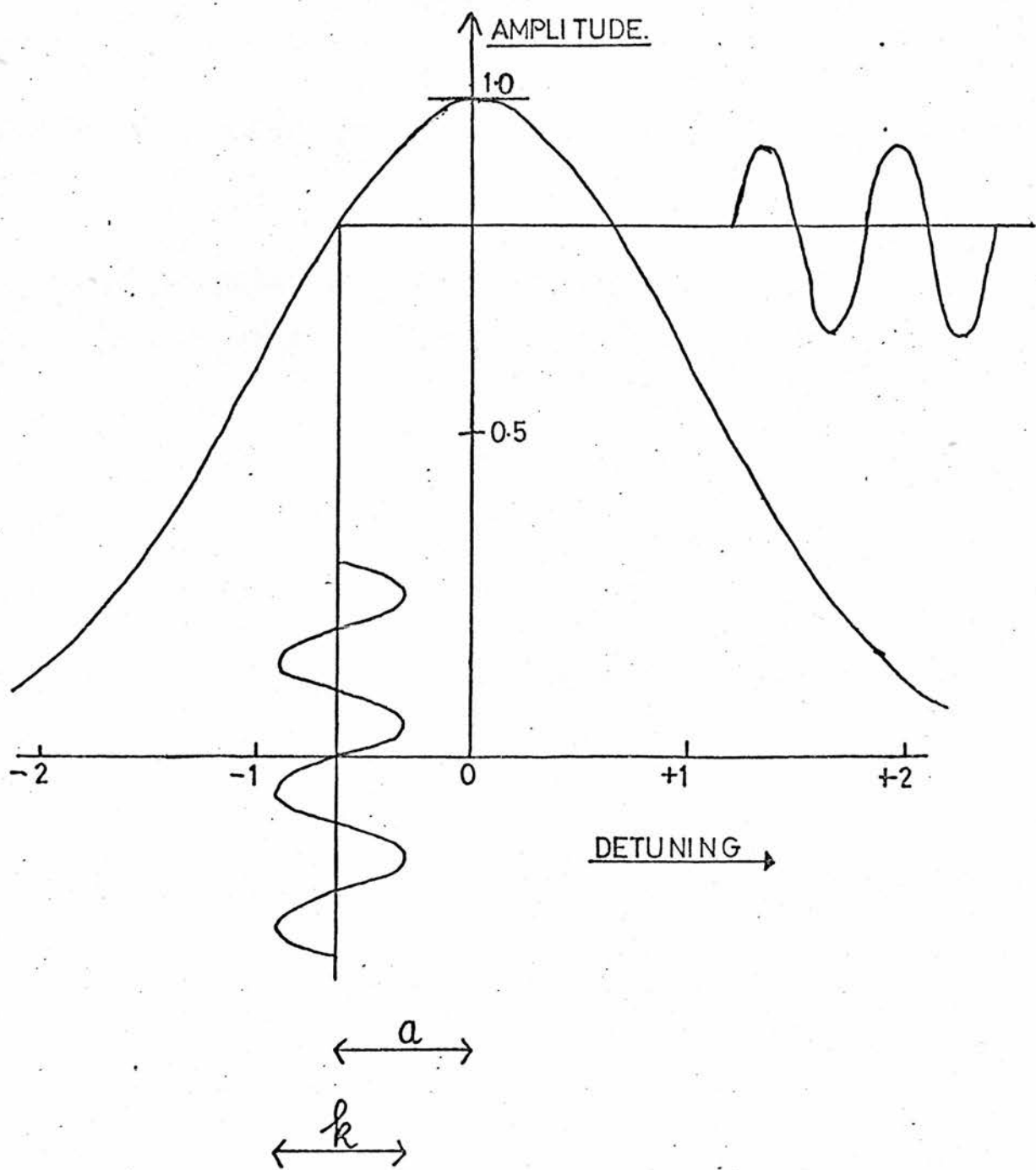


FIGURE 5.1
LORENTZ LINESHAPE - SCAN BROADENING

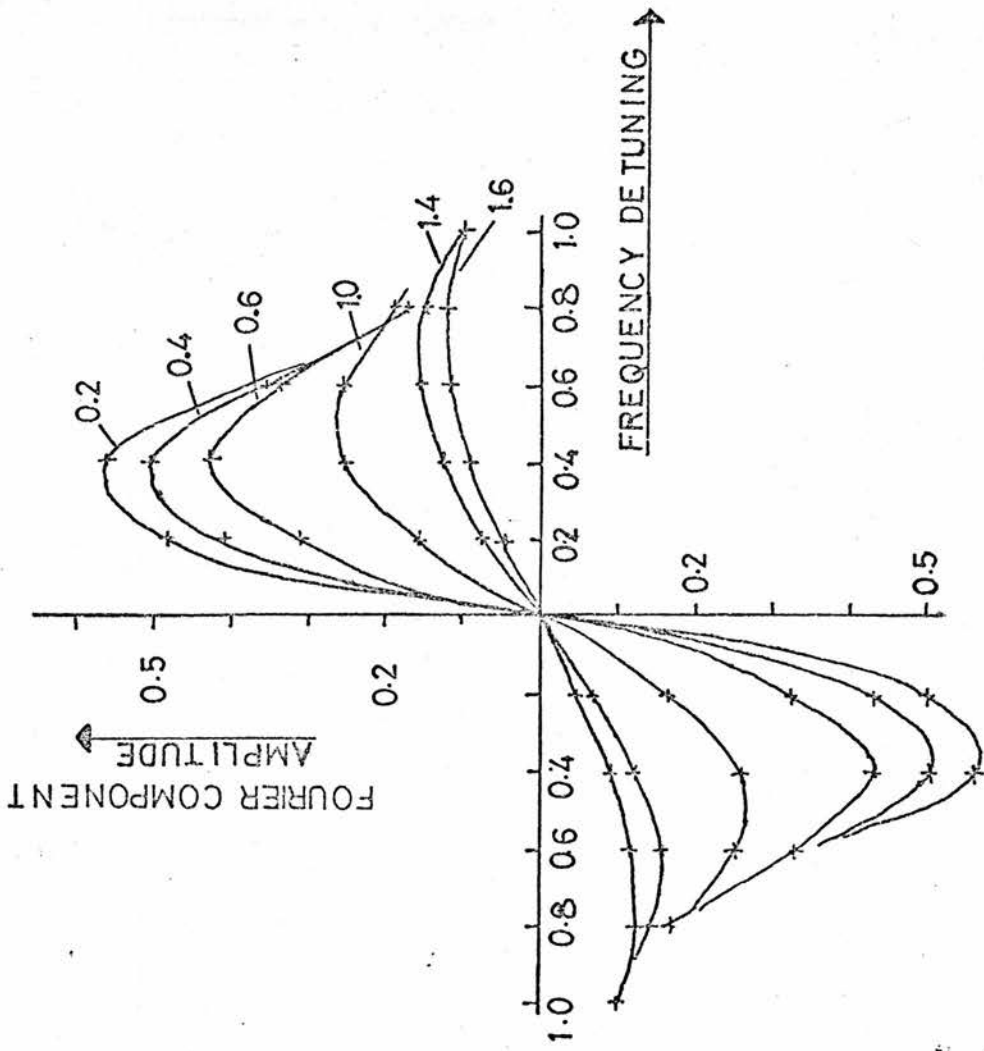


FIGURE 5.2

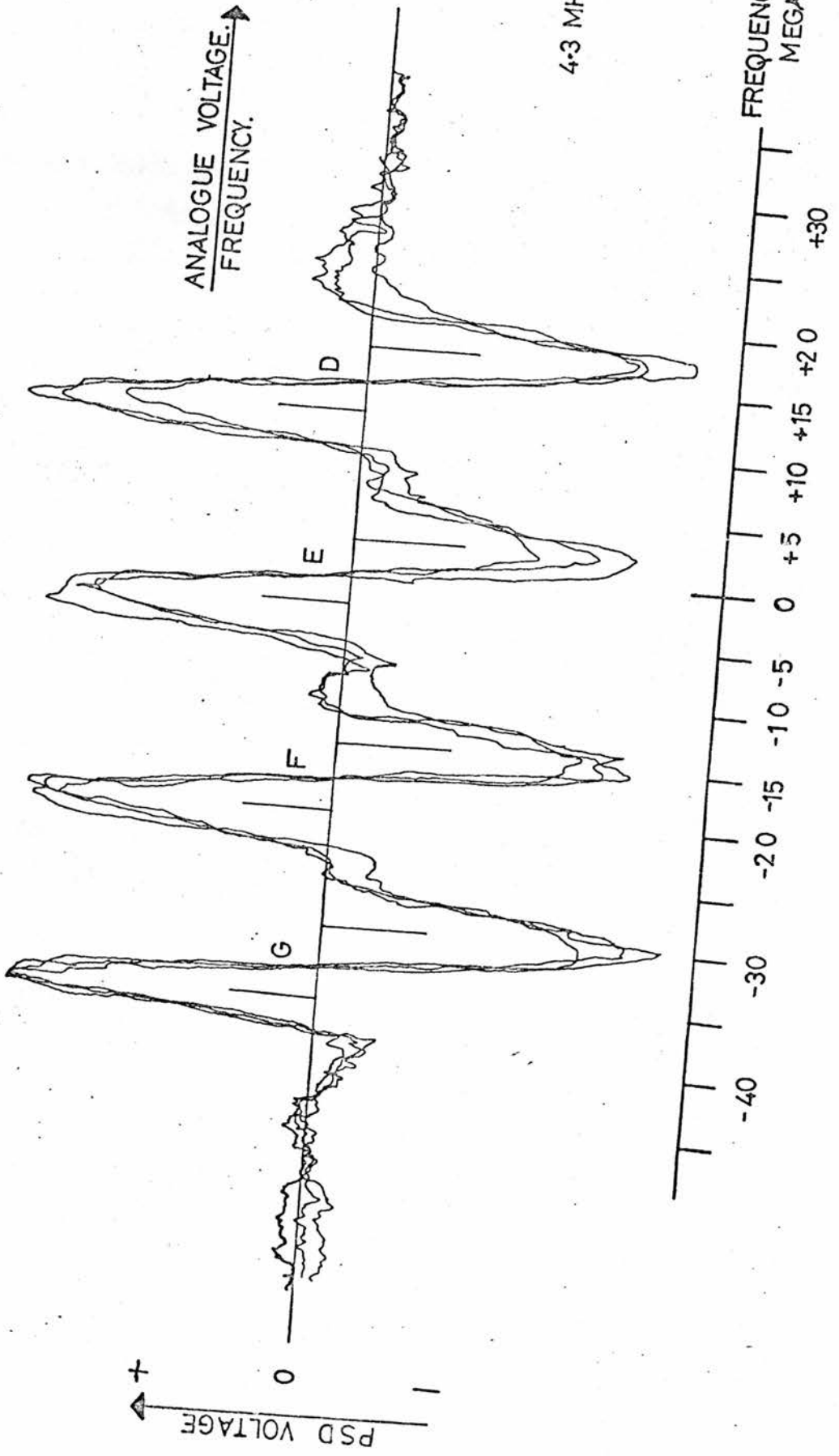
THIRD HARMONIC BROADENING FOR VARIOUS MODULATION AMPLITUDES.

The unlocked laser was modulated at a frequency near 1 KHz., and the A.C. peak to peak voltage modulation applied to the PZT was observed on an oscilloscope connected to the piezoelectric. The magnitude of this A.C. voltage was variable, and the piezoelectric tube had a calibrated sensitivity. (Section 2.4.) The imposed optical frequency modulation was therefore known for various applied voltages. As the unlocked laser was scanned over its d e f g peaks, the output of a phase sensitive detector monitoring the third harmonic component in the light output of this laser was displayed as the Y signal on an X-Y recorder. The X scan was provided by a linear analogue output of known voltage to frequency sensitivity from the beat frequency unit (Section 2.7). The X axis of the chart recorder scale was therefore calibrated in terms of frequency. A variable radio frequency signal from an oscillator could also be injected into the beat frequency system where it was displayed and counted as would be a laser beat frequency. This provided the means for convenient quick check on the sensitivity of the frequency scan on the chart recorder. The analogue output was used to give an X shift on the chart recorder, and in this way, the recorder X scale was calibrated in frequency terms since the oscillator frequency could be varied and resulted in different pen displacements on the recorder.

A typical result of four superimposed scans is shown in Figure 5.3. for the peaks d e f g. The width of the features, as defined by the maximum - minimum separation, was measured by dropping a perpendicular to the zero line from the mean position of the extrema. The width of the recording was converted to a frequency separation by the conversion factor determined above. In this way the widths of the features could be measured to better than 0.5 MHz. A check on these measurements was also possible. The unlocked laser was scanned over the group of four components and a pen recorder scan traced out as described. The input to the beat frequency apparatus was then replaced by the signal generator which was tuned to move the recorder pen to the positions of the maxima and minima of each component. The input frequency was counted for each pen position, and the peak widths measured directly from the frequency measurements. The results of this agreed with the earlier measurements to within the accuracy of the measurement and peak estimation technique.

A series of experiments was carried out for different modulation voltages and measurements of the peak separations for various a.c. voltages (or frequency modulations) were made. The results are shown in Figure 5.4., together with theoretical values obtained from the calculation outlined earlier for different frequency modulations. No distinction is made here between the d, e, f or g peaks. The theoretical model was normalised to have a zero scan width of 1.7 MHz. peak to peak which is the value for zero scan width obtained by extrapolating the experimental results.

FIGURE 5.3
THIRD DERIVATIVE SCAN



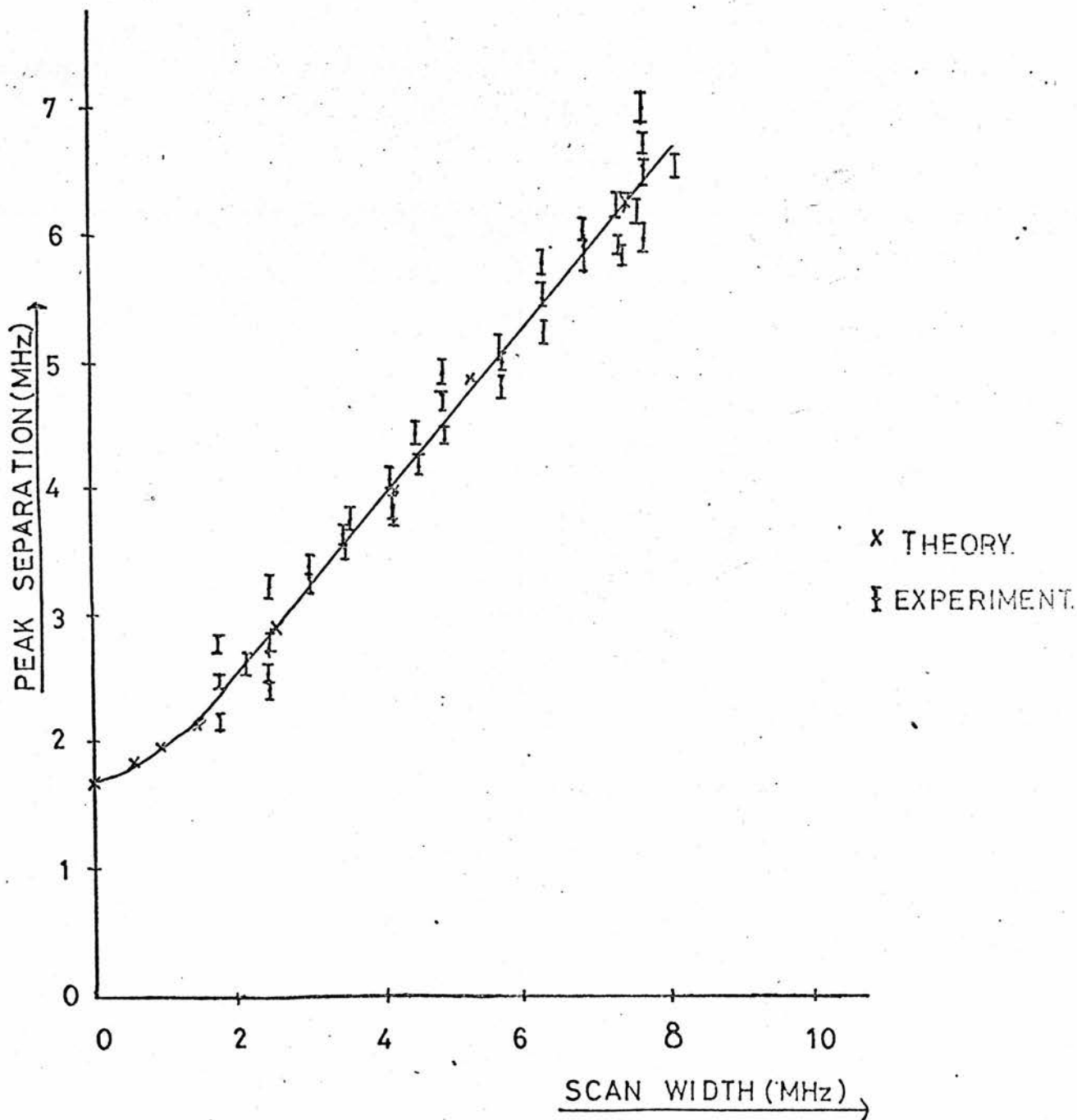


FIGURE 5.4

THIRD DERIVATIVE SCAN BROADENING.

The experimental results indicate that the d e f and g components appear to have comparable widths. The experimental points and the theoretical predictions agree within the spread of the measured values, and the slope of the line gives a broadening of some 0.5 MHz., per 1 MHz., scan width. The experiments were carried out for frequency scans up to about 8 MHz. For larger scans the scan becomes comparable with the separation of the hyperfine components (some 13 MHz). The theory, which was derived for an isolated Lorentzian lineshape, would then not apply as the effects of the neighbouring lines would begin to appear since the modulation encompassed sections of adjacent features. For scan widths smaller than those measured, a low signal to noise ratio made precise identification of the small maxima and minima impossible.

5.2.2. Frequency Shifts

The effects of variations of the scan width on the beat frequency between two locked lasers were investigated. Two lasers were locked, using third derivative techniques, to components d and g respectively. The beat frequency was counted for integration times of 10 seconds and the results of subsequent averages plotted as shown in Figure 5.5. Successive measurements are plotted and are joined together. This does not, however, indicate that the beat frequency follows this path but is done to clarify the experimental points.

The scan on the laser locked to component d was maintained at 6 MHz., but that on the laser locked to g was varied, and the change in the d - g beat frequency for different scan widths is shown in Figure 5.6. The error bars indicate the accuracy of estimating the centre of the beat frequency envelope. The beat frequency increases as the scan width on the laser locked to line g is increased, and the linear variation has a slope of 13 KHz. per MHz. frequency modulation width. This result emphasises the need for identical scan widths on any two lasers which are compared in a beat frequency experiment. A scan difference of 1.5 MHz. near the optimum scan of 6 MHz., would create a frequency shift of 20 KHz., or 1 part in 10^{10} . For comparison or reproducibility studies at this level, the scan widths must therefore be controlled to within 1.5 MHz.

It seems likely that these shifts are due to the large applied modulation which encompasses parts of more than one component. As a means of investigating the nature of the shifts still further, a comparison between lasers locked to the d and f components will shortly be made. In this case, the modulation on the f component will be increased, and any shift measured. The presence of components e and g on either side of f might well give rise to a different shift from the measurements described above.

FIGURE 5.5

VARIATION OF BEAT FREQUENCY WITH SCAN WIDTH.

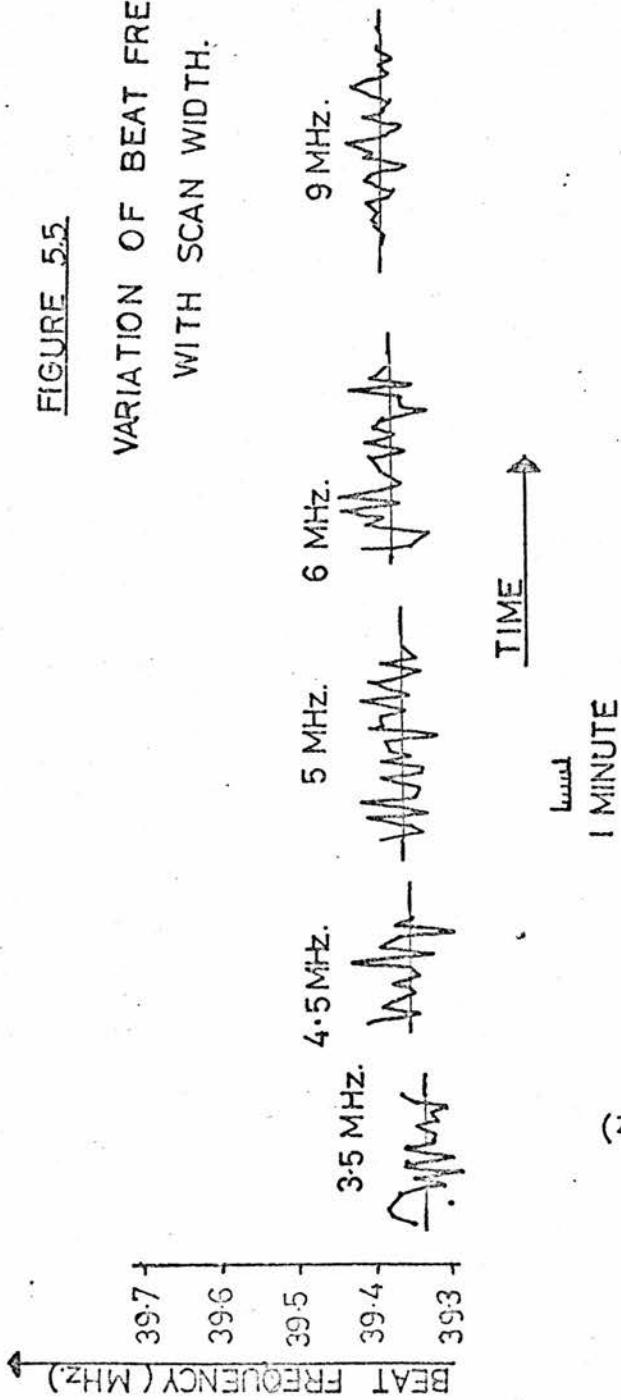
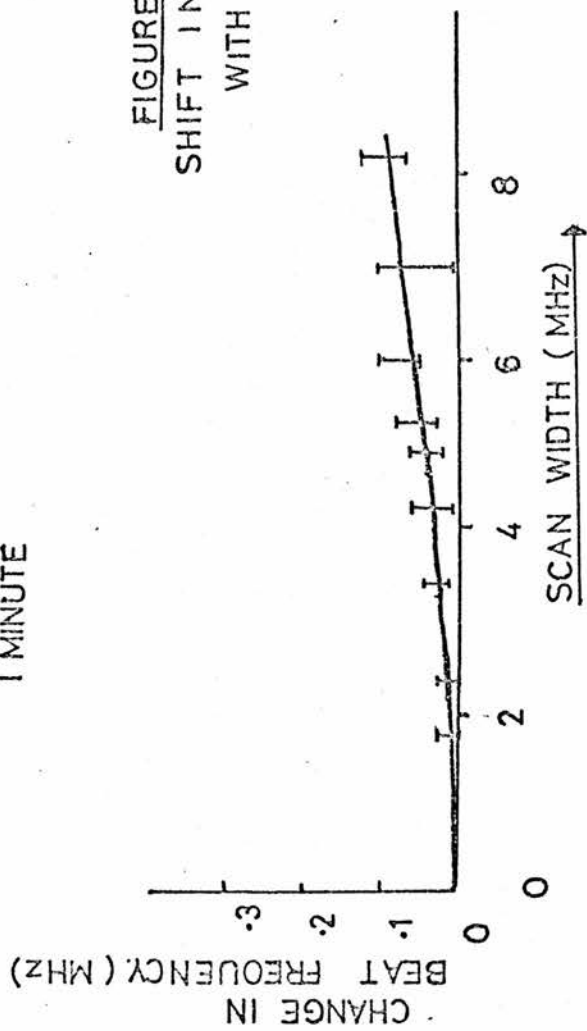


FIGURE 5.6
SHIFT IN BEAT FREQUENCY WITH SCAN WIDTH.



5.2.3. Broadening by the scan - First Derivative Detection

The peak to peak modulation widths necessary for satisfactory observation of the saturated absorption features by first derivative techniques are smaller than those for third derivative methods. Nevertheless, broadening of the observed peak width may be measured. As might be expected, the broadening is small under normal operating conditions, but a knowledge of the variation with modulation amplitude is important for experiments to be discussed later in the chapter.

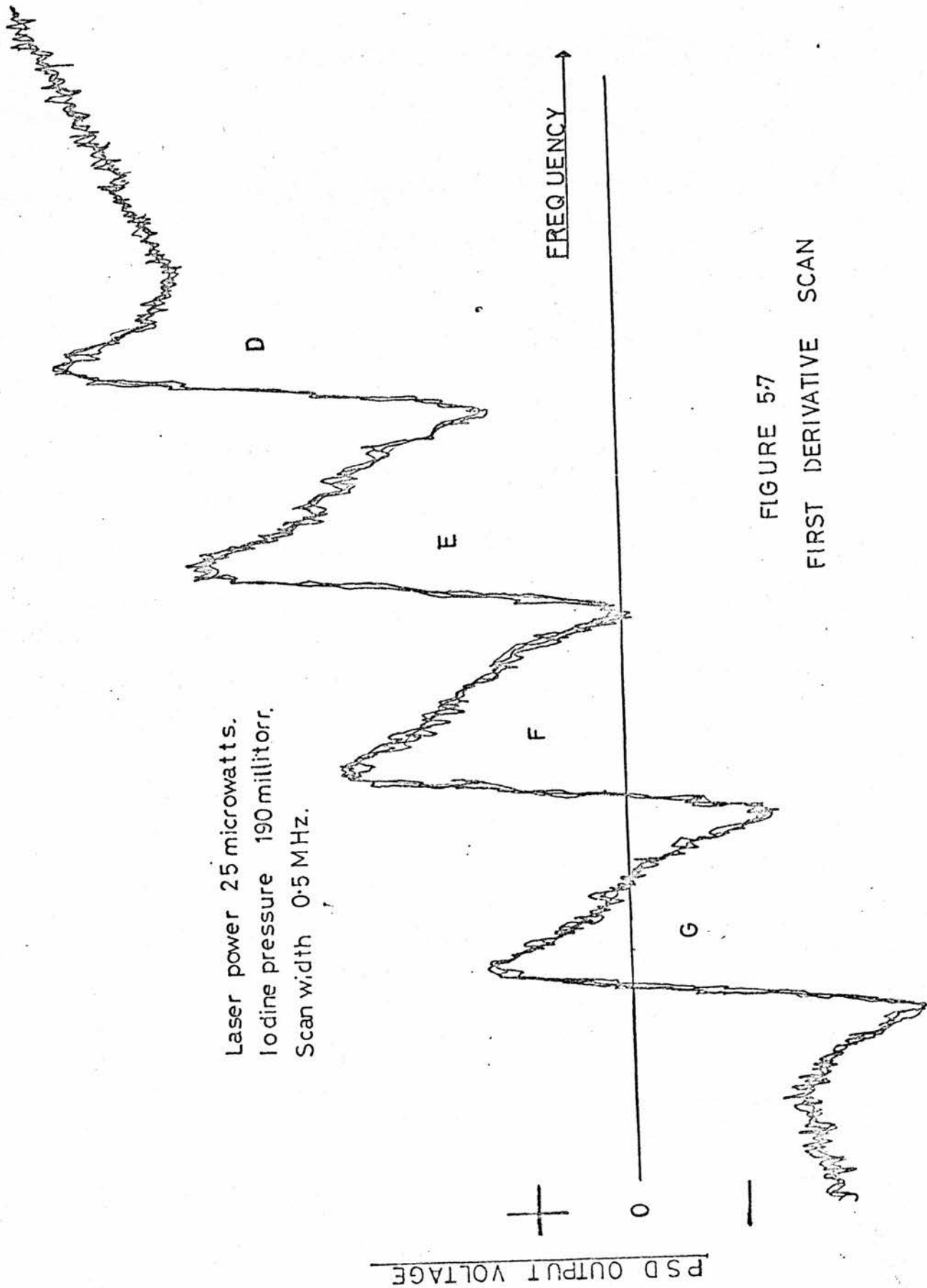
The measurement of peak widths, observed in first derivative form, involved a technique similar to that discussed in Section 5.2.1. except that the p.s.d. reference frequency for the scanned laser was at the fundamental modulation frequency, and not three times it. The reference laser was locked to component d in the third derivative mode. A typical p.s.d. output scan versus frequency as observed on a chart recorder is shown in figure 5.7. In this case, the laser power was 25 microwatts and the iodine pressure was 190 millitorr. The p.s.d. time constant was 0.1 seconds. The peak widths for each of the four components were estimated by measuring the peak separations on the chart recorder and converting this to a frequency width from the known dispersion of the X sensitivity. This measurement may be made with an accuracy better than 0.5 MHz. The measurement was made for a series of modulation amplitudes which were again measured by observing the peak to peak a.c. voltage on the piezoelectric tube using an oscilloscope.

A theoretical evaluation of the expected broadening was carried out following the technique outlined in 5.2.1. The first Fourier component is involved in this treatment and:

$$a_1 = \frac{1}{\pi} \int_{-\pi}^{\pi} \frac{\cos \omega t \, d(\omega t)}{(a + k \cos \omega t)^2 + 1} \quad (5.6.)$$

was evaluated for a range of a and k using a complex integration technique for a Lorentzian of F.W.H.M. 2. Figure 5.8. shows the computed broadening for k values of 0, 0.6, 0.8, 1.0, and 1.2. The dotted line is the locus of the maximum of the first harmonic component and indicates the broadening to be expected from observations of the peak widths using these modulation amplitudes. As with the calculations described in Section 5.2.1., the computed curve does not indicate the magnitude of the experimentally observed first derivative signals. Obviously a zero scan would give no signal and large scans would become dominated by the shape of the gain curve.

These predictions were compared with experiment, and Figure 5.9. shows the results of measurements on the broadening of component d for a range of peak to peak scan widths. The solid line is the theoretical prediction and



Laser power 25 microwatts.
Iodine pressure 190 millitorr.
Scan width 0.5 MHz.

FIGURE 5.7
FIRST DERIVATIVE SCAN

FIGURE 58

COMPUTED SHAPE OF SCAN BROADENED
FIRST DERIVATIVE LINESHAPE.

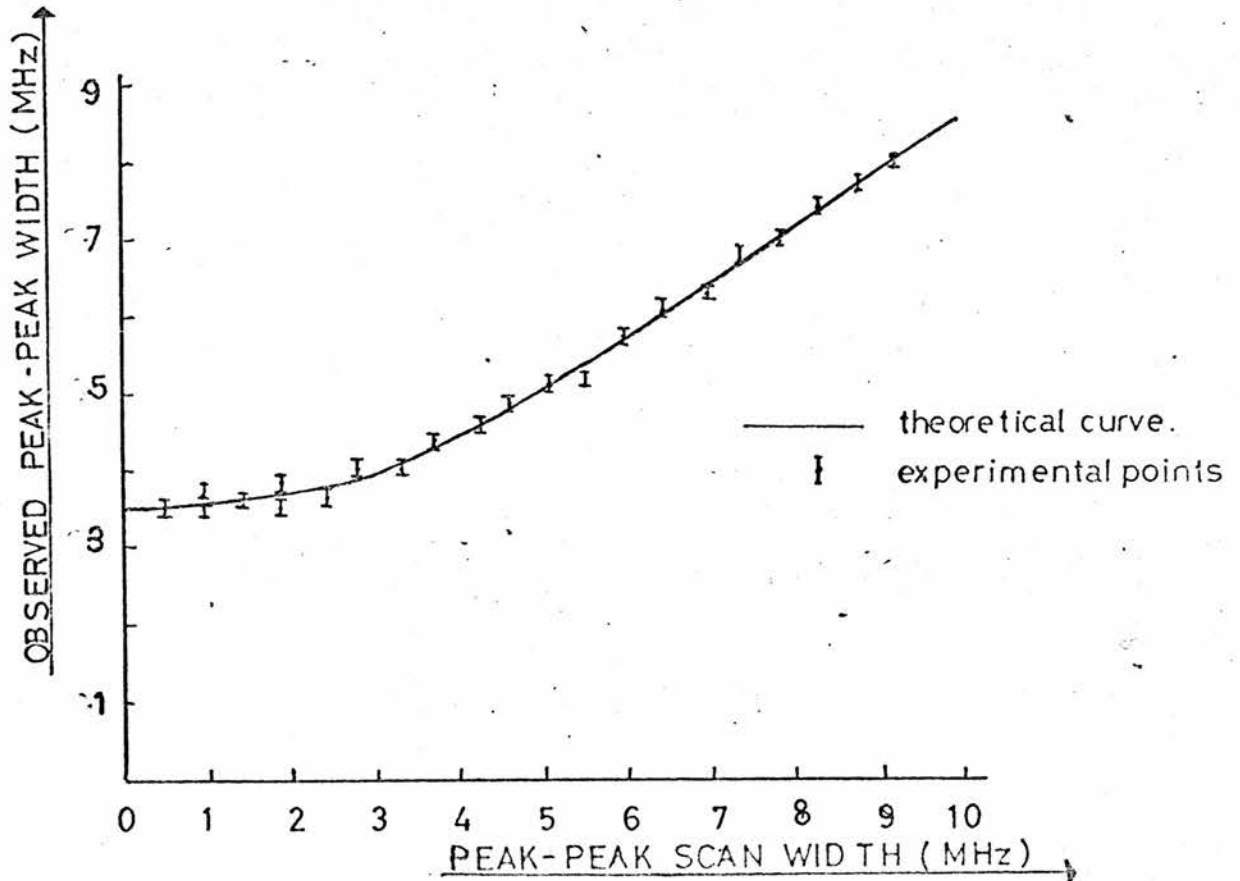
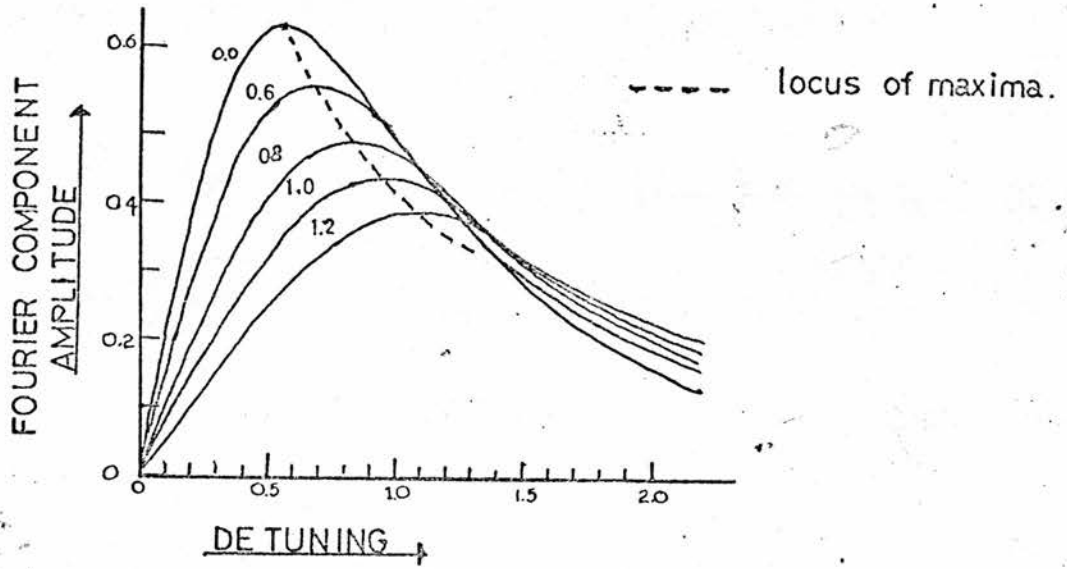


FIGURE 59

OBSERVED SCAN BROADENING

the dots indicate the measured values which have an error of ± 0.25 MHz. The broadening introduced by scan widths of up to 2 MHz., is almost negligible. Typically, scans of 0.5 MHz. are used and give satisfactory observation of the features.

One difficulty with third harmonic measurement techniques discussed later in the chapter is that small changes in the non scan-broadened feature width give rise to a large change in the k value which may be defined as (a.c. scan amplitude)/(F.W.H.M. of feature) because of the large scans involved. These small changes are easily brought about by, for example, laser power variations. In this way the small changes in observed peak width are masked by large scan width changes. This renders third derivative observation unsuitable for sensitive measurement of small broadenings. The first derivative technique, however, uses such small scans that factors of two or three increase in non scan broadened widths and give rise to negligible increases in the observed feature widths.

5.3. Power Broadening

The broadening effects of the laser power on the observed third harmonic detected linewidths were measured by the scan/recorder method already described. A graph may be plotted showing the variation of observed width with laser power.

From the slope of this line it is possible to make an estimate of the dipole moment of the 11-5 band of the B - X iodine transition about which there seems to be some uncertainty. La Paglia (96) calculated values for the similar Π - X transition of iodine and found that the dipole moment μ depended strongly on the internuclear separation. At the equilibrium molecular separation value, $\mu \sim 6 \times 10^{-3}$ debyes, but varied through two orders of magnitude over a range of 1 Å around the equilibrium value of 5.3 Å. Chutjian and James (78) calculate values of μ for the B - X system for a selection of vibrational transitions, not however including the 11 - 5 band, and report values between 0.145 debyes and 0.21 debyes. Evidently, the value of μ may vary considerably over various vibrational lines.

The relationship between the F.W.H.M. of the saturated absorption line-shape and the laser power may be written, with minor modification from Bennett (31) as:

$$\Delta\nu = \sqrt{(\Delta\nu_0)^2 + \left[\frac{\mu E}{h}\right]^2} \quad (5.7.)$$

Where $\Delta\nu$ is the observed F.W.H.M., $\Delta\nu_0$ is the width at zero laser power, μ the dipole moment of the transition, E is the laser field strength and h, Planck's constant. E may be related to the laser power density P by the following relation

$$E \text{ (volts/cm)} = \sqrt{12 \pi P} \quad (\text{mW/mm}^2) \quad (5.8.)$$

However, any broadening measurements made using third harmonic detection must be regarded with some suspicion. We have already seen that the scan

broadening contribution to the observed width is considerable in third derivative detection methods. The effect of scan broadening will vary as the non scan broadened width varies due to the changing laser power. In the limit of infinite power broadened width, the scan broadening would be negligible. As the power broadened width decreases, the scan contribution increases and so the observed linewidth is larger than that due to power broadening alone. This indicates that the slope of the graph observed in these experiments is too small.

This difficulty may be removed by making power broadening measurements on component widths observed in first derivative form. The third derivative results, however, still have a great deal of relevance and indicate the behaviour of the system as the laser power is changed. The scan broadening does introduce a shift of the centre of the line, as discussed in section 5.2., of 13 KHz., per MHz. Power variations in an iodine laser stabilized using third harmonic technique must be made small enough to keep this shift below an effective scan width variation of 1 MHz., if the stabilized laser frequency is to be reproducible and possess a long term stability of ± 2 in 10^{10} .

The first harmonic saturated absorption curves were observed in exactly the same way as the third harmonic curves described earlier in this section, except that the p.s.d. reference frequency was the fundamental modulation frequency. A typical scan over d, e, f, and g is shown in Figure 5.7. and illustrates the reproducibility of the technique. The peaks were identified sufficiently well for peak to peak separations to be measured to within an accuracy of about 250 KHz. The X axis variation is caused by instability in the reference laser which varied over the few seconds taken to trace out a given peak. This instability gave an overall measurement accuracy for a particular scan of about 500 KHz. Figure 5.10. shows the result of the power broadening for a range of laser powers. The square of the observed linewidth is plotted to the laser power output for reasons to be discussed below. The power output may be easily related to the power density inside the laser cavity from a knowledge of the output mirror transmission, and the beam diameter.

During power broadening measurements, the pressure broadening contribution is constant, as are the fundamental natural and interaction line broadening contributions. The scan contribution variation may be neglected as described in Section 5.2.3. Equation 5.7. may be rewritten using equation 5.8. as :

$$\Delta\nu = \sqrt{(\Delta\nu_0)^2 + \left(\frac{\mu}{2} \sqrt{12\pi P}\right)^2} \quad (5.9.)$$

where $\Delta\nu$ is in MHz., μ is in debye units (1 debye = 10^{-18} esu. cm.) and P is in mW per square mm. The zero power broadened width from Figure 5.10. is about (1.5 x 1.73) MHz. F.W.H.M., and so we may write:

$$\Delta\nu^2 = 6.5 + 3\pi \mu^2 P. \quad (5.10.)$$

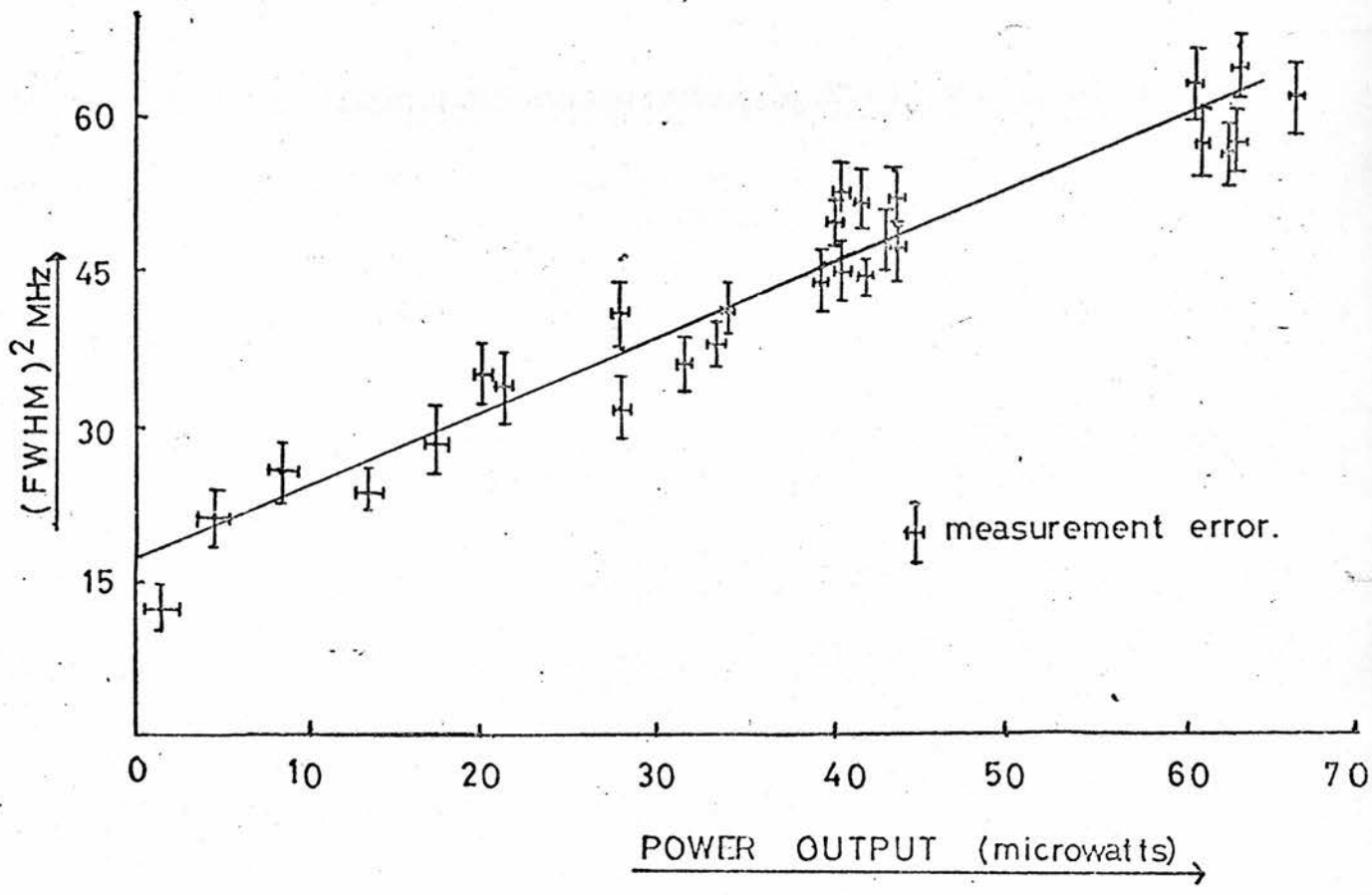


FIGURE 5.10
OBSERVED POWER BROADENING

The slope of the curve of Figure 5.10. therefore carries information about the value of μ , and measurement of the slope indicates a value of 0.22 debyes for the dipole moment of this transition. The accuracy of the measurement is determined by the possible variation in slope of the curve and, for the measurements so far taken, is estimated to give an uncertainty of ± 0.02 debyes. This is consistent with the results of Chutjian and James (78) The power broadening contribution to observed F.W.H.M. lineshape may also be expressed as 63 KHz. per μW output power. This represents a power broadening of about 60 KHz., F.W.H.M., $mW^{-1} mm^{-2}$ for power densities between the laser mirrors.

One difficulty and additional source of error in these measurements is concerned with the estimation of the intracavity power density. The difficulty arises from the Gaussian variation of electric field strength across the laser beam diameter. The output power of the laser is measured as integrated over the beam area on a large photocell and this figure has been used to estimate the intracavity power density by multiplying by the mirror transmission coefficient and dividing by the beam area. This beam area has been evaluated assuming the beam diameter is the spot size ω . (93). Obviously, this is an arbitrary definition of beam size and so the results must be interpreted with some caution. The power density closer to the beam centre than ω will be higher than that used in the dipole moment calculations and the power density further out from ω will be less than that used in the calculations. This method of averaging the electric field might therefore be open to question. However, intuitively, one feels that the use of the spot size in these calculations is a reasonable approximation to make, and is likely to give a sensible estimate of power density.

5.4. Pressure Broadening

The experiments of Chutjian, Link and Brewer (70) on iodine pressure shifts and broadening have already been referred to in Chapter 3. Their experiments were not saturated absorption experiments, however, but rather involved iodine molecules moving in all directions. These will be referred to as linear experiments. The nature of saturated absorption implies that only zero longitudinal velocity molecules contribute to the saturated absorption signal. Furthermore, those molecules suffering collisions during their interaction with the radiation field contribute less to the observed linewidth than those interacting uninterruptedly during their passage through the beam. The mean free path of a molecule at typical operating pressures is about 3 mm., and so most molecules do indeed traverse the interaction area, which is some 1 mm. in diameter, without suffering a collision. We should reasonably expect collisional broadenings to be smaller in saturated absorption work than those in linear absorption work. Chutjian et al. (70)

report a broadening, evaluated from a Stern-Volmer plot of energy level lifetime to pressure, of 2.6 MHz., per torr increase in the observed linewidth of the transition.

Using the scan method already discussed, experiments were performed to measure this broadening under saturated absorption conditions. Over a temperature range from 4°C to 25°C, the iodine vapour pressure varies from 45 millitorr to 350 millitorr (Section 4.2.), so a broadening of less than 1 MHz., might well be expected in a non-pressure broadened linewidth of about 2 MHz. As this would represent a considerable change in linewidth, first derivative observation of the broadened features was again necessary to avoid swamping the small pressure broadening by a large variation in scan broadening. The iodine pressure was slowly varied by changing the temperature of a water bath surrounding the sidearm of an iodine absorption tube inside the cavity of the laser which was to be scanned. Observations were carried out at temperature intervals of about 1 degree; the temperature was allowed to warm up slowly from an original ice-water mixture at 4°C to room temperature (22°C). For temperatures above this, warm water was added to the bath. Measurements were made both with the temperature increasing and then decreasing. The results for a particular temperature were consistent, showing that there was no lag or lead of bath and iodine temperatures for the two series of measurements. The upper pressure limit was set by the increase in absorption coefficient which then exceeded the laser gain and stopped laser action. The lower pressure limit was reached when there were no longer sufficient molecules to give a measurable absorption signal. Throughout the experiments the laser power was maintained constant, thereby ensuring a constant power broadening linewidth contribution.

The results of these measurements are shown in Figure 5.11, where the first derivative peak to peak width of component d is plotted for different iodine pressures. The zero pressure intercept is 2.15 MHz., which represents a linewidth of 3.75 MHz F.W.H.M. The error in this measurement may be estimated as about ± 0.1 MHz., peak to peak. This may be accounted for by:

- i) A natural lifetime of 410×10^{-9} seconds leading to a full width contribution of 390 KHz. ; a peak to peak width of 230 KHz.
- ii) A power broadening width contribution of 1.28 MHz. peak to peak (2.21 MHz. F.W.H.M.) for a constant laser output power of 35 microwatts (see section 5.3.)
- iii) A scan width contribution of less than 100 KHz. peak to peak (173 KHz. F.W.H.M.)
- iv) Interaction linewidth some 40 KHz. (70 KHz. F.W.H.M.)

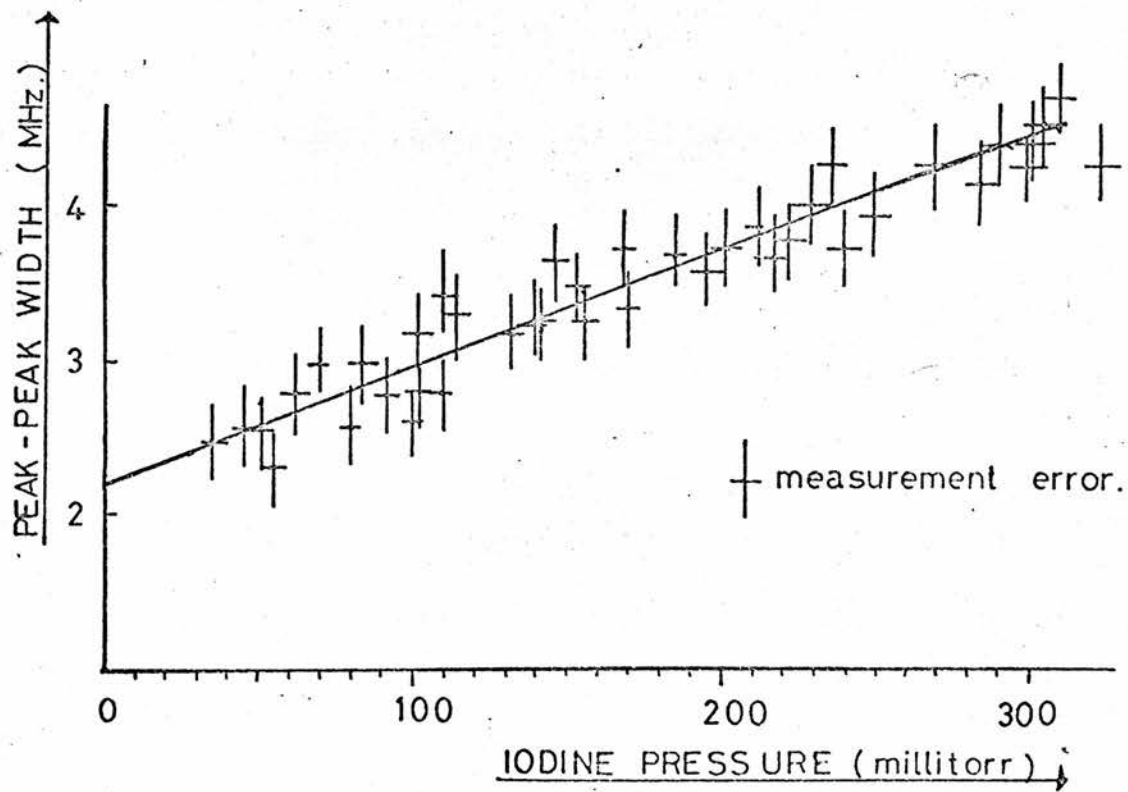


FIGURE 5-11

OBSERVED PRESSURE BROADENING

These factors give a total F.W.H.M. observed linewidth of 2.84 MHz., which reveals a discrepancy of almost 1 MHz. Some sign of a discrepancy has also been observed by other workers but not, however, with the accuracy of these experiments (66). It is likely that the extra contribution arises from predissociation (section 3.4.8). No estimate of the theoretically expected magnitude of this effect has yet been made. Figure 5.11 shows a linear variation of linewidth against pressure. The iodine pressure values have been measured as described in section 4.2. The slope gives a broadening coefficient for the F.W.H.M. of 11.9 MHz. per torr, and a similar slope is also observed in Stern-Volmer plots for components e, f and g. The mean value is 11 MHz. per torr. The Stern-Volmer equation (3.8.) therefore gives a value for the self quenching coefficient, σ^2 , of 305 \AA^2 .

This must be compared with the result of Chutjian et al. (70) of $\sigma^2 = 70 \text{ \AA}^2$ for this transition and of 65 \AA^2 from Chapman and Shotton (69). Neither of these results were observed in saturated absorption. Chutjian et al. measured the lifetime of selected vibrational levels from $v' = 0 - 25$ of the $B^3\Pi_{ou}^+$ state of iodine from the direct decay of fluorescence excited by a pulsed, tunable dye laser. Unfortunately, this method is likely to excite a blend of vibrational levels as the dye laser emission bandwidth was sufficiently broad to encompass several absorption lines.

The second result, however, was from experiments on the upper absorbing state lifetime, where a pulse of 633 nm. laser radiation excited ground state iodine molecules in an extracavity tube. The observed fluorescent decay of a single vibrational level enabled the lifetime to be measured (410 ± 15 nanoseconds). A plot of lifetime to iodine pressure gave a value for σ^2 .

The discrepancy found in the work reported in this thesis is almost certainly due to the presence of water vapour in the iodine tube. Of three iodine cells used in these experiments, all filled within a week of each other, two gave similar results, while the third gave absorption lines about twice as broad at room temperature. The variation of water vapour pressure from 4°C to 20°C is from 6 torr to 18 torr, and so is vastly greater than that of iodine. However, there is no means of knowing the water partial pressure inside the tube, and so the observed broadening may not be attributed to the full water vapour pressure change. Shotton (94) has intimated that he observed larger self quenching coefficients when water vapour was not totally excluded from iodine tubes. The water vapour pressure does not register on the conductivity type pirani vacuum gauges used to check the variation of iodine pressure with temperature in a sealed off iodine tube and so it is not easy to know of this contamination. A further set of iodine tubes are shortly to be filled under more carefully controlled conditions. The iodine will be dried by passing over phosphorous pentoxide before entering the absorption tube. In this way,

it is expected that the observed discrepancy will be resolved and a value for the self quenching coefficient observed under saturated absorption conditions will be measured using the method already described.

Pressure shifts are expected to be small, and the evidence of Dahlstrom and Hanes (66) indicates that an upper limit to the shift of 60 KHz. per torr may be expected for iodine - iodine collisions.

In Section 5.7., experiments are discussed which show that the offset frequency between lasers locked to the same line and operated under identical conditions is less than 20 KHz. when any of the three iodine cells is used as a reference. This leads one to suspect that the pressure shift induced by the different water pressures in the three tubes is less than 20 KHz. Furthermore, the side arms of any two tubes may be operated at temperatures of 22°C and 32°C respectively and the lasers still show no mutual offset frequency greater than 20 KHz. The change in water vapour pressure over this range is several tens of torr and it must be concluded that the collision induced shift with water vapour must be small.

5.5. Beat Frequency measurements for different integration times

To assess the performance of the control systems and to measure the reproducibility of the beat frequency between any two chosen hyperfine components, the beat frequency system was used (section 4.2.7.) In this case, two lasers were locked to two different lines of the d,e,f,g group and the beat frequency was counted, as described before. The lasers used in these experiments were both operated with 6 MHz. wide scans at 1.59 KHz. modulation frequency and were locked using third derivative techniques with a p.s.d. time constant of 1 second. The zero voltage level of the p.s.d. output stages were initially set to zero within 5 mV and both were within 10 mV of zero voltage after an experiment lasting an hour.

The integration time, normally, was 1 second on the beat frequency system reversible counter, but a longer 10 second integration period was made available by counting the beat frequency on a second frequency counter with a longer integration time. The results of this experiment are illustrated in a beat frequency plot illustrated in Figure 5.12. The displayed counter reading was noted and then plotted against time as shown. The results for 1 and 10 second integration times are shown and indicate the smoothing expected for the longer integration period. Also shown in the figure is the beat signal when one laser was unlocked, retuned to the same component and relocked. The discrepancy between the centre frequencies indicates the precision by which the stabilization system reproduces the same frequency. The lasers may be relocked to within ± 20 KHz., thereby indicating a reproducibility of the reference frequency of better than ± 2 part in 10^{10} .

FIGURE 5.12

BEAT FREQUENCY MEASUREMENTS FOR 1 AND 10 SECOND INTEGRATIONS

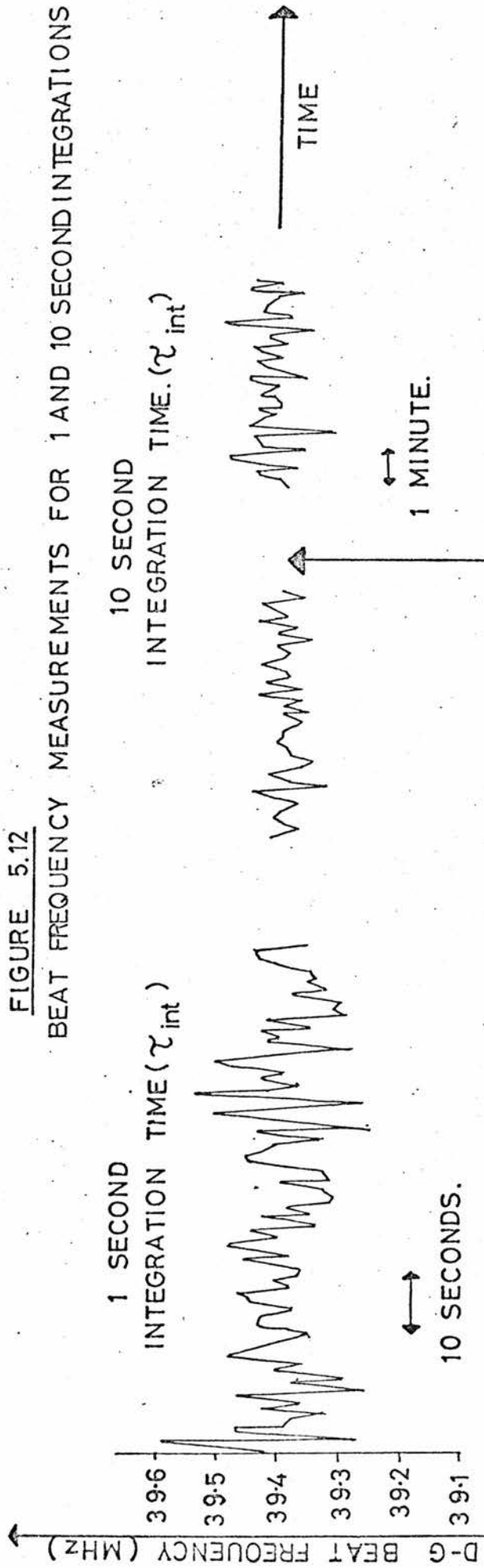
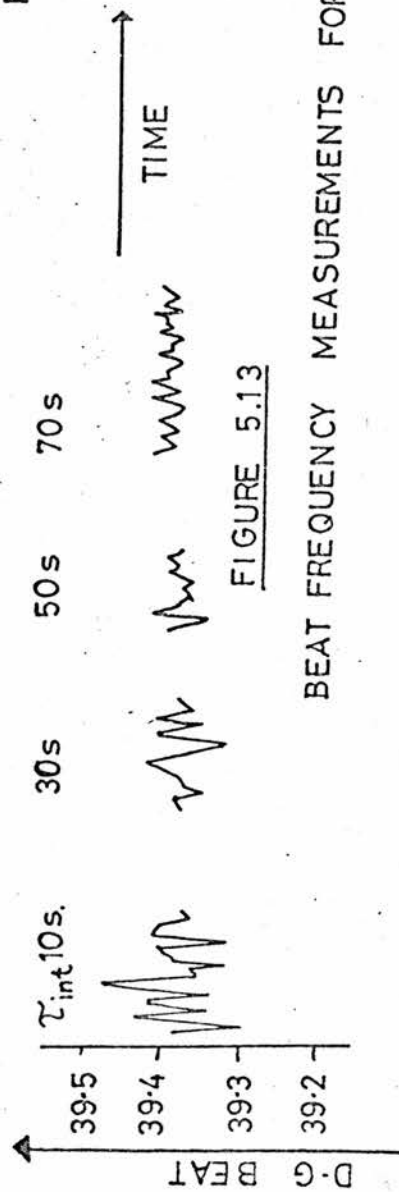


FIGURE 5.13

BEAT FREQUENCY MEASUREMENTS FOR LONGER INTEGRATION TIMES



For an averaging time of one second, the laser frequencies remained within ± 2 parts in 10^9 for periods of a minute as shown in the Figure. This performance is maintained for similar plots which were made for times of up to 5 minutes. It is possible to display the analogue voltage generated within the beat frequency apparatus as a function of time on a chart recorder. A suitable capacitor placed across the recorder input terminals ensured a one second time constant. Using this apparatus, runs of an hour were possible, and such an experiment showed that the centre of the beat frequency remained within ± 1 part in 10^{10} of its original value. After the lasers were warmed up for an hour, both remained in lock for some two hours before one laser reached the end of the control range on its piezoelectric.

For an integration time of ten seconds, the beat frequency between the two lasers was constant to within 4 parts in 10^{10} , as shown in Figure 5.12. This performance is maintained when an analogue voltage to time plot is made over an hour, as for the 1 second integration time.

5.6. Long Term Stability and Allan Variance Plots

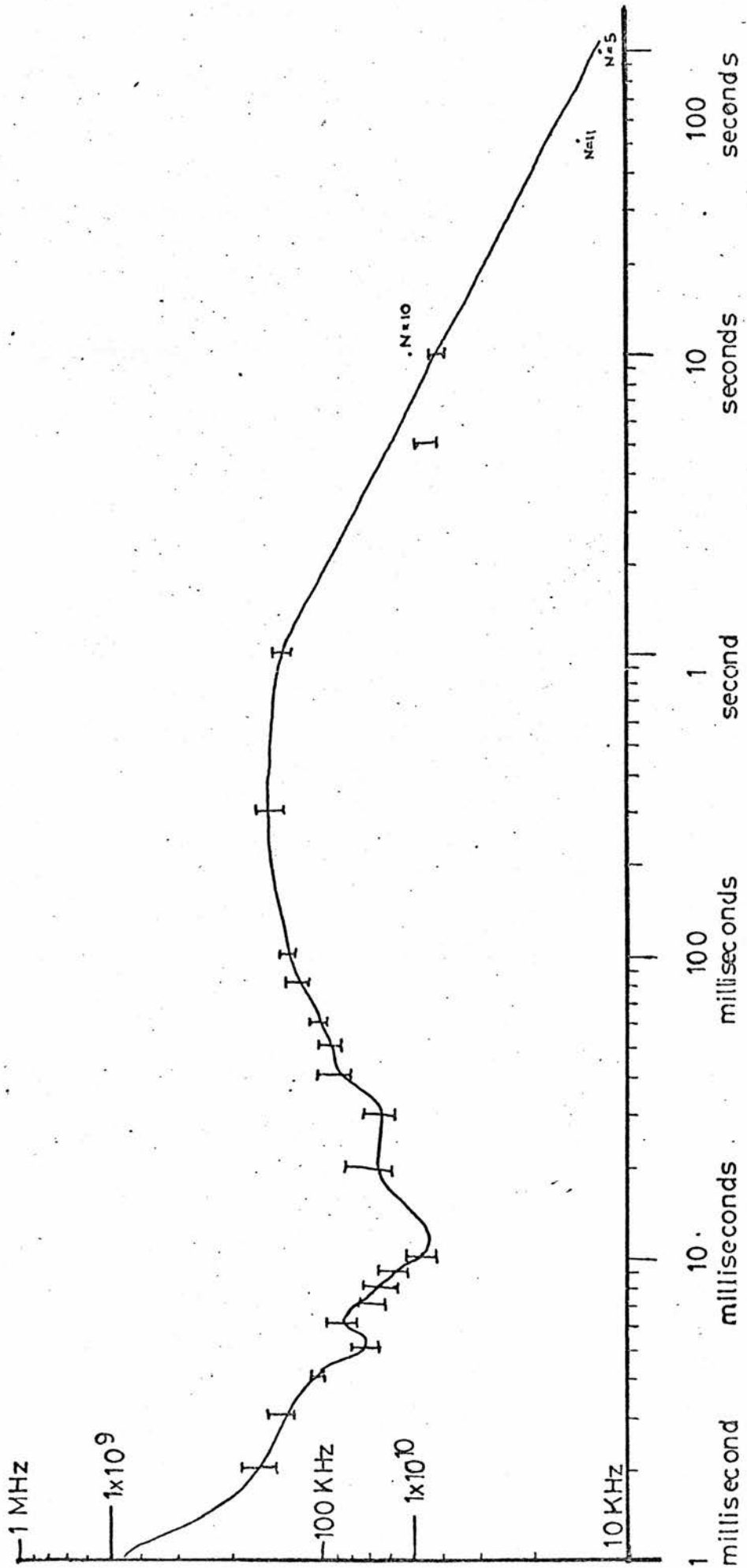
The performance of the laser over long integration times carries information about the stability of the iodine reference frequency. More fundamental information about the nature of the reference may be obtained from Allan Variance measurements where the nature of the limiting noise source affecting the laser stability is revealed.

The performance of two servo-locked lasers was investigated over integration times longer than the 10 second times discussed in the last section. A frequency counter, which had variable integration times up to 99 seconds was used, and typical stability figures for the d - g component beat are shown in Figure 5.13. As expected, the fluctuations gradually became smaller, and resulted in variations of some 30 KHz. peak to peak for integration times of 70 seconds.

One method of characterising long term frequency stability is the Allan Variance which was discussed in Section 1.6. The average value of the standard deviation of this variance, $\langle\sigma(2,\tau)\rangle$, is a suitable parameter to characterise long term frequency stability (33) and this is plotted as a function of integration time in Figure 5.14. These measurements were performed with the aid of a Hewlett Packard computing counter programmed to compute $\langle\sigma(2,\tau)\rangle$ for integration periods from one millisecond to ninety-nine seconds. The number of samples taken was 100 for integration times up to about 10 seconds. However, each variance measurement takes 200 times the averaging period (neglecting counter dead times). This requires a 30 minute observation time for a single variance

FIGURE 5.14

ALLAN VARIANCE MEASUREMENTS



measurement at 10 seconds integration time. To reduce the time involved in computing variance measurements for these integration periods, the number of samples was reduced to about 10. This, however, reduced the confidence level of the measurements made for long periods; the number of samples is indicated on the figure. The error bars indicate the spread of variance measurements made for a given integration time.

It was possible to initiate the integration period of the counter by triggering on an input waveform. Three separate experiments were performed by random triggering, triggering on the mains cycle and, finally, triggering on the scan waveform. This made little difference to the Variance measurements over integration times up to about 1 second. The measurements made with mains synchronisation, however, were typically a few parts in 10^{11} better for integration periods of about 10 seconds, and Figure 5.14 shows the Allan Variance plot for mains synchronised integration periods. The effects of the imposed frequency modulation are not apparent in this plot as they would correspond to variations with a period of ≈ 0.5 milliseconds which is off the scale to the left. Mains variations would manifest themselves at 10 milliseconds, corresponding to 100 Hz. or 20 milliseconds corresponding to 50 Hz. However, the Allan Variance shows no sign of any peaks at these times, or any differences between mains synchronised or non mains synchronised Variance measurements. Any mains synchronised variations which do exist on the laser evidently are not sufficiently large to be observed by this method. Comparison of these measurements with long integration time measurements, such as those shown in Figure 5.12, show satisfactory agreement.

The maximum sample time available on the counter was 99 seconds, and the plot of the Variance indicates that the laser stability was improving at these periods. The slope of this line is $(-\frac{1}{2})$ which is the slope to be expected from white frequency noise. This implies that improvements to the servo mechanism to increase the D.C. gain at these frequencies should improve the performance of the laser. A line with zero slope would indicate that the character of the frequency fluctuation was flicker or $(1/f)$ noise. This type of noise represents the fundamental limitation of any system and it would be impossible to improve the performance of the laser by any modifications to the servo system.

These servo-system improvements could take the form of an increase in the servo-system time constant, thereby increasing the gain at low frequencies. However, any increase in the time constant would reduce the servo-system action at higher frequencies. It might then be possible to increase the amplifier gains in the p.s.d. unit to counteract this effect and still avoid oscillation in the servo-system. This aspect of optimum servo-system design is still under development, and more experiments are necessary to study the long term stability of lasers with different servo-system gains and time constants.

5.7. Frequency Offsets - Beat Frequency experiments with lasers locked to the same line

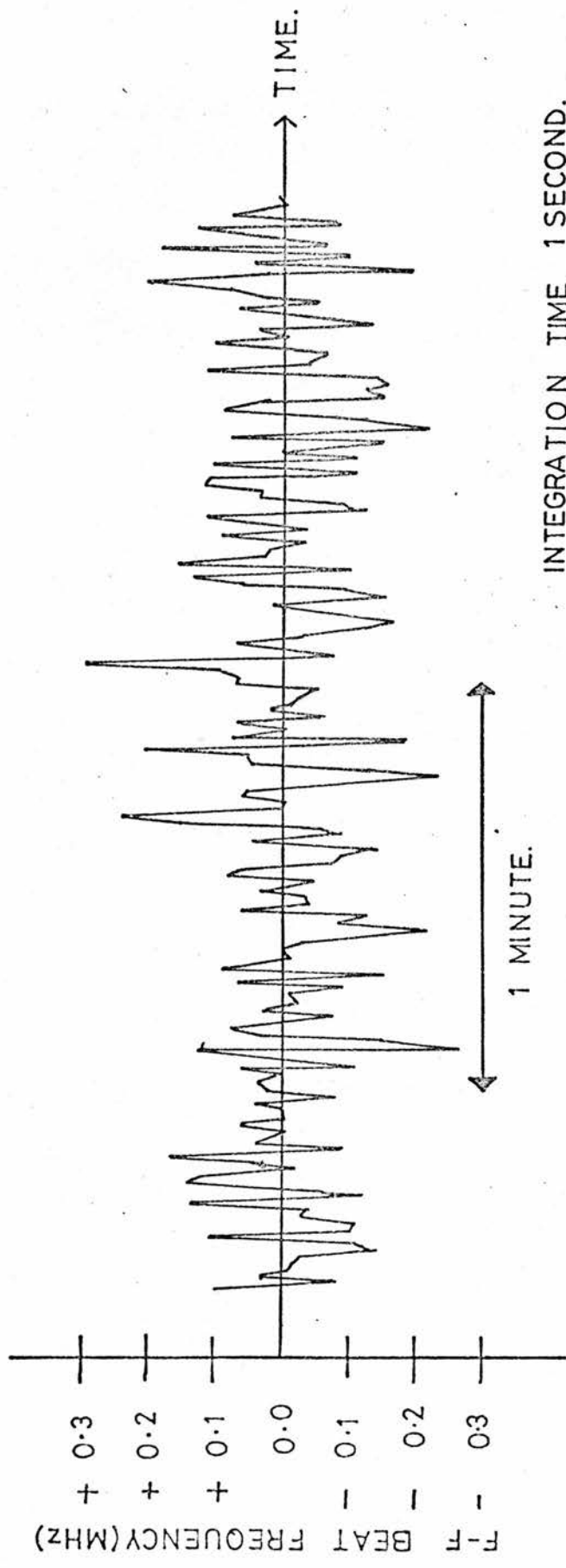
If a beat frequency experiment is carried out between two lasers locked to the same saturated absorption line and operated under nominally the same conditions, then, ideally, the beat frequency is zero. In practice, any offsets between the locking points show up as a non zero mean beat frequency. This experiment, therefore, carries information about the differences in the stabilized laser frequency to be expected from differently constructed lasers. These differences may arise from electronic differences in the servo-system, differences in the iodine pressure, power shifts and broadening, or scan width contribution introduced from dissimilar experimental conditions. Such an experiment was performed with two lasers locked to line g. One was operated with an AIM phase sensitive detector system and the second with a Brookdeal system. The zeros of the p.s.d.s were set to zero voltage to within 5 mV and the phase settings between input and reference signals were adjusted individually to give maximum third differential signal. Any phase errors would, ideally, have shown up as a reduction in signal and would not have introduced a frequency offset. The scan widths were both adjusted to be equal to 6 MHz., and the p.s.d. time constants were both 1 second. In both servo-systems integrating filters were used. (Chapter 3.8.)

Observations of the beat frequency for 1 second averaging times are plotted in Figure 5.15. This shows an estimated offset from zero of less than 1×10^{-11} . The relocking of both lasers on the same day and on different days reproduced this beat to better than 1×10^{-10} . The beat frequency measurements indicated peak deviations from zero frequency within $\pm 5 \times 10^{-9}$ for 1 second averaging times. These performances were achieved in a normal laboratory environment with other work proceeding and no special precautions were taken to ensure especially quiet surroundings. Very little change was observed when similar experiments were carried out during the evening.

During these measurements the mains supply voltage varied because of voltage reductions arising from a national miners' strike. This test of insensitivity to mains fluctuations indicated that the stabilized frequency remained within 1×10^{-10} for 5 - 7% mains voltage variations.

5.8. Separation of Hyperfine Component Centres

The separation of the centres of components d, e, f and g were measured by beating together two lasers locked to different components. The beat frequency was, of course, the separation of the component line centres. For two lasers operating under the same conditions, the individual frequency shifts discussed in this chapter were assumed to be the same and so the beat frequency represented the unperturbed separation. Relocking of the two lasers to their respective saturated absorption features reproduced the beat frequency



INTEGRATION TIME 1 SECOND.

SCAN WIDTH 6MHZ.

IODINE TEMPERATURE 20 °C

LASER POWERS 50 μW

FIGURE 5.15

BEAT FREQUENCY VARIATIONS BETWEEN
TWO LASERS LOCKED TO THE SAME COMPONENT.

to within some ± 20 KHz. giving rise to a measurement accuracy of 1 in about 500 for the beat frequency.

A second measurement of the line centre separations to somewhat poorer accuracy was possible using the scan technique and recorder trace calibration method discussed in section 5.2. One laser was locked to a particular component, usually d or g, and the second scanned over d, e, f and g. The p.s.d. output was recorded as a function of frequency on a chart recorder. From the known calibration of the recording or from settings to the line centres from a signal generator input, as described before, the centre separations were again measured. An extreme component was chosen as a reference to eliminate the different sensitivities of the beat frequency analogue output voltage for positive and negative beat frequencies. In this experiment, therefore, all the beat frequencies were either negative indicating the reference laser is tuned to a high frequency component d and the second laser is scanned from low to high frequency passing through g, f, e, and finally d at zero beat frequency, or positive, in which case, the reference was locked to component g and the second laser scanned in the order d, e, f and g. The accuracy of these measurements was about ± 0.3 MHz. and the results are shown in table 5.16.

Table 5.16 also shows the earlier experimental results of Dahlstrom and Hanes (66). The laser used in their experiments was stabilized using first derivative locking and the separations were measured by observing the p.s.d. output on an oscilloscope as this laser was swept in frequency. The light from this laser was mixed with that of a second tunable stable laser (not locked to an iodine reference). The oscilloscope trace was brightened when the beat between these lasers passed through a frequency determined by the tuning of an RF receiver. Thus two bright points were shown on the screen; when the beat frequency was plus the separation and also when it was minus the separation. A frequency calibration of the scan was then possible, but was limited in accuracy to ± 1 MHz. because of the instability of the reference laser and tuning errors in the receiver.

A theory published by Kroll (Section 3.6.) treats the hyperfine splitting as the sum of a nuclear electric quadruple interaction in both electronic states and a magnetic hyperfine interaction for the excited state only. Theoretical investigation of the neighbouring P.(33) line has also been made (83). Table 5.16 shows that the theoretical and experimental results are in agreement to within the experimental accuracy. This agreement confirms the validity of the theory in explaining the hyperfine splitting. The quadrupole coupling constants may be deduced from measurements of the hyperfine component splitting and by comparisons with the expected separations calculated from Kroll's theory.

Separation	Beat Frequency Centre Separations (MHz.)	Analogue Output Scans (MHz.)	Dahlstrom and Hanes (MHz.)	Theory (Kroll) (MHz.)
d - e	12.88 \pm 0.02	12.7 \pm 0.3	13.3 \pm 1.0	12.7
d - f	26.24 \pm 0.02	27.5 \pm 0.3	27.3 \pm 1.0	26.0
d - g	39.43 \pm 0.02	40.2 \pm 0.3	40.6 \pm 1.0	38.9

TABLE 5.16

Hyperfine Component Centre Separations

5.9. Summary and Conclusions

The experiments described in this thesis have traced the successful development and operation of a laser stabilized by saturated absorption in iodine. The preliminary results indicate that the frequency stability and reproducibility exceed those of any other visible stabilized laser. This laser, therefore, has shown itself worthy of further study and investigation which could well lead to its establishment as an international length standard. The techniques developed have already proved successful in the investigation of stability, reproducibility, and susceptibility to perturbations, and further experiments using these established methods should reveal any outstanding frequency shifts or line broadening mechanisms, particularly that of pressure broadening. The construction of further lasers in a more compact form is already in progress and intercomparison of these, both at the N.P.L., and internationally, should lead to confirmation of the reproducibility and stability figures discussed in this thesis.

The technique of saturated absorption spectroscopy provides the possibility of spectroscopic resolution comparable to the best already available in the visible spectral region, and applications involving the use of a tunable dye laser are particularly exciting (95).

The development of the iodine stabilized laser raises the possibility of new, precise measurements of fundamental constants. At the Bureau International des Poids et Mesures at Sèvres, Paris, an iodine stabilized laser is shortly to be constructed using the techniques described in this thesis and will be used in a precise measurement of the acceleration due to gravity g . The long term stability and reproducibility of the laser frequency will enable studies to be made of the variation of g with time.

At the N.P.L., iodine stabilized lasers are to be used in experiments to measure the speed of light and the Rydberg constant. A joint project between N.P.L., and Cambridge University Department of Geodesy and Geophysics is already in progress to investigate long period earth strain effects using a Michelson type fringe counting interferometer with a Lamb Dip stabilized laser. Considerable increases in the sensitivity and an extension of the range of observable strain periods can be expected using an iodine stabilized laser source.

The development of this laser has also enabled hitherto unexplored areas of physics to be investigated. The interesting but perplexing subject of collisions under saturated absorption conditions is already receiving close study. As a first step, the other line broadening features, such as power broadening and natural widths, will shortly be investigated in an atomic beam system. This will be developed, it is hoped, as a joint project with Sussex University. Measurements of parameters such as these under the typical beam conditions, notably absence of collisions, should provide confirmation of the

measurements reported here. The collisional effect should be the only major difference between the two experiments and may therefore be studied more closely. Any differences between the frequency emitted by a beam stabilized laser and a tube stabilized laser will be revealed by this study.

It is almost certain that either this laser or the methane stabilized 3.39 μ m laser will replace the Krypton 86 Lamp as the primary length standard. Table 5.17 summarises the properties of the iodine laser studied in this thesis and compares them, where possible, with the methane laser. As yet, iodine lasers are in their infancy and considerable improvements in performance are certain to be made in the next series of experiments. In particular, reproducibility and both short and long term stabilities will be improved in second generation lasers. Experimentally, the programme in the next few months will involve wavelength measurements on the d,e,f and g iodine components against Krypton 86, and the making of more careful pressure broadening measurements using tubes of dry iodine. A series of conditions will be established detailing the variations in laser parameters which must not be exceeded if one is to achieve a specified frequency stability. Lasers prepared both at N.P.L., and similar laboratories will be compared and the possibility of frequency shifts arising from different constructional techniques will be investigated.

The iodine stabilized laser, therefore, provides a most useful new laser light source. Because of its advantages over other previously constructed lasers and because of its potential as a spectroscopic tool it represents a most exciting development in the field of stabilized laser physics.

TABLE 5-17.
STABILIZED LASER PERFORMANCE.

Absorber	IODINE 127	METHANE
Wavelength	633 nm.	3.39 μ m
Short term stability	2×10^9 (200 KHz)	1×10^{12} (100 Hz)
Long term stability	$> 1 \times 10^{11}$ (500 Hz)	1×10^{13} (10 Hz)
Reproducibility	$> 2 \times 10^{10}$ (20KHz)	1×10^{11} (1KHz)
Pressure shift	< 60 KHz/torr	75 KHz/torr.
Pressure broadening	< 2.6 MHz/torr.	8 MHz/torr.
Absorber pressure	0.2 torr	0.04 torr
Power shift	< 20 KHz for x3 power rise.	—
Zeeman shift	$< 10^{13}$ for earths field.	—

APPENDIX I

The following is a list of the known absorption coincidences. The references are not exhaustive, but refer to the primary publication in each case.

- i) I_2 with the 514.5 nm line of Ar II and the 508.5 nm line of the Cd laser. (51, 52)
- ii) I_2 with the 568.2 nm line of the Kr II laser. (53)
- iii) I_2 at 501.7 nm., Br_2 at 514.5 nm., Cl_2 at 488.0 nm., all lines from the Ar II laser. (54)
- iv) NO_2 with 11 lines between 457.9 nm. and 520.8 nm. from Ar II and Kr II lasers. (55)
- v) K_2 with the 633 nm. line of the He - Ne laser. (56, 57)
- vi) Na_2 with seven lines from the Ar II laser. (57, 58)
- vii) Rb_2 and Cs_2 with several lines from the Ar II laser and the 633 nm. line of the He - Ne laser. (57, 58)
- viii) $^{14}NH_3$ and $^{15}NH_3$ with several lines in the $10\mu m$ region from CO_2 and NO_2 lasers. (59)
- ix) CH_3Br with the $10.6\mu m$ line of the CO_2 laser. (60)
- x) H_2CO with various infrared lines of the He - Xe and He - Ne lasers. (61, 62)
- xi) dimethyl ether with the $3.51\mu m$ line of the He - Xe laser. (63)
- xii) CH_4 , C_3H_8 and C_2H_6 with lines from the 7 - 8 μm region from Ne and Xe lasers. (64)
- xiii) CH_4 and the $3.39\mu m$ line from He - Ne lasers. (65)
- xiv) I_2^{127} with the 633 nm line from He - Ne lasers. (66)
- xv) I_2^{129} with the 633 nm line from He - Ne lasers. (67)
- xvi) SF_6 with the $10.6\mu m$ line from the CO_2 laser. (68)

REFERENCES

1. Comptes Rendus des Seances, 11 eme Conference Generale des Poids et Mesures
Paris 1960. Paris, Gauthier - Villars p.85.
2. Rowley, W.R.C., Wilson, D.C., Nature 200 745-747 1963.
3. White, A.D., Rev. Sci. Inst. 37 968-969 1966.
4. Lamb, W.E., Phys. Rev. 134A 1429-1450 1964.
5. Mielenz, K.D., Nefflen, K.F., Rowley, W.R.C., Wilson D.C., Engelhard, E.
Appl. Opt. 7 289-293 1968.
6. Turner, R., Baird, K.M., Taylor, M.J., Van der Hoeven, C.J.
Rev. Sci. Inst. 35 996-1001 1964.
7. Basov, N.G., Letokhov, V.S. Soviet Physics USPEKHI 11 855-880 1969.
8. Bagaev, S.N., Kolomnikov, Y.D., Lisitsyn, V.N., Chebotayev, V.P.
IEEE Journal of Quantum Electronics QE 4 868-870 1968.
9. Lee, P., Skolnick, M.L. Appl. Phys. Lett. 10 303-305 1967.
10. Jaseja, T.S., Murray, J., Townes, C.H., Phys. Rev. 133A 1221-1225 1964.
11. Bruce, C.F. Appl. Opt. 10 880-882, 1971.
12. Collinson, J.A. Bell Syst. Tech. J. 44 1511-1519 1965.
13. Van Bueren, H.G. Phys. Lett. 2 340-341 1962.
14. Tomlinson, W.J., Fork, R.L. Appl. Opt. 8 121-129 1969.
15. Tang, C.L., Statz, H. Phys. Rev. 128 1013-1020 1962.
16. Wallard, A.J., Woods, P.T. Institute of Physics Plasma Physics Group
Meeting, November 1971, S.E.R.L. Baldock, U.K.
17. Collinson, J.A. B.S.T.J. 44 1511-1519 1965.
18. Engelhard, E.J.G. J. Opt Soc. America. 61 216-217 1971.
19. White, A.D. Appl. Phys. Lett. 10 24-26 1967.
20. Sosnowski, T.P., Johnson W.B. IEEE J. Quant. Elect. QE 5 151-156 1969.
21. Gyorffry, B.L., Borenstein, M., Lamb, W.E. Phys. Rev. 169 340-359 1968.
22. Meyer, F.J. IEEE J. Quant. Elect. QE 3 690 1967.
23. White, H.E. Atomic Spectra. McGraw Hill, London 1934.
24. Arrathoon, R., Siegman, A.E. Appl. Phys. Lett. 13 197-199 1968.
25. Smith, P.W. IEEE J. Quant. Elect. QE 1 343-348 1965.
26. Smith, P.W. IEEE J. Quant. Elect. QE 2 666-668 1966.
27. Harris, S.E., McDuff, O.P. IEEE J. Quant. Elect. QE 1 245-262 1965.
28. Hercher, M. Applied Optics 8 1103-1106 1969.
29. Barber, H.F. Applied Optics 7 559-561 1968.
30. Manger, H., Rothe, H. Phys. Lett. 7 330-331 1963.
31. Bennett, W.R. Applied Optics Supplement Number 2 on Optical Masers
32. Allan, D.W. Proc. IEEE 54 221-230 1966.
33. Barnes, J.A. et al. IEEE Trans. Inst. Meas. IM 20 105-119, 1971.
34. Hellwig, H., Bell, H.E., Karlaschoff, P., Bergquist, J.C. J. Appl. Phys.
43 450-452 1972.
35. Boyne, H.S. IEEE Trans. on Inst. and Meas. IM 20 19-22 1971.
36. Malacara, D., Berriel, L.R., Rizo, I. Am. J. Phys. 37 276-284 1969.

37. Ramsay, J.V., Tomaka, K. Jap. J. Appl. Phys. 5 918-923 1966.
38. Field, R.L. Rev. Sci. Inst. 38 1720-1722 1966.
39. Hochuldi, U., Haldeman, P. Rev. Sci. Inst. 36 1493-1494 1965.
40. Hochuldi, U., Haldeman, P., Hardwick, D. IEEE J. Quant. Elect. QE 3
612-613 1967.
41. Moore, W.T. Private communication.
42. Rowley, W.R.C. IEEE. Trans. on Inst. and Meas. IM 15 146-149 1966.
43. Rowley, W.R.C., Wallard, A.J., Wilson, D.C., Woods, P.T. unpublished.
44. White, A.D. Rev. Sci. Inst. 38 1079-1084 1967.
45. Lisitsyn, V.N., Chebotayev, V.P. Soviet Physics JETP 27 227-229 1968.
46. Hall J.L. "The lineshape problem in laser saturated molecular absorption"
Lectures in Theoretical Physics 12. ed. Mahanthapa, Brittin,
pub. Gordon & Breach Co. New York 1970
47. Letokhov, V.S. Soviet Physics 27 665-669 1968.
48. Greenstein, G. unpublished.
49. Freed, C. IEEE J. Quant. Elect. QE 4 404-408 1968.
50. Jaseja, T.S., Javan, A., Murray, J., Townes, C.H. Phys. Rev. 133A
1221-1225 1964.
51. Steinfeld, J.D., Campbell, J.D., Weiss, N.A. J. Mol. Spec. 29 204-215 1969.
52. Ezekiel, S., Weiss, R. Phys. Rev. Lett. 20 91-93 1968.
53. Sakurai, K., Broida, H.P. J. Chem. Phys. 50 557-559 1969.
54. Holzer, W., Murphy, W.F., Bernstein, H.J. J. Chem. Phys. 52 469-470 1970.
55. Sakurai, K., Broida, H.P. J. Chem. Phys. 50 2404-2410 1969.
56. Tango, W.J., Link, J.K., Zare, R.N. J. Chem. Phys. 49 4264-4268 1968.
57. Baumgartner, G., Demtröder, W., Stock, M. Z. Phys. 232 462-472 1970.
58. Demtröder, W., McClintock, M., Zare, R.N. J. Chem. Phys. 51 5495-5508 1969.
59. Shimizu, T., Oka, T. J. Chem. Phys. 53 2536-2537 1970.
60. Ronn, A.M., Lide, D.R. J. Chem. Phys. 47 3669-3670 1967.
61. Letokhov, V.S. JETP. Lett. 6 101-103 1967.
62. Sakurai, K., Shimoda, K., Takami, M. J. Phys. Soc. Jap. 21 1838 1966.
63. Wang, S.C., Siegman, A.E. IEEE J. Quant. Elec. QE 6 576-577 1970.
64. Brunet, H. IEEE J. Quant. Elect. QE 2 382-384 1966.
65. Barger, R., Hall, J.L. Phys. Rev. Lett. 22 4-8 1969.
66. Dahlstrom, C., Hanes, G.R. Appl. Phys. Lett. 14 362-364 1969.
67. Knox, J.D., Yoh-Han Pao. Appl. Phys. Lett. 16 129-131 1970.
68. Rabinowitz, P., Keller, R., Larouette, J.T. Appl. Phys. Lett. 14 376-378 1969.
69. Shotton, K.C., Chapman, G.D. J. Chem. Phys. 56 1012-1013 1972.
70. Chutjian, A., Link, J.K., Brewer, L. J. Chem. Phys. 46 2666-2675 1967.
71. Brewer, L., Berg, R.A., Rosenblatt, C.M. J. Chem. Phys. 38 1381-1388 1963.
72. Sakurai, K., Capelle, G., Broida, H.P. J. Chem. Phys. 54 1220-1223 1971.

73. Barger, R., Hall, J.L. private communication.
74. Hall, J.L., Barger, R., Uzgiris, E. presented at ICPEAC Conference in Amsterdam 1971.
75. Breene, R.C., Shift and Shape of Spectral Lines, New York, 1961.
76. Arrathoon, R., Siegman, A.E. Appl. Phys. Lett. 13 197-199 1969.
77. Ozier, I. Phys. Rev. Lett. 27 1329-1332 1971.
78. Chutjian, A., James, A. J. Chem. Phys. 51 1242-1249 1969.
79. Chapman, G. Bull. Canad. Assoc. Physicists 27 55 1971.
80. Ramsay, N.F. Molecular Beams p.118. Clarendon Press, Oxford 1956.
81. Series, G.W. Rep. Prog. Phys. 22 280-328 1959.
82. Kroll, M. Phys. Rev. Lett. 23 631-633 1969.
83. Hanes, G., Lapierre, J., Bunker, P., Shotton, K.C. J.Mol. Spect. 39 506-515 1971.
84. Wallard, A.J., Woods, P.T. To be published.
85. Yoh, J., George, N. Report AFOSR - 70 - 0899 TR.
86. Prescott, L.J., Van der Ziel, A. Appl. Phys. Lett 5 48-49 1964.
87. Carscadden, A., Bletzinger, P., Friar, E.M. J. Appl. Phys. 35 3432-3 1964.
88. Hernquist, K.G. RCA Review 30 429-434 1969.
89. Rózsa, K., Salamon, T. Optics and laser Technology 151-153 August 1970.
90. Baird, K.M., Hanes, G. Metrologia 5 32-33 1969.
91. Wallard, A.J., Journal of Physics E. 5 926-930 1972.
92. Kaye, G.W.C., and Laby, T.H. Tables of Physical and Chemical Constants London : Longmans, Green. 1959.
93. Kogelnik, H. Li, T. Appl. Optics 5 1550-1570 1966.
94. Shotton, K.C. private communication.
95. Hänsch, T.W., Shahin, I.S., Schawlow, A.L. Phys. Rev. Lett. 27 707-710 1971.
96. La Paglia, S.R. J. Chem. Phys. 48 537-538 1968.

JOURNAL TITLE ABBREVIATIONS

Listed in the order in which they appear in the list of references

Rev. Sci. Inst.	Review of Scientific Instruments
Phys. Rev.	Physical Review
Appl. Opt.	Applied Optics
Appl. Phys. Lett.	Applied Physics Letters
Bell Syst. Tech. J.	Bell Systems Technical Journal
E.S.T.J.	
Phys. Lett.	Physics Letters
J. Opt. Soc. America	Journal of the Optical Society of America
J. Quant. Elect.	Journal of Quantum Electronics
Proc. IRE	Proceedings of the Institute of Radio Engineers
Proc. IEEE	Proceedings of the Institute of Electronic and Electrical Engineers
Trans. Inst. and Meas.	Transactions on Instrumentation and Measurement
Am. J. Phys.	American Journal of Physics
Jap. J. Appl. Phys.	Japanese Journal of Applied Physics.
J. Mol. Spec.	Journal of Molecular Spectroscopy
J. Chem. Phys.	Journal of Chemical Physics
Z. Phys.	Zeitschrift für Physik
Bull. Canad. Assoc. Phys.	Bulletin of the Canadian Association of Physicists